Development and Validation of Human Body Finite Element Models for Pedestrian Protection

Wansoo Pak

Dissertation submitted to the faculty of the Virginia Polytechnic Institute and State University in partial fulfillment of the requirements for the degree of

Doctor of Philosophy
in
Biomedical Engineering

Costin D. Untaroiu, Chair
Francis S. Gayzik
Warren N. Hardy
Yong Woo Lee
Alexandrina Untaroiu

September 17, 2019
Blacksburg, VA

Keywords: *finite element modeling, impact biomechanics, pedestrian safety, computational biomechanics*

Development and Validation of Human Body Finite Element Models for Pedestrian Protection

Wansoo Pak

Abstract

The pedestrian is one of the most vulnerable road users. According to the World Health Organization (WHO), traffic accidents cause about 1.34 million fatalities annually across the world. This is the eighth leading cause of death across all age groups. Among these fatalities, pedestrians represent 23% (world), 27% (Europe), 40% (Africa), 34% (Eastern Mediterranean), and 22% (Americas) of total traffic deaths. In the United States, approximately 6,227 pedestrians were killed in road crashes in 2018, the highest number in nearly three decades.

To protect pedestrians during Car-to-Pedestrian Collisions (CPC), subsystem impact tests, using impactors corresponding to the pedestrian's head and upper/lower leg were included in regulations. However, these simple impact tests cannot capture the complex vehicle-pedestrian interaction, nor the pedestrian injury mechanisms, which are crucial to understanding pedestrian kinetics/kinematics responses in CPC accidents. Numerous variables influence injury variation during vehicle-pedestrian interactions, but current test procedures only require testing in the limited scenarios that mostly focus on the anthropometry of the 50th percentile male subject. This test procedure cannot be applied to real-world accidents nor the entire pedestrian population due to the incredibly specific nature of the testing. To better understand the injury mechanisms of pedestrians and improve the test protocols, more pre-impact variables should be considered in order to protect pedestrians in various accident scenarios.

In this study, simplified finite element (FE) models corresponding to 5th percentile female (F05), 50th percentile male (M50), and 95th percentile male (M95) pedestrians were developed and validated in order to investigate the kinetics and kinematics of pedestrians in a cost-effective study. The model geometries were reconstructed from medical images and exterior scanned data corresponding to a small female, mid-sized male, and tall male volunteers, respectively. These models were validated based on post mortem human surrogate (PMHS) test data under various loading including valgus bending at knee joint, lateral/anterior-lateral impact at shoulder, pelvis, thorax, and abdomen, and lateral impact during CPC. Overall, the kinetic/kinematic responses predicted by the pedestrian FE models showed good agreement against the corresponding PMHS test data. To predict injuries from the tissue level up to the full-body, detailed pedestrian models, including sophisticated musculoskeletal system and internal organs, were developed and validated as well. Similar validations were performed on the detailed pedestrian models and showed high-biofidelic responses against the PMHS test data.

After model development and validation, the effect of pre-impact variables, such as anthropometry, pedestrian posture, and vehicle type in CPC impacts were investigated in different impact scenarios. The M50-PS model's posture was modified to replicate pedestrian gait posture. Five models were developed to demonstrate pedestrian posture in 0, 20, 40, 60, and 80 % of the gait cycle. In a sensitivity study, the 50th percentile male pedestrian simplified (M50-PS) model in gait

predicted various kinematic responses as well as the injury outcomes in CPC impact with different vehicle type.

The pedestrian FE models developed in this work have the capability to reproduce the kinetic/kinematic responses of pedestrians and to predict injury outcomes in various CPC impact scenarios. Therefore, this work could be used to improve the design of new vehicles and current pedestrian test procedures, which eventually may reduce pedestrian fatalities in traffic accidents.

Development and Validation of Human Body Finite Element Models for Pedestrian Protection

Wansoo Pak

General Audience Abstract

The pedestrian is one of the most vulnerable road users. According to the World Health Organization, traffic accidents cause about 1.34 million fatalities annually across the world. This is the eighth leading cause of death across all age groups. Among these fatalities, pedestrians represent 23% (world), 27% (Europe), 40% (Africa), 34% (Eastern Mediterranean), and 22% (Americas) of total traffic deaths. In the United States, approximately 6,227 pedestrians were killed in road crashes in 2018, the highest number in nearly three decades.

To protect pedestrians in traffic accidents, subsystem impact tests, using impactors corresponding to the pedestrian's head and upper/lower leg were included in regulations. However, these simple impact tests cannot capture the complex vehicle-pedestrian interaction, nor the pedestrian injury mechanisms, which are crucial to understanding pedestrian kinetics/kinematics responses in traffic accidents. Numerous variables influence injury variation during vehicle-pedestrian interactions, but current test procedures only require testing in the limited scenarios that mostly focus on the anthropometry of the average male subject. This test procedure cannot be applied to real-world accidents nor the entire pedestrian population due to the incredibly specific nature of the testing. To better understand the injury mechanisms of pedestrians and improve the test protocols, more pre-impact variables should be considered in order to protect pedestrians in various accident scenarios.

In this study, simplified pedestrian computational models corresponding to small female, average male, and large male pedestrians were developed and validated in order to investigate the kinetics and kinematics of pedestrians in a cost-effective study. Overall, the kinetic/kinematic responses predicted by the pedestrian models showed good agreement against the corresponding test data. To predict injuries from the tissue level up to the full-body, detailed pedestrian computational models, including sophisticated musculoskeletal system and internal organs, were developed and validated as well. Similar validations were performed on the detailed pedestrian models and showed high-biofidelic responses against the test data. After model development and validation, the pre-impact variables were examined using the average male pedestrian model, which was modified the position to replicate pedestrian gait posture. In a sensitivity study, the average male pedestrian model in gait predicted various kinematic responses as well as the injury outcomes in lateral impact with different vehicle types.

The pedestrian models developed in this work have the capability to reproduce the kinetic/kinematic responses of pedestrian and to predict injury outcomes in various pedestrian impact scenarios. Therefore, this work could be used to improve the design of new vehicles and current pedestrian test procedures, which eventually many reduce pedestrian fatalities in traffic accidents.

Acknowledgements

I would like to begin by thanking my advisor, Dr. Costin D. Untaroiu. His guidance in research enlightened me in a positive way. The honest and instant feedback that he provided made me not settle and motivated me to always improve. Thank you to the remaining members of my committee, Dr. Francis S. Gayzik, Dr. Warren N. Hardy, Dr. Yong Woo Lee, and Dr. Alexandirna Untaroiu, for your advice and aid with my research. I would also like to thank the members of Dr. Untaroiu's group: Keegan Yates, Yunzhu Meng, Wade Baker, and Daniel Grindle. You all were great supporters and were always willing to help. Finally, I am blessed to have supportive parents. You have always encouraged me to pursue my goals and believed in my success. I would not have been able to make it this far without the unconditional love and support.

Table of Contents

Abstract ii

General Audience Abstract iv

Chapter 1 1

Introduction

1.1 BACKGROUND 1

1.2 SUMMARIES OF CHAPTER 5

REFERENCE 6

Chapter 2 8

Finite Element Model of a High-Stature Male Pedestrian for Simulating Car-to-Pedestrian Collisions 8

ABSTRACT 8

2.1 INTRODUCTION 8

2.2 METHODS 9

2.3 RESULTS 13

2.4 DISCUSSION 20

2.5 CONCLUSION 22

REFERENCE 22

Chapter 3 26

Development and Validation of a Finite Element Model of a Small Female Pedestrian 26

ABSTRACT 26

3.1 INTRODUCTION 26

3.2 METHODS 27

3.3 RESULTS 31

3.4 DISCUSSION 34

REFERENCE 36

Chapter 4 41

Development and Validation of a Finite Element Model of an Average Male for Investigating Pedestrian Accidents 41

ABSTRACT 41

4.1 INTRODUCTION 41

4.2 METHODS 42

4.3 RESULTS 47

4.4 DISCUSSION 56

4.5 CONCLUSION 58
REFERENCE 58
Chapter 5 63
Pedestrian Biomechanical and Injury Responses regarding Pre-Impact Posture and Vehicle Type 63
ABSTRACT 63
5.1 INTRODUCTION 63
5.2 METHODS 64
5.3 RESULTS 68
5.4 DISCUSSION 72
REFERENCE 74
Chapter 6 79
Conclusion
6.1 LIMITATIONS AND FUTURE WORK 79
6.2 CONCLUSION 80
REFERENCE 80
Appendix A 82

Chapter 1

Introduction

1.1 BACKGROUND

The pedestrian is one of the most vulnerable road users. According to the World Health Organization (WHO), the total number of fatalities recorded in traffic accidents is about 1.35 million each year worldwide [2]. This is the eighth leading cause of death for people across all age groups. From this high mortality rate, more than half of road traffic deaths are of the most vulnerable road users, which includes pedestrians. In 2018, pedestrian fatalities represented 23% (world), 27% (Europe), 40% (Africa), 34% (Eastern Mediterranean), and 22% (Americas) of total traffic deaths. In the United States, approximately 6,227 pedestrians were killed in road crashes in 2018, the highest number in nearly three decades [3].

Historically, the major challenge of automotive safety research improving the design of vehicles and restraint systems to reduce the risk of occupant injury. Consequently, vehicle occupant fatalities have declined 46% since 1975 [4]. Pedestrian fatalities have been increased while the total crash fatalities have been decreased (Figure 1.1, a), therefore, the percentage of total fatalities with respect to the pedestrian have increased almost continuously since 2008 (Figure 1.1, b) [5, 6].

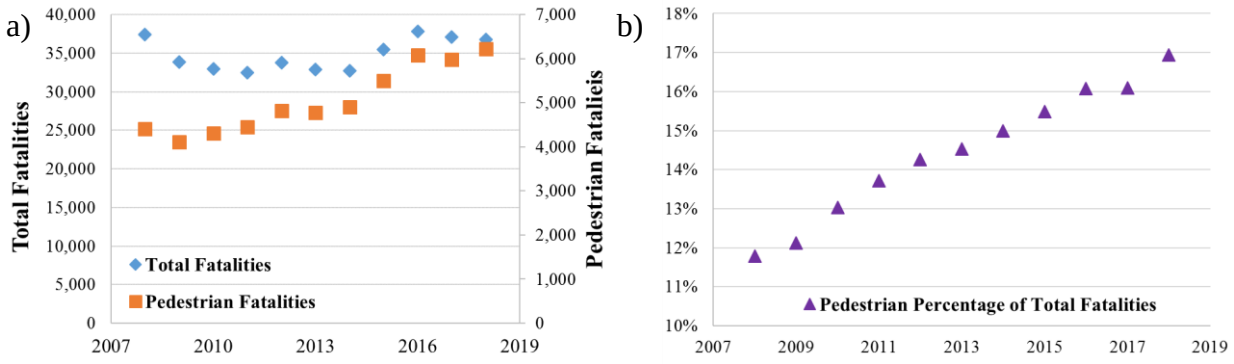

Figure 1.1 Total fatalities and pedestrian fatalities in Traffic crashes (left) and the pedestrian percentage of total fatalities (right)

Due to the high fatality rate of pedestrians in traffic accidents, pedestrian protection during Car-to-Pedestrian Collision (CPC) has generated increased attention. Many countries have developed their own regulations on new cars in order to protect pedestrians. In these regulations, the new vehicles are tested with subsystem impactors that correspond to an adult/child head and adult upper/lower leg.

For example, the European New Car Assessment Program (Euro NCAP) performs the headform, upper legform, and legform tests for pedestrian protection (Figure 1.2, a) [7]. In the head impact

tests, the acceleration of the headform's center of gravity are recorded. In the legform impact tests, the knee bending angle at the top of tibia section, angle at the bottom of femur section, and acceleration at tibia section are measured. In the upper legform impact tests, the forces at the upper/lower femur section and bending moment at the center of femur, 50mm above and 50mm below of center of femur are measured. During legform tests, the bending moment and acceleration of the tibia and medial collateral ligament (MCL), anterior cruciate ligament (ACL), and posterior cruciate ligament (PCL) elongations are measured.

The Japan New Car Assessment Program (JNCAP) performs head impact tests for pedestrian protection. The Head Injury Criterion (HIC) is evaluated by projecting the adult headform (165mm in diameter and 4.5kg in mass) and the child headform (165mm in diameter and 3.5kg in mass) at 35km/h to the selected locations of divided vehicle bonnet and windshield area [8]. The impact angle is chosen according to the type of vehicle being tested: sedan, SUV, and One Box. In the legform impact tests, the bending moment at the tibia and elongation of MCL, ACL, and PCL are measured [9].

The Korean New Car Assessment Program (KNCAP) has similar test procedures to the Euro NCAP procedures, except it does not include the upper legform impact test to the bonnet leading edge and the impact area is different [10]. The test procedure includes the headforms (adult and child) and legforms (upper or lower) impact assessment. The headform specification is same as JNCAP's specifications for both adult and child tests. Six impact tests are carried out with the headform projected to the vehicle with 40km/h speed at 50° for child and 65° for adult (Figure 1.2, b). The lower legform (926mm and 13.4kg) and the upper legform (350mm and 9.5kg) impact to the front bumpers with 40km/h speed at three points.

The China New Car Assessment Program (CNCAP) performs head and leg impact tests for the pedestrian protection [11]. The adult (65°) or child (50°) headform is projected at 40km/h to the test vehicle and the HIC15 values are measured. For the leg test, the Transport Research Laboratory (TRL) upper leg or FLEX leg impactor (Humanetics, Farmington Hills, MI, USA) is selected based on the test vehicle bumper height. The legform impacts the vehicle front horizontally at speed of 40km/h and the bending moments of tibia and MCL, ACL, and PCL ligament elongations are calculated for lower legform. The impacting force and bending moments are calculated for the upper legform tests.

The Australasian New Car Assessment Program (ANCAP) performs headform, upper legform (10.5kg), and lower legform tests for pedestrian protection [12]. The test measurements are identical to the Euro NCAP tests.

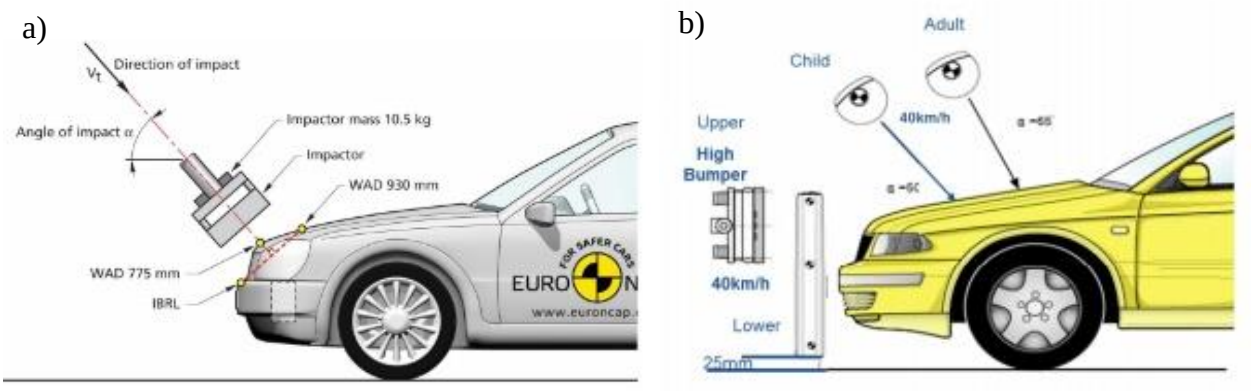

Figure 1.2 Upper legform test in Euro NCAP (left) and the impactor test in KNCAP (right)

These subsystem tests have led to reducing the stiffness of new vehicle front-end components, which has reduced the risk of injuries in traffic accidents [13]. However, these simple impact tests cannot capture the complex vehicle-pedestrian interaction, nor the pedestrian injury mechanisms, which are crucial to understanding the pedestrian kinetics/kinematics responses in CPC accidents. Furthermore, the effect of the front bumper design is not relevant in higher severity crashes (above 40 km/h vehicle impact speed used in the subsystem tests). This finding was confirmed by the finite element (FE) analyses of the TRL legform, FLEX legform, and full human model [14]. Therefore, the current test results from current protocols obtained in subsystem tests may not applicable in the severe pedestrian accidents.

The current test protocols are focused mostly on 50th percentile male anthropometries, so their findings cannot be applied to the entire pedestrian population. In addition, the 50th percentile male anthropometry has discrepancies between countries (Table 1.1). As in the case of Anthropometric Testing Device (ATD), the pedestrian subsystem impactors are manufactured mostly from polymeric and metallic materials, so they are usually stiffer than corresponding human parts. While some improvements were made especially in TRL legform, there are still some questions regarding impactor biofidelity [15].

Table 1.1 50th percentile male anthropometry parameters [1]

	Weight (kg)	Height (cm)	Shoulder height (mm)	Hip height (mm)	Knee height (mm)
UK	79.75	175.5	1455.3	931.5	467.3
USA	82.1	178.1	1459.7	934.3	468.7
China	60	169.1	1388.6	860.4	413

Another major limitation of the current subsystem tests is the fact that the body parts are isolated, which prevent them from reproducing the full-scale pedestrian response. It can be observed in FE simulations that the deformation of vehicle hood, caused by the pedestrian torso and upper extremity-hood interaction, can significantly influence the head pre-impact conditions. The boundary conditions on the impactors are also different from those of pedestrian body regions. For example, the current legform is not connected to the ankle joint and does not include the foot, which may affect the lower limb kinetic/kinematic responses. Similarly, the headform impactor is

isolated so the influence of the neck muscles and the cervical vertebral on the kinetic/kinematic responses of the head is neglected. Hence, the current test protocols should be improved to better represent the full-scale pedestrian response and should be conducted in a way to represent the entire pedestrian population.

A number of variables influence injury variation during vehicle-pedestrian interactions, however current regulations only require testing in the specific scenario that the average male pedestrian is set to mid-stance and impacted laterally with the centerline of the vehicle at 40 km/h. To better understand the injury mechanisms of pedestrian in vehicle-pedestrian interaction, more pre-impact variables should be considered such as the pedestrian anthropometry, posture, vehicle type, and speed. Guo et al. study showed drastically different pedestrian kinematic responses in CPC simulation when pedestrian model anthropometry was varied [1]. The taller European size pedestrian model impacted the vehicle's windshield with their shoulder while the Chinese size pedestrian model impacted the vehicle's bonnet with their hip and their head struck the windshield. In addition, statistical significance of sustaining head injury was observed for shorter pedestrian compared to medium height pedestrian [16]. With respect to the lower extremity, heavier pedestrians tend to results in severe injuries compared to medium weight pedestrian possibly due to the greater inertia [16].

A pedestrian's walking posture can influence its kinetic/kinematic responses in a CPC. When a pedestrian is impacted laterally by vehicle with the struck side leg facing forwards, smaller head impact velocity and Wrap Around Distance (WAD) are observed compared to the posture of the struck side leg facing backwards [17]. The height of H-point also changes during on the gait cycle. In addition, the posture of the arms also affects the upper body and head kinematics [18, 19]. There are discrepancies between head contact times when are posture varies, even if there has no significant difference visually [20]. However, a full-scale tests have not examined the effects of the arm posture that may have on full-body kinematics because the upper extremities were tied together during CPC testing for its repeatability [21].

The speed of vehicle play important role in pedestrian accidents. Rosen et al. study concluded that the fatality risks at 50km/h vehicle speed are more than twice as high as the risk at 40km/h and more than five times higher than the risk at 30km/h [22]. In addition, the fatality risk was estimated to be about 50% when vehicle impact velocity was 75km/h.

In 2015, nearly 88.7% of pedestrian fatalities were caused by front impacts of passenger cars and light trucks including SUVs, pickups, and vans [23]. Recently, the light truck and vans (LTV) sales are increasing; a new concern regarding pedestrian protection has emerged. Most passenger cars impact pedestrians below their center of gravity. However, the larger or taller vehicles such as LTV, Sport Utility Vehicle (SUV), and Multi-Purpose Vehicle (MPV) impact pedestrians at or above their center of gravity [24]. Pedestrian collisions with LTVs report greater pedestrian morbidity and mortality than pedestrian collisions with passenger cars [26, 27]. In addition, the injury risks of the head and chest are greater when struck by the LTV rather than by a passenger car.

Pedestrian kinetic/kinematic responses and injury biomechanics are heavily influenced by each of these variables. Combined variables effect may cause thoroughly different results as well. To verify the correlation between two or more combination of variables, a combined human and vehicle variables study is essential. While the PMHS tests provide the most biofidelic response, this method is not suitable for various test scenarios due to its high-cost and unreproducible nature.

Hence, the development of FE pedestrian models could be a better alternative that characterizes the whole-body response of vehicle-pedestrian interactions and assesses the pedestrian injuries in a repeatable and inexpensive manner. To investigate the kinetics and kinematics in a cost-effective study, FE models corresponding to six-years-old child (6YO), 5th percentile female (F05), 50th percentile male (M50), and 95th percentile male (M95) pedestrian in simplified models have been developed and validated. To predict injuries from tissue level up to full-body, detailed pedestrian models including sophisticated musculoskeletal system and internal organs have been developed and validated. After model development and validation, the pre-impact variables were investigated in different impact scenarios.

1.2 SUMMARIES OF CHAPTER

The manuscript "**A finite element model of a midsize male for simulating pedestrian accidents**" [25] about the development and validation of a 50th percentile male pedestrian model was published in *Journal of Biomechanical Engineering* on October 19, 2017. The work presented in this paper was primarily carried out by C.D. Untaroiu and I have participated in the model development and validation work. The article is available at: http://computationalnonlinear.asmedigitalcollection.asme.org/article.aspx?articleid=2653833.

The manuscript "**A finite element model of a six-year-old child for simulating pedestrian accidents**" [28] about the development and validation of a child pedestrian model was published in *Accident Analysis & Prevention* on October 17, 2016. The work presented in this paper was primarily carried out by Y. Meng and I have participated in the model development and validation work. The article is available at: https://www.sciencedirect.com/science/article/pii/S0001457516303633.

The subsequent chapters of this work, including title and summary are:

Chapter 2: **Finite Element Model of a High-Stature Male Pedestrian for Simulating Car-to-Pedestrian Collisions**

The 95th percentile male pedestrian simplified model was developed and validated in this chapter. The kinetics/kinematics of taller male pedestrian population can be studied with this model.

Chapter 3: **Development and Validation of a Finite Element Model of a Small Female Pedestrian**

The 5th percentile female pedestrian simplified model was developed and validated in this chapter. The kinetics/kinematics of small female pedestrian population can be studied with this model.

Chapter 4: **Development and Validation of a Finite Element Model of an Average Male for Investigating Pedestrian Accidents**

The 50th percentile male pedestrian detailed model was developed and validated in this chapter. The kinetics/kinematics as well as the injury outcomes of the average male pedestrian population can be studied with this model.

Chapter 5: **Pedestrian Biomechanical and Injury Responses regarding Pre-Impact Posture and Vehicle Type**

The influence of the pedestrian gait and vehicle type was studied with the average male pedestrian simplified model. Different kinetics/kinematics and injury predictions were observed with respect to the pedestrian posture in gait cycle and vehicle type.

Chapter 6: **Conclusion**

Limitations, future works, and conclusion of this study.

REFERENCE

[1] R. Guo, Q. Yuan, C. Sturgess, A. M. Hassan, Y. Li, and Y. Hu, "A study of an Asian anthropometric pedestrian in vehicle–pedestrian accidents using real-world accident data," *International journal of crashworthiness*, vol. 11, pp. 541-551, 2006.

[2] WHO, "Global Status Report on Road Safety," 2018.

[3] R. Retting, "Pedestrian Traffic Fatalities by State: 2018 Preliminary data," GHSA2019.

[4] IIHS, "General statistics," 2016.

[5] NHTSA, "Traffic Safety Facts (2017 Data)," 2019.

[6] NHTSA, "Early Estimate of Motor Vehicle Traffic Fatalities in 2018," 2019.

[7] EuroNCAP, "Pedestrian Testing Protocol v8.5," 2019.

[8] JNCAP, "Pedestrian Head Protection Performance Test procedure," 2018.

[9] JNCAP, "Pedestrian Leg Protection Performance Test Procedure," 2018.

[10] Y.-W. Yun, J.-W. Lee, G.-H. Kim, and P. Gyung-Jin, "Pedestrian Protection Test and Results: Utilization for Regulations in Korea," in *In 23rd International Technical Conference on the Enhanced Safety of Vehicles (ESV)*, 2013.

[11] CNCAP, "CNCAP Management Regulation," 2018.

[12] ANCAP, "ANCAP Assessment Protocol-Pedestrian Protection v9.0.2," 2018.

[13] J. Strandroth, M. Rizzi, S. Sternlund, A. Lie, and C. Tingvall, "The correlation between pedestrian injury severity in real-life crashes and Euro NCAP pedestrian test results," *Traffic injury prevention*, vol. 12, pp. 604-613, 2011.

[14] K. Mizuno, T. Ueyama, D. Nakane, and S. Wanami, "Comparison of reponses of the Flex-PLI and TRL legform impactors in pedestrian tests," *SAE International journal of passenger cars-mechanical systems*, vol. 5, pp. 203-213, 2012.

[15] Y. Matsui, H. Ishikawa, A. Sasaki, J. Kajzer, and G. SCHROEDER, "New biofidelic corridor and biofidelity test procedure for pedestrian legform impactors," *Traffic injury prevention*, vol. 5, pp. 390-397, 2004.

[16] G. Zhang, L. Cao, J. Hu, and K. H. Yang, "A field data analysis of risk factors affecting the injury risks in vehicle-to-pedestrian crashes," in *Annals of Advances in Automotive Medicine/Annual Scientific Conference*, 2008, p. 199.

[17] J. Elliott, C. Simms, and D. P. Wood, "Pedestrian head translation, rotation and impact velocity: The influence of vehicle speed, pedestrian speed and pedestrian gait," *Accident Analysis & Prevention*, vol. 45, pp. 342-353, 2012.
[18] R. Paas, C. Masson, and J. Davidsson, "Head boundary conditions in pedestrian crashes with passenger cars: six-degrees-of-freedom post-mortem human subject responses," *International journal of crashworthiness*, vol. 20, pp. 547-559, 2015.
[19] G. Schroeder, "Injury mechanism of pedestrians during a front-end collision with a late model car," in *JSAE Spring Convention, 2000*, 2000.
[20] C. Klug, F. Feist, M. Raffler, W. Sinz, P. Petit, J. Ellway, *et al.*, "Development of a Procedure to Compare Kinematics of Human Body Models for Pedestrian Simulations," in *IRCOBI Conference Proceedings*, 2017.
[21] J. R. Kerrigan, J. R. Crandall, and B. Deng, "Pedestrian kinematic response to mid-sized vehicle impact," *International journal of vehicle safety*, vol. 2, pp. 221-240, 2007.
[22] E. Rosén and U. Sander, "Pedestrian fatality risk as a function of car impact speed," *Accident Analysis & Prevention*, vol. 41, pp. 536-542, 2009.
[23] NHTSA, "Traffic Safety Facts," 2015.
[24] J. R. Crandall, K. S. Bhalla, and N. Madeley, "Designing road vehicles for pedestrian protection," *BMJ: British Medical Journal*, vol. 324, p. 1145, 2002.
[25] C. D. Untaroiu, W. Pak, Y. Meng, J. Schap, B. Koya, and S. Gayzik, "A Finite Element Model of a Midsize Male for Simulating Pedestrian Accidents," *Journal of biomechanical engineering*, vol. 140, p. 011003, 2018.
[26] B. Y. Henary, J. Crandall, K. Bhalla, C. N. Mock, and B. S. Roudsari, "Child and adult pedestrian impact: the influence of vehicle type on injury severity," in *Annual Proceedings/Association for the Advancement of Automotive Medicine*, 2003, p. 105.
[27] D. E. Lefler and H. C. Gabler, "The emerging threat of light truck impacts with pedestrians," Rowan University, 2001.
[28] Y. Meng, W. Pak, B. Guleyupoglu, B. Koya, F. S. Gayzik, and C. D. Untaroiu, "A finite element model of a six-year-old child for simulating pedestrian accidents," *Accident Analysis & Prevention*, vol. 98, pp. 206-213, 2017.

Chapter 2

Finite Element Model of a High-Stature Male Pedestrian for Simulating Car-to-Pedestrian Collisions

Wansoo Pak, Yunzhu Meng, Jeremy Schap, Bharath Koya, Scott F. Gayzik, Costin D. Untaroiu

Manuscript published in *International Journal of Automotive Technology* on June 1, 2019 [1]. The published article can be found at: https://link.springer.com/article/10.1007/s12239-019-0042-7 (Acquired permission to publish on the dissertation)

ABSTRACT

Among road traffic deaths, pedestrian accounted for 22% of all fatalities in the world, 26% in Europe, and 22% in the U.S. To investigate the injury risk of the high-stature population, a Finite Element (FE) model corresponding to a male 95th percentile (M95) pedestrian was developed and validated in this study. The model mesh was obtained by morphing the Global Human Body Models Consortium male 50th percentile pedestrian model to the reconstructed geometry of a recruited high-stature human subject. The lower extremity, shoulder, and upper body of the FE model were validated against the Post Mortem Human Surrogate (PMHS) test data recorded in valgus bending, lateral, and anterior-lateral blunt impact tests. Then, a vehicle-pedestrian impact simulation was performed using the whole-body model. In the component validations, the M95 pedestrian model showed higher stiffness than the PMHS test corridors developed for 50th percentile male. The kinematic trajectories predicted by the FE model were well correlated to the corresponding PMHS test data in whole-body validation. Therefore, the model could be used to investigate various pedestrian accidents and/or to improve safety regulations and vehicle front-end design for high-stature pedestrian protection.

2.1 INTRODUCTION

Among the road traffic deaths, pedestrian fatalities represented 22% (World), 26% (Europe), and 22% (U.S.) of total traffic fatalities [2]. In the United States, approximately 5,000 pedestrians are killed and 70,000 are injured in road crashes annually [3]. Historically, the major challenge of automotive safety research was to better improve the design of both vehicles and restraint systems to mitigate injuries for vehicle occupants. Recently, the pedestrian protection during CPC has generated increased attention with testing protocols that involve three subsystem tests for adult pedestrian protection (leg, thigh, and head impact tests) and a head impact test for the child

pedestrian [4]. These subsystem impact tests can reduce the stiffness of vehicle front-end components to mitigate impact force and consequently reduce the risk of injuries. However, neither the complicated vehicle-pedestrian interaction nor the injury mechanisms can be characterized from these subsystem impact tests.

To describe the whole-body response during vehicle-pedestrian interactions, several pedestrian FE models representing 50th percentile male have been developed and validated previously [5-8]. Nevertheless, the model anthropometry plays a major role in pedestrian kinematics and injury mechanisms during a CPC [9-11]. For example, the head contact velocity to the car hood is influenced by pedestrian height in vehicle-pedestrian crash simulation [12]. In addition, the results of CPC PMHS tests showed that the specimen anthropometry could influence the pedestrian kinematics and lower extremity injuries [13]. Therefore, pedestrian FE models with various anthropometries need to be developed to cover various human population.

The primary goal of this study was to develop and validate a human FE model corresponding to a 95th percentile male anthropometry in walking posture.

2.2 METHODS

2.2.1 Development of the finite element model of a 95th percentile pedestrian male

The male 95th percentile pedestrian simplified (M95-PS) model was developed based on anthropometry of a recruited male subject (186.7 cm and 102.1 kg). Fifteen anthropometric measurements describing the subject demonstrated a close match to the anthropometry of a 95th percentile male based on previous research [14, 15]. A multi-modality protocol was used to acquire data in a standing posture (Figure 2.1, a) [16]. External anthropometry was collected via a 3D scanner (Faro, Platinum Model arm, 8ft. (2.4 m), Lake Mary, FL) (Figure 2.1, b). The subject was instructed to walk towards a line on the floor and to stop with both feet parallel to assume a natural posture. The feet of the subject were traced on poster board and an apparatus was used to put light contact on the back during surface scanning to reduce the effect of swaying (Figure 2.1, b). A photo target was used to keep the head in the Frankfurt plane. The external anthropometry data and surface scans were integrated together for the generation of a NURBS patchwork of the large male outer surface in this neutral standing posture. Surface data was symmetrized using methods described in a previous study [17].

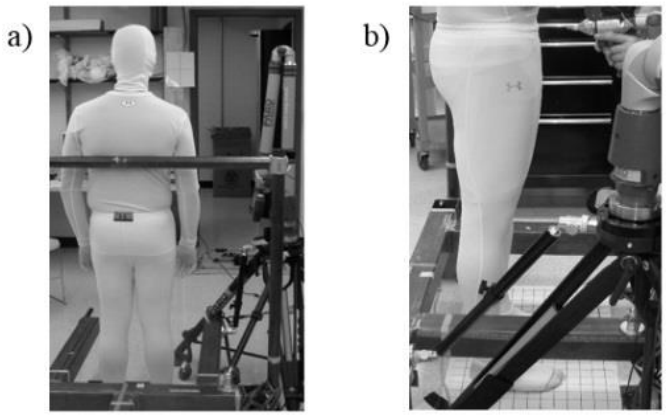

Figure 2.1 The subject was scanned in the standing posture using a 3D laser scanner in a neutral standing posture. The upper body was scanned first followed by the lower body.

The mesh of M95-PS model was obtained by morphing a previously developed male 50th percentile pedestrian simplified (M50-PS) model [18]. The average male FE model (also in the neutral standing posture) was morphed to target geometry by using the outer surface and landmark data acquired from the high-stature male subject using a radial basis interpolation approach [15]. Due to the morphing procedure, all modeling aspects including the number of nodes, element, material types, and contact definitions are carried forward from the M50-PS model. The only difference is the location of the nodes. The defined material properties of the M95-PS model thus are based on the GHBMC occupant model [19].

It should be mentioned that M95-PS model was developed as a simplified version in order to evaluate the kinematics and kinetics of pedestrians relatively quickly during a CPC scenario. Hence, the model did not include internal viscera of the body, but rather was filled with substitute component. In addition, the brain was replaced with a single mass node at the location of brain center of gravity and constrained to the skull. The model was designed to match the standard requirements of the Euro NCAP test protocol [4], which calls for a heel to heel distance for the 95th percentile male of 337 ± 10 mm and H-point height of 1040 mm ± 5%. The model meets the H-point target due to the recruitment of a specific large male subject based on anthropometry, however, the heel to heel distance was achieved by repositioning the model using meshing software (Hyperworks, Altair Engineering, Troy, MI) and local re-meshing. The upper extremities were also adjusted using the same approach, to match the pre-test posture [20] (Figure 2.2).

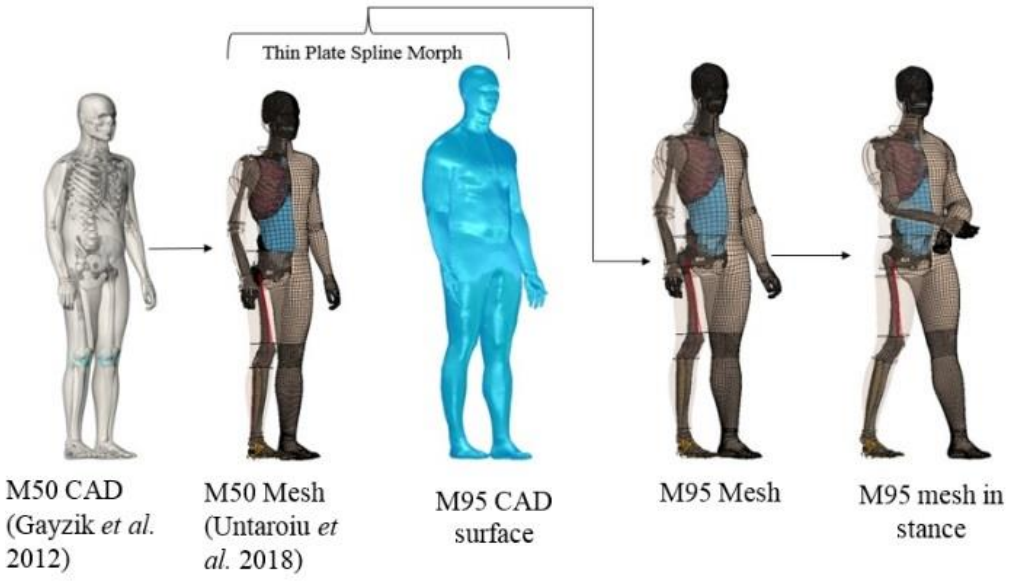

Figure 2.2 The schematic FE model mesh development procedure.

2.2.2 Validation of the knee joint under valgus bending

Combined valgus bending and shear loading of the knee joint have been recognized as primary injury mechanisms during a pedestrian accident [21]. To validate the injury biomechanics of the knee joint under lateral loading, a four-point knee bending test reported in the literature was simulated [21]. The tested knee joints were acquired from 24 adult PMHS (68.3 ± 9.8 ages, 172 ± 7.8 cm height, and 75.2 ± 14.4 kg weight). The knee joint FE model was extracted from the M95-PS model in standing posture (straight knee) and then re-positioned manually to fit into the simulation setup (Figure 2.3). The ends of the three bones (femur, fibula, and tibia) were positioned approximately in the center of cups and then they were rigidly constrained to the bone cups in a depth of 76 mm (the interior length of the cup). Each part of the apparatus was defined as rigid, except the load cell part attached to the bone cup, which was deformable in order to calculate the time histories of bending moment. The bone cups were attached to extension beams that were linked to the rotational joint supports. The initial anterior-posterior knee axis was approximately parallel with the axis defined by the support centers. The support on the femur side was allowed to slide horizontally, while the other support was fixed. To load the knee joint under valgus bending, the extension beams were rotated at a knee angular rate of approximately 1 deg/ms in correspondence with a 40 km/h CPC impact [22].

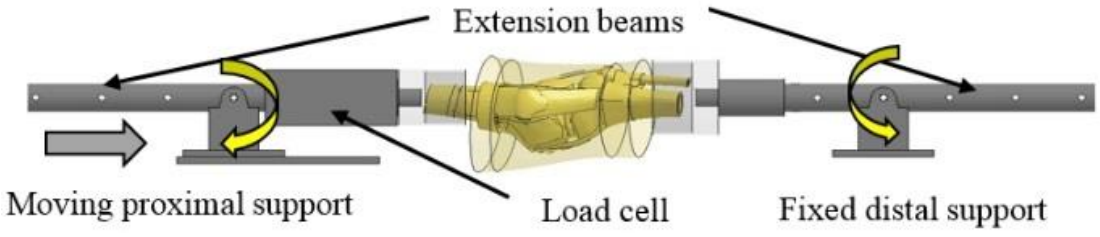

Figure 2.3 The FE simulation setup of four-point knee joint bending.

2.2.3 Validation of the thoraco-abdominal region and pelvis under lateral impact loading

The upper body region of the whole-body FE model was validated against test data recorded on 14 PMHS specimens (53.8 ± 13.9 age, 67.2 ± 16.2 kg weight) subjected to blunt lateral/anterior-lateral impact loading [23]. During the PMHS test, the specimen was suspended upright with arms overhead, then released prior the impact. Based on the test scenario, eight FE simulations performed using the pedestrian FE model under various combinations of impacted regions (pelvis, abdomen, and thorax) and impactor velocities. To avoid interference between arm and impactor during its validation, the arm parts were removed but concentrated masses corresponding to each arm were applied near the scapular region to maintain the correct pedestrian total mass (Figure 2.4). The pelvis was loaded laterally with the impactor aligned adjacent to the greater trochanter (Figure 2.4, a). The center of the impactor was aligned to the xiphoid process for the thorax impact and 7.5 cm down from the xiphoid process for the abdomen impact. Then, the impactor was rotated 60° from the anterior-posterior direction of the model before it impacted the model (Figure 2.4, b, c). During the simulation, the time histories of the impact force were recorded to compare to corresponding PMHS test data.

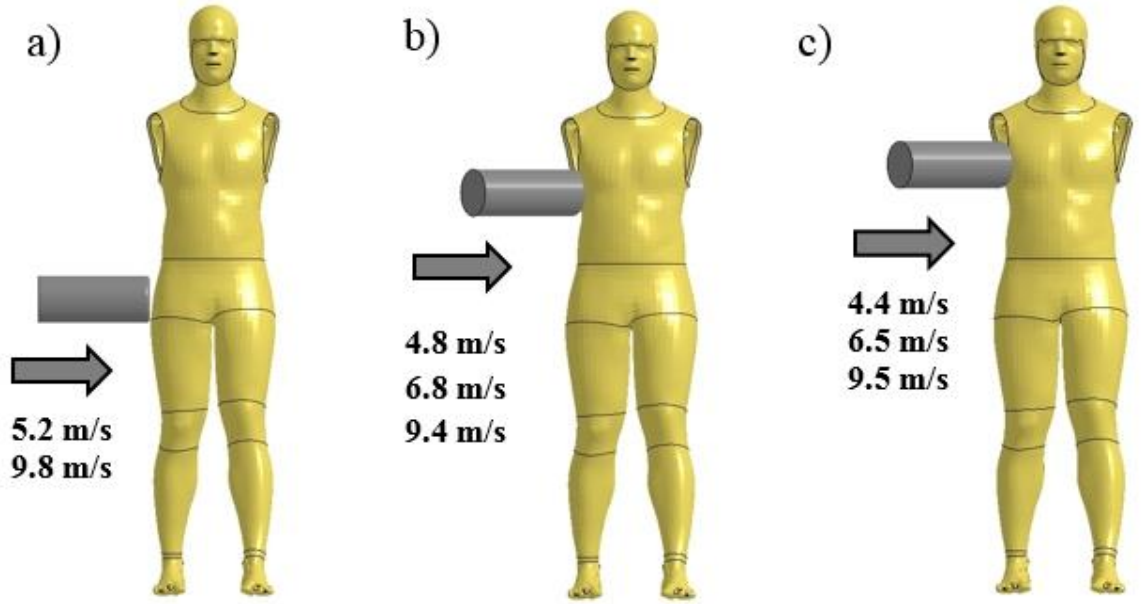

Figure 2.4 The upper body FE simulation setup for the M95-PS model: a) Pelvis, b) Abdomen, c) Thorax.

2.2.4 Validation of the shoulder under lateral impact

The shoulder and arm were reported as the most frequent injured upper extremity parts [24] during pedestrian accidents. In order to validate the upper extremity, a lateral impact simulation at the shoulder region was performed based on PMHS test data [25]. A rigid impactor with a mass of 23 kg and 150 mm diameter was aligned to the acromion of the right shoulder joint (Figure 2.5, a). Two FE impact simulations were performed on the M95-PS model at initial impactor velocities of 4.5 m/s and 6.8 m/s.

2.2.5 Validation of the whole-body

The male 95th percentile (M95) whole-body FE model was validated in a CPC simulation based on PMHS test data [20]. The pedestrian model was positioned laterally at the centerline of a FE model of the mid-sized sedan used in testing to represent the most frequent accident scenario [26] (Figure 2.5, b). The posture of the FE model was set to mid-stance with the legs apart walking towards the vehicle centerline and the rearward leg being impacted first by the vehicle. This configuration is based on the pedestrian testing protocol of European new car assessment programme [4]. In testing, the PMHS was supported by a harness and released approximately 20-30 ms before the vehicle contact. In FE simulation, prior to the impact at approximately 5 ms, the gravity acceleration was assigned to the pedestrian model and a force corresponding to its body weight was applied upward by the ground model to initiate the foot-ground contact. Then, the pedestrian model was impacted by the vehicle FE model, which was validated by its manufacturer against pedestrian subsystem test data [27]. Markers were attached to the PMHS head, first thoracic vertebra (T1), and sacrum and their kinematics were recorded relative to the car during testing [20]. Nodes corresponding to these markers were defined in the pedestrian FE model at the head's Center of Gravity (CG), and about 60mm behind of the T1 and sacrum due to the consideration of the screw length (Figure 2.4) [18]. In addition, a TDAS bag was attached to the PMHS during testing. While the bag dimensions and the attachment to the PMHS was not documented [20], the TDAS mass (about 4.3 kg) was added as four concentrated mass nodes rigidly to the lumbar spine (L1-L4). Static/dynamic friction coefficients were defined as the average values reported in literature [28]: 0.26/0.25 (fabric-to-steel) for vehicle-to-pedestrian contact and 0.61/0.45 (fabric-to-fabric) for pedestrian-to-pedestrian contact.

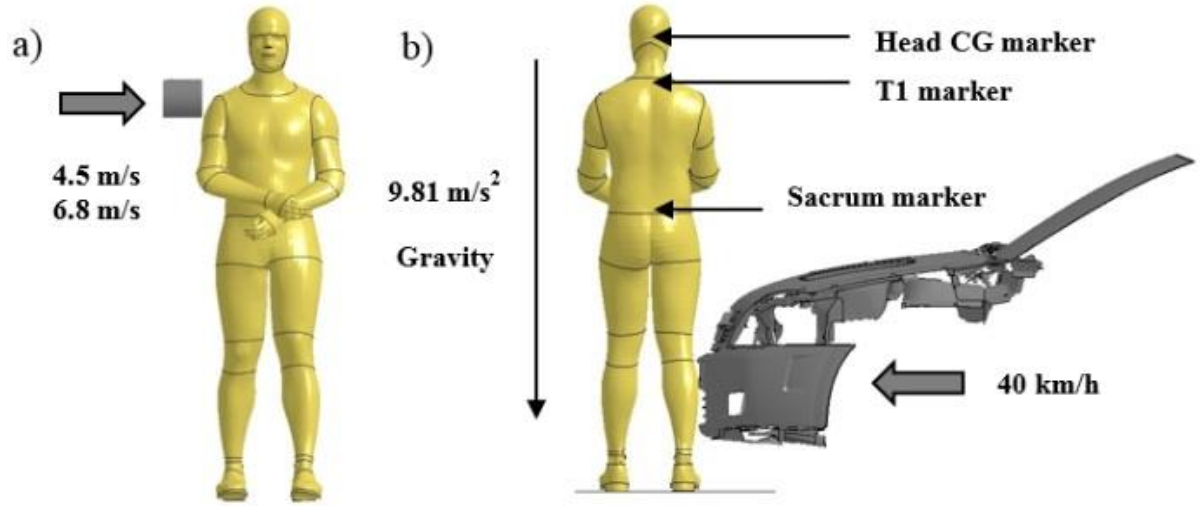

Figure 2.5 a) The shoulder lateral impact FE simulation setup, b) FE simulation setup for the CPC validation.

2.3 RESULTS

Each of validation responses predicted by the M95-PS model were compared to the corresponding PMHS test corridors. The results of validation simulation results at the component level were filtered (SAE 180) to reduce the numerical noise.

2.3.1 Validation of the pedestrian model at component level

Overall, the resulting curves of angular bending knee stiffness for the M95-PS model have a relatively similar trend as the curves corresponding to PMHS tests (Figure 2.6). It should be mentioned that the PMHS test curves were scaled to represent a 50th percentile adult male anthropometry [21]. Initially, the load cell bending moment predicted by the FE model was lower than in testing, probably caused by possible differences in the setup inertia (simulation vs. testing), which was approximated in the FE simulation. Then, the model predicted higher stiffness than the scaled test curves possibly due to its higher weight. In terms of injury prediction, the M95-PS model predicted ruptures of MCL and ACL ligaments in a range from 14° to 17.5° knee angles. This soft tissue injury is the second most frequent injuries observed in all PMHS tests (52.5% MCL rupture only and 10 % ACL & MCL ruptures) [21].

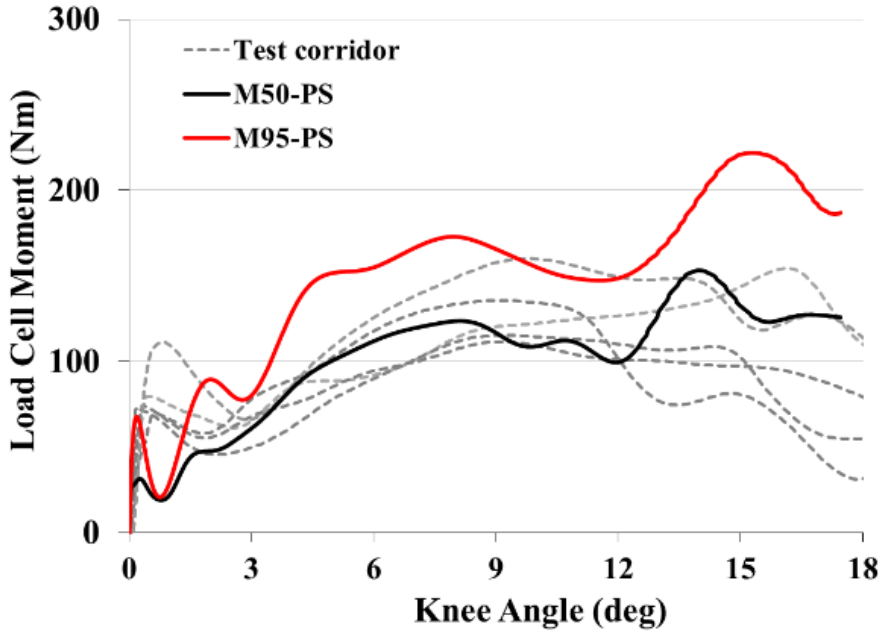

Figure 2.6 The response of knee joint under bending loading: PMHS test data vs. FE simulations

The impact force time histories predicted by the M95-PS model under pelvic lateral loading were close to the mean corridor at lower impact velocity (5.2 m/s) (Figure 2.7, a), and close to the upper boundary corridor at higher impact velocity (9.8 m/s) (Figure 2.7, b). It should be mentioned that the individual test corridors were normalized to represent a 50th percentile adult male [23].

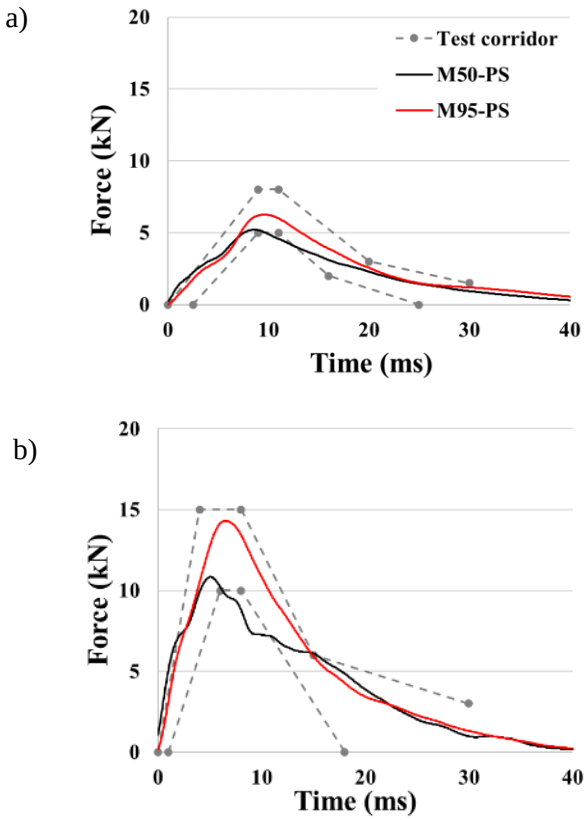

Figure 2.7 The time histories of impact force at pelvis: FE models vs. PMHS test corridors. a) 5.2 m/s, b) 9.8 m/s initial impactor velocity

The time histories of impact force predicted by the upper body region of the M95-PS model was compared against the PMHS test data [23] recorded at thorax (Figure 2.8) and abdomen (Figure 2.9) locations. Due to its higher inertia, the M95-PS model predicted stiffer response than that of M50-PS model. At the beginning of loading (approximately 0 to 5 ms), the impact force predicted by the M95-PS model was close to the upper corridor of the PMHS test data. However, after first peak force, a larger decrease of the impact force predicted by the M95-PS model compared to the normalized PMHS corridor was observed in both thorax (Figure 2.8) and abdomen simulations (Figure 2.9).

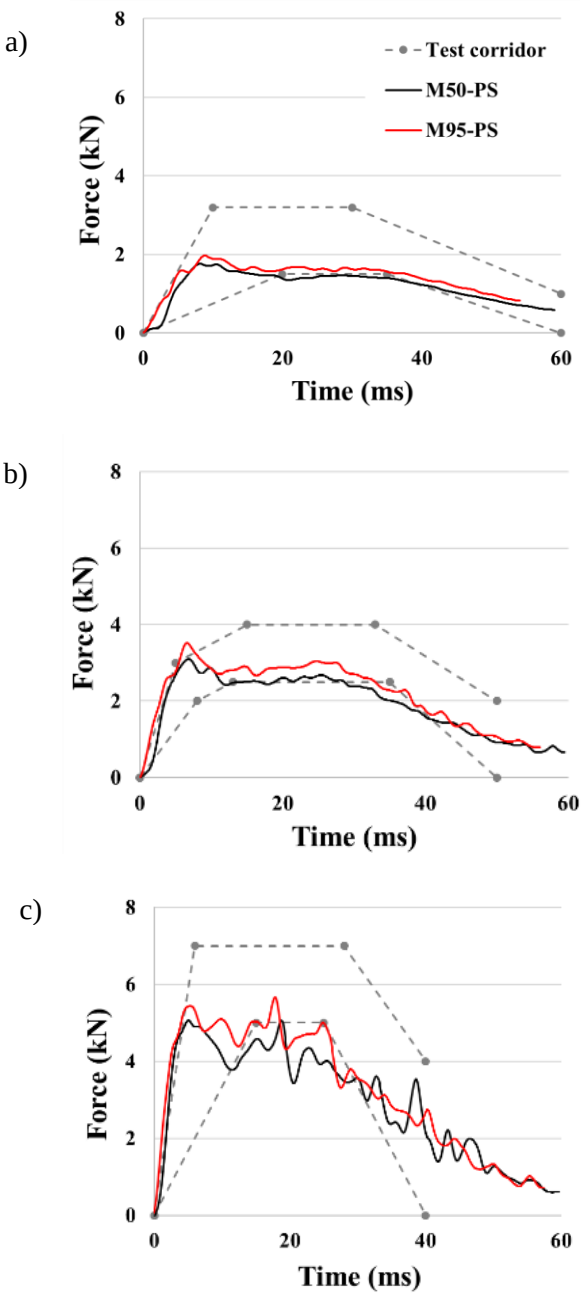

Figure 2.8 The time histories of impact force at thorax: FE models vs. PMHS test corridors. a) 4.4 m/s, b) 6.5 m/s, c) 9.5 m/s initial impactor velocity

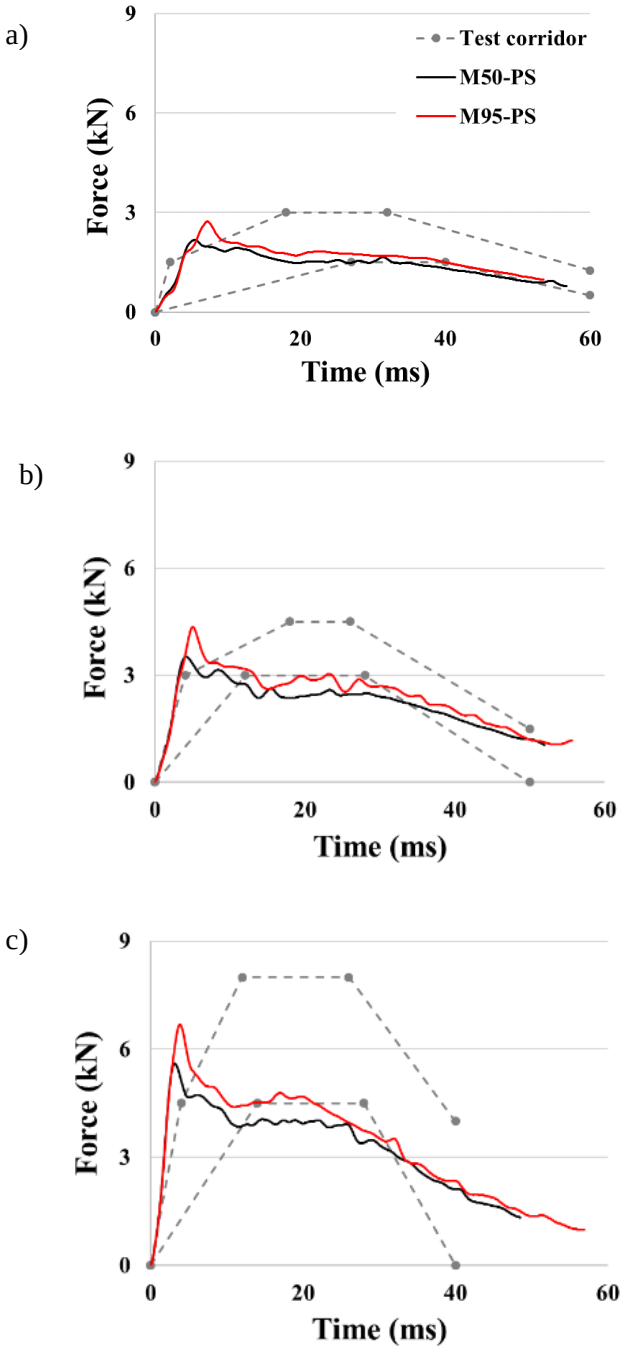

Figure 2.9 The time histories of impact force at abdomen: FE models vs. PMHS test corridors. a) 4.8 m/s, b) 6.8 m/s, c) 9.4 m/s initial impactor velocity

A six line corridor [25] was developed based on shoulder impact data obtained from literature [29-32] (average 73.3 ± 14.0 age, 62.2 ± 16.4 kg weight, and 370.6 ± 36.9 mm shoulder breath). Up to the peak force, M95-PS's force predictions were close to the upper boundaries of the test corridor (Figure 2.10) and higher than the corresponding response predicted by the M50-PS model [18].

The marker trajectories relative to the vehicle were calculated and compared to PMHS test data. The upper body trajectories predicted by the M95-PS model are close to the trajectories recorded on tall PMHS test data (Figure 2.11). The kinematic response between the FE model and PMHS test during vehicle-pedestrian interaction was also illustrated (Figure 2.12). The M95-PS model (189.5 cm and 102.5 kg) predicted similar response to a tall PMHS (184.3 cm and 91.6 kg). A higher WAD was observed in the FE model (2,335 mm) than in taller PMHS test (2200 and 2230 mm) due to the higher stature of the M95-PS model.

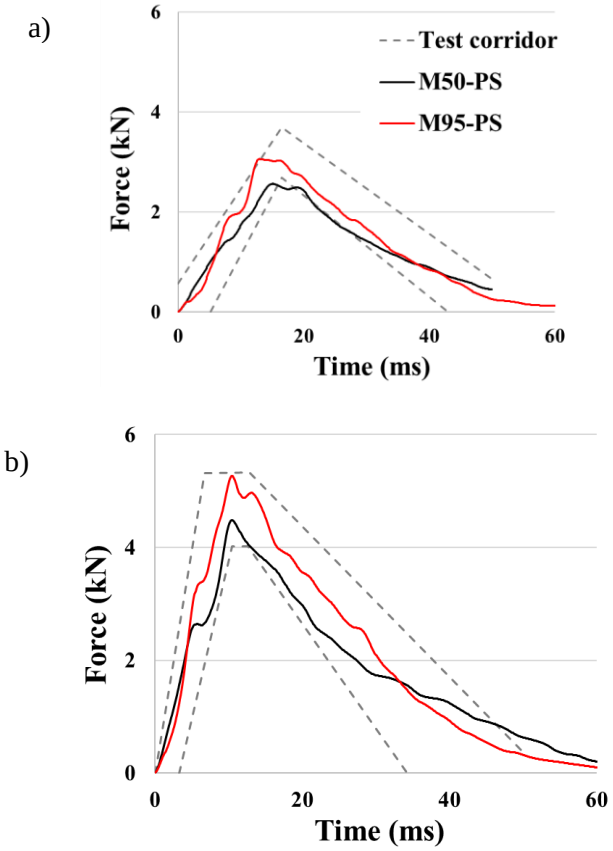

Figure 2.10 The time histories of impact force in lateral shoulder impact: FE models vs. PMHS test corridors. a) 4.5 m/s, b) 6.8 m/s initial impactor velocity

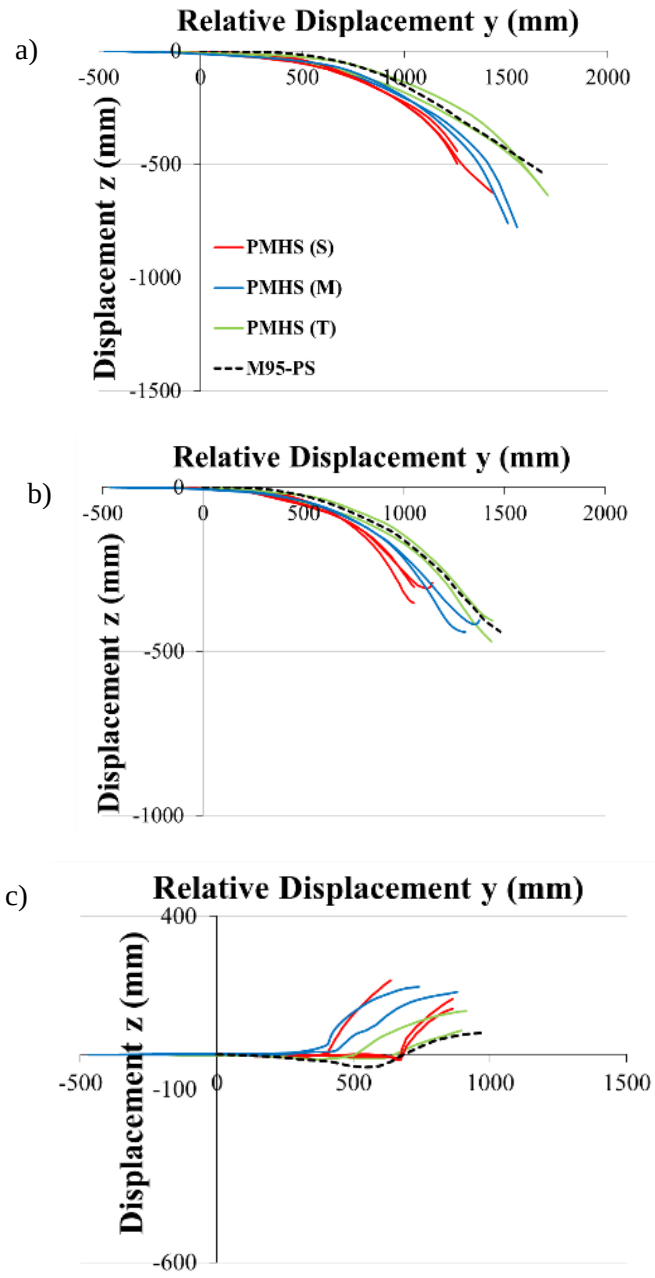

Figure 2.11.\ Kinematic trajectories of the M95-PS model relative to the vehicle: FE models vs. PMHS tests. a) Head CG, b) T1, c) sacrum, S: short, M: mid-sized, T: tall specimen

In terms of injuries, the FE model predicted knee ligament injuries in both right (ACL/MCL) and left (ACL/LCL) lower extremities. In testing, the most common injury pattern in PMHS right lower extremity (five of eight) was bone fractures (mostly tibia fractures) and knee ligament damages recorded in one PMHS [18]. In the left lower extremity, the typical injury pattern in PMHS tests was LCL/ACL rupture (5 tests) similar to the injuries predicted by the M95-PS model.

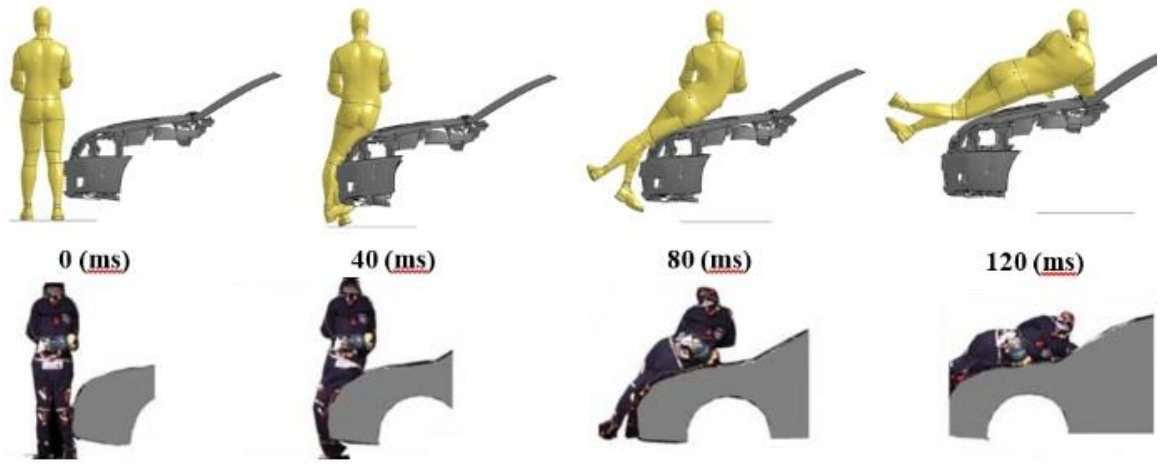

Figure 2.12 Comparison of the kinematic responses: M95-PS model (top) vs. PMHS (bottom)

2.4 DISCUSSION

This study presents the development and validation of a simplified full body human FE model corresponding to a 95th percentile male in mid-stance posture. This is the first human FE model that is based on geometric data acquired from a subject with anthropometric characteristics close to those of 95th percentile male. Previous pedestrian 95th percentile human FE models [11] or ATD [9, 13] were obtained by a simple scaling process. In addition, this pedestrian FE model will be publicly available for academic researchers while the previous models are mostly proprietary. The mesh of the model was obtained by a morphing approach that reduced considerably the development effort. The model characteristics including material properties and contact definitions were duplicated from the M50-PS model [18]. Overall, the M95-PS model has approximately 539,000 nodes and 839,000 elements.

The M95-PS model was validated at component level, similar to the M50-PS model, against impact loadings similar to those observed in CPC scenarios. It should be mentioned that the majority of test data presented in literature were obtained on subjects with anthropometry close to that of a 50th percentile male subject. While various scaling procedures were proposed in literature [33], their validations are difficult to be performed mostly due to the variations in human properties and various test setups used in component tests. Therefore, it was decided to compare the model responses to existing 50th percentile male test corridors, which could be considered an inherent limitation of this study. In the future, the model could be further validated when test data corresponding to 95th percentile male subjects becomes available.

The M95-PS model showed, as expected, a higher stiffness than the M50-PS model and PMHS scaled test data during the knee validation under valgus bending. In addition, in terms of injury prediction, the M95-PS model predicted the second most frequent ligament injuries observed in PMHS tests. Since scaling the test data to 95th percentile is challenging, additional tests of tall specimens are recommended in the same test configurations or in an improved test configuration that will allow an accurate calculation of the knee stiffness at its center location. In a CPC event,

the knee could be subjected to complex conditions, which may include shearing load in addition to bending depending on the position of the vehicle bumper relative to the knee. Therefore, more model improvements and validations could increase the users' confidence in its biofidelity. Improvement of the knee model may include adding the structures neglected in the current model (e.g. surrounding muscles and tendons), improving the geometry of knee capsule (which was approximated, not reconstructed from medical images), and/or modeling the synovial fluid. Updating material properties of the knee ligaments with an anisotropic material model [34] and validation of each ligament against test data may also improve the biofidelity of the knee.

The upper body validation responses under blunt lateral/anterior-lateral loadings at the regions of shoulder, pelvis, thorax, and abdomen was within the PMHS test corridor, but mostly close to the upper boundaries. Since the pelvic flesh plays a significant role in lateral impact pelvic test, it is believed that a more biofidelic material model of flesh may improve the response of the model in this loading condition. Therefore, it is recommended to update the flesh material model when compression test data on pelvic flesh specimens becomes available. For the anterior-lateral impact test on the thorax and abdomen, the M95-PS model predicted close to the lower boundaries of PMHS test responses after peak impact force. While the internal organs were not modeled and included in the current version of FE model, the rib cage is the main contributor to its stiffness. Therefore, it is believed that modeling internal organs [35-37] and including them into the rib cage cavity will improve the damping properties of the upper body and consequently the overall correlation of the model with the PMHS test data.

In conclusion, as expected, the responses of M95-PS model components were usually close to upper boundaries of test corridors and showed higher stiffness than the corresponding responses of M50-PS model components. These results and the model stability during these simulations generate confidence in the model. In addition, a simple and reliable scaling relationship from M95-PS to M50-PS was not determined, which may suggest that the material properties and test setup may play a role in addition to anthropometry.

Overall, the kinematic trajectories predicted by the M95 pedestrian FE model were close to the corresponding trajectories recorded on tall PMHS subjects. The M95-PS model predicted longer contact time between the head and the vehicle and larger WAD. This could be caused by a higher stature of the FE model compared to the tallest PMHS (189.5 cm of FE model vs. 179 and 184.3 cm of PMHSs). In terms of injury, similar patterns of ligament ruptures were observed, but no bone fractures were predicted in long bones. This could be caused by the current elastic-plastic material model with plastic strain failure criteria assigned to cortical bone, which should be improved as it was suggested previously [38, 39] or due to the anthropometric differences between the M95-PS model and tested PMHS. In vehicle-pedestrian interaction, the front end vehicle geometry including front bumper shape plays a significant role [12, 13]. Hence, more CPC validation using tall subjects, various gait postures [40, 41], and various types of vehicles (e.g. sport utility vehicle, truck, and compact sized car) is suggested to be performed when test data will be available. Furthermore, to better understand the overall contributions of pedestrian anthropometry, vehicle geometry, and lower limb material/failure properties, sensitivity studies [42-44] should be performed in the future. In addition to male models (M50-PS, M95-PS), pediatric and female FE models should be developed and used in automotive safety studies to

cover the broader human anthropometry [45, 46] and other safety fields as well (e.g. sport, aerospace, military, etc.) [47-49].

2.5 CONCLUSION

This study presents the development and validation of a simplified full body human FE model corresponding to a 95th percentile male in mid-stance posture. Overall, the model showed good results and promising capability to predict the injury risk of pedestrians in lateral car impact. Therefore, the model could be used by automotive safety engineers to improve the design of vehicle front-end parts for better protection of the tall pedestrian population.

ACKNOWLEDGEMENT

Funding for this study was provided by the Global Human Body Models Consortium (GHBMC). All findings and views reported in this manuscript are based on the opinions of the authors and do not necessarily represent the consensus or views of the funding organization.

REFERENCE

[1] W. Pak, Y. Meng, J. Schap, B. Koya, S. F. Gayzik, and C. D. Untaroiu, "Finite Element Model of a High-Stature Male Pedestrian for Simulating Car-to-Pedestrian Collisions," *International Journal of Automotive Technology*, vol. 20, pp. 445-453, 2019.

[2] WHO, "Road traffic injuries," 2016.

[3] NHTSA, "Traffic Safety Facts 2016," 2018.

[4] EuroNCAP, "Pedestrian Testing Protocol Version 9.0.2," 2018.

[5] Y. Takahashi, Y. Kikuchi, A. Konosu, and H. Ishikawa, "Development and validation of the finite element model for the human lower limb of pedestrians," *Stapp car crash journal*, vol. 44, pp. 335-55, 2000.

[6] C. D. Untaroiu, J. B. Putnam, J. Schap, M. L. Davis, and F. S. Gayzik, "Development and preliminary validation of a 50th percentile pedestrian finite element model," in *ASME 2015 IDETC/CIE Conference*, Boston, MA, USA, 2015, p. 7.

[7] P. J. Arnoux, D. Cesari, M. Behr, L. Thollon, and C. Brunet, "Pedestrian lower limb injury criteria evaluation: a finite element approach," *Traffic Inj Prev*, vol. 6, pp. 288-97, Sep 2005.

[8] M. Iwamoto, K. Omori, H. Kimpara, Y. Nakahira, A. Tamura, I. Watanabe, *et al.*, "Recent Advances in THUMS: Development of Individual Internal Organs, Brain, Small Female, and Pedestrian Model," in *4th European LS-DYNA Conference*, Ulm (Germany), 2003.

[9] R. Fredriksson, J. Shin, and C. D. Untaroiu, "Potential of pedestrian protection systems--a parameter study using finite element models of pedestrian dummy and generic passenger vehicles," *Traffic injury prevention*, vol. 12, pp. 398-411, 2011.

[10] C. D. Untaroiu, J. Shin, J. R. Crandall, R. Fredriksson, O. Bostrom, Y. Takahashi, *et al.*, "Development and validation of pedestrian sedan bucks using finite-element simulations:

a numerical investigation of the influence of vehicle automatic braking on the kinematics of the pedestrian involved in vehicle collisions," *International Journal of Crashworthiness,* vol. 15, pp. 491-503, 2010.

[11] R. Watanabe, T. Katsuhara, H. Miyazaki, Y. Kitagawa, and T. Yasuki, "Research of the relationship of pedestrian injury to collision speed, car-type, impact location and pedestrian sizes using human FE model (THUMS Version 4)," *Stapp car crash journal,* vol. 56, pp. 269-321, 2012.

[12] Y. Okamoto, T. Sugimoto, K. Enomoto, and J. Kikuchi, "Pedestrian head impact conditions depending on the vehicle front shape and its construction--full model simulation," *Traffic injury prevention,* vol. 4, pp. 74-82, 2003.

[13] C. Untaroiu, J. Shin, J. Ivarsson, J. Crandall, Y. Takahashi, A. Akiyama, *et al.*, "Pedestrian kinematics investigation with finite element dummy model based on anthropometry scaling method," in *Proc. 20th Int. Technical Conf. Enhanced Safety of Vehicle*, 2007.

[14] C. C. Gordon, T. Churchill, C. E. Clauser, B. Bradtmiller, and J. T. McConville, "Anthropometric survey of US army personnel: methods and summary statistics 1988," DTIC Document1989.

[15] N. A. Vavalle, S. L. Schoell, A. A. Weaver, J. D. Stitzel, and F. S. Gayzik, "Application of radial basis function methods in the development of a 95th percentile male seated fea model," *Stapp car crash journal,* vol. 58, p. 361, 2014.

[16] F. Gayzik, D. Moreno, C. Geer, S. Wuertzer, R. Martin, and J. Stitzel, "Development of a full body CAD dataset for computational modeling: a multi-modality approach," *Annals of biomedical engineering,* vol. 39, p. 2568, 2011.

[17] F. Gayzik, D. Moreno, K. Danelson, C. McNally, K. Klinich, and J. D. Stitzel, "External landmark, body surface, and volume data of a mid-sized male in seated and standing postures," *Annals of biomedical engineering,* vol. 40, pp. 2019-2032, 2012.

[18] C. D. Untaroiu, W. Pak, Y. Meng, J. Schap, B. Koya, and S. Gayzik, "A Finite Element Model of a Midsize Male for Simulating Pedestrian Accidents," *Journal of biomechanical engineering,* vol. 140, p. 011003, 2018.

[19] D. Schwartz, B. Guleyupoglu, B. Koya, J. D. Stitzel, and F. S. Gayzik, "Development of a computationally efficient full human body finite element model," *Traffic injury prevention,* vol. 16, pp. S49-S56, 2015.

[20] J. R. Kerrigan, J. R. Crandall, and B. Deng, "Pedestrian kinematic response to mid-sized vehicle impact," *International journal of vehicle safety,* vol. 2, pp. 221-240, 2007.

[21] D. Bose, K. S. Bhalla, C. D. Untaroiu, B. J. Ivarsson, J. R. Crandall, and S. Hurwitz, "Injury tolerance and moment response of the knee joint to combined valgus bending and shear loading," *J Biomech Eng,* vol. 130, p. 031008, Jun 2008.

[22] C. Untaroiu, K. Darvish, J. Crandall, B. Deng, and W. Jenne-Tai, "A finite element model of the lower limb for simulating pedestrian impacts," *Stapp car crash journal,* vol. 49, p. 157, 2005.

[23] D. C. Viano, "Biomechanical responses and injuries in blunt lateral impact," SAE Technical Paper 0148-7191, 1989.

[24] J.-L. Martin, A. Lardy, and B. Laumon, "Pedestrian injury patterns according to car and casualty characteristics in France," in *55th AAAM Annual Conference Annals of Advances in Automotive Medicine*, 2011.

[25] S.-W. Koh, J. M. Cavanaugh, M. J. Mason, and S. A. Petersen, "Shoulder injury and response due to lateral glenohumeral joint impact: an analysis of combined data," *Stapp car crash journal,* vol. 49, p. 291, 2005.
[26] R. Fredriksson, E. Rosén, and A. Kullgren, "Priorities of pedestrian protection—a real-life study of severe injuries and car sources," *Accident analysis & prevention,* vol. 42, pp. 1672-1681, 2010.
[27] J. R. Kerrigan, D. P. Parent, C. Untaroiu, J. R. Crandall, and B. Deng, "A new approach to multibody model development: pedestrian lower extremity," *Traffic Inj Prev,* vol. 10, pp. 386-97, Aug 2009.
[28] V. Kothari and M. Gangal, "Assessment of frictional properties of some woven fabrics," 1994.
[29] J. H. Bolte IV, M. H. Hines, R. G. Herriott, J. D. McFadden, and B. R. Donnelly, "Shoulder impact response and injury due to lateral and oblique loading," *Stapp car crash journal,* vol. 47, p. 35, 2003.
[30] J. H. Bolte, M. H. Hines, J. D. McFadden, and R. A. Saul, "Shoulder response characteristics and injury due to lateral glenohumeral joint impacts," *Stapp car crash journal,* vol. 44, pp. 261-280, 2000.
[31] S. Compigne, Y. Caire, T. Quesnel, and J.-P. Verries, "Non-injurious and injurious impact response of the human shoulder three-dimensional analysis of kinematics and determination of injury threshold," *Stapp car crash journal,* vol. 48, pp. 89-123, 2004.
[32] D. R. Marth, "Biomechanics of the shoulder in lateral impact," MS Thesis, Wayne State University, 2002.
[33] A. Petitjean, X. Trosseille, N. Yoganandan, and P. F. A., "Normalization and scaling for human response corridors and development of injury risk curves," in *Accidental Injury*, ed: Springer, 2015, pp. 769-792.
[34] J. A. Weiss and J. C. Gardiner, "Computational Modeling of Ligament Mechanics," *Critical Reviews in Biomedical Engineering,* vol. 29, pp. 1-70, 2001.
[35] Y. C. Lu and C. D. Untaroiu, "A statistical geometrical description of the human liver for probabilistic occupant models," *Journal of Biomechanics,* vol. 47, pp. 3681-3688, Nov 28 2014.
[36] K. M. Yates, Y. C. Lu, and C. D. Untaroiu, "Statistical shape analysis of the human spleen geometry for probabilistic occupant models," *J Biomech,* vol. 49, pp. 1540-1546, Jun 14 2016.
[37] K. M. Yates and C. D. Untaroiu, "Finite element modeling of the human kidney for probabilistic occupant models: Statistical shape analysis and mesh morphing," *J Biomech,* vol. 74, pp. 50-56, Jun 6 2018.
[38] N. Yue and C. D. Untaroiu, "A numerical investigation on the variation in hip injury tolerance with occupant posture during frontal collisions," *Traffic Inj Prev,* vol. 15, pp. 513-22, 2014.
[39] C. D. Untaroiu, N. Yue, and J. Shin, "A finite element model of the lower limb for simulating automotive impacts," *Ann Biomed Eng,* vol. 41, pp. 513-26, Mar 2013.
[40] C. D. Untaroiu, M. U. Meissner, J. R. Crandall, Y. Takahashi, M. Okamoto, and O. Ito, "Crash reconstruction of pedestrian accidents using optimization techniques," *International Journal of Impact Engineering,* vol. 36, pp. 210-219, Feb 2009.

[41] C. D. Untaroiu, J. R. Crandall, Y. Takahashi, M. Okamoto, O. Ito, and R. Fredriksson, "Analysis of running child pedestrians impacted by a vehicle using rigid-body models and optimization techniques," *Safety Science,* vol. 48, pp. 259-267, Feb 2010.

[42] Y. Han, J. K. Yang, K. Mizuno, and Y. Matsui, "Effects of Vehicle Impact Velocity, Vehicle Front-End Shapes on Pedestrian Injury Risk," *Traffic Injury Prevention,* vol. 13, pp. 507-518, 2012.

[43] J. B. Putnam, J. T. Somers, and C. D. Untaroiu, "Development, calibration, and validation of a head-neck complex of THOR mod kit finite element model," *Traffic injury prevention,* vol. 15, pp. 844-54, 2014.

[44] L. M. Saez, L. J. G. Casanova, E. A. Fazio, and A. G. Alvarez, "Behaviour of high bumper vehicles in pedestrian scenarios with full finite element human models," *International Journal of Crashworthiness,* vol. 17, pp. 1-10, Feb 2012.

[45] C. V. Zegeer and M. Bushell, "Pedestrian crash trends and potential countermeasures from around the world," *Accident Analysis & Prevention,* vol. 44, pp. 3-11, 2012.

[46] Y. Meng, W. Pak, B. Guleyupoglu, B. Koya, F. S. Gayzik, and C. D. Untaroiu, "A finite element model of a six-year-old child for simulating pedestrian accidents," *Accident Analysis & Prevention,* vol. 98, pp. 206-213, 2017.

[47] W. A. Baker, M. R. Chowdhury, and C. D. Untaroiu, "Validation of a booted finite element model of the WIAMan ATD lower limb in component and whole-body vertical loading impacts with an assessment of the boot influence model on response," *Traffic Inj Prev,* vol. 19, pp. 549-554, Jul 4 2018.

[48] W. A. Baker, C. D. Untaroiu, D. M. Crawford, and M. R. Chowdhury, "Mechanical characterization and finite element implementation of the soft materials used in a novel anthropometric test device for simulating underbody blast loading," *J Mech Behav Biomed Mater,* vol. 74, pp. 358-364, Oct 2017.

[49] W. A. Baker, M. R. Chowdhury, and C. D. Untaroiu, "A Finite Element Model of an Anthropomorphic Test Device Lower Limb to Assess Risk of Injuries During Vertical Accelerative Loading," *J Biomech,* 2018.

Chapter 3

Development and Validation of a Finite Element Model of a Small Female Pedestrian

Wansoo Pak, Yunzhu Meng, Jeremy Schap, Bharath Koya, Scott F. Gayzik, Costin D. Untaroiu

Manuscript submitted in *Computer Methods in Biomechanics and Biomedical Engineering* on August 6, 2017. (In review)

ABSTRACT

Pedestrians are the most vulnerable road user and represent about 23% of the road traffic deaths in the world. A finite element (FE) model corresponding to a 5th percentile female pedestrian (F05-PS) was developed by morphing the Global Human Body Models Consortium (GHBMC) 50th percentile male pedestrian (M50-PS) model to the reconstructed geometry of a recruited small female subject. The material properties of the pedestrian model were assigned based on GHBMC M50-PS model. In model validation, the knee lateral stiffness and force time histories of F05-PS upper body showed similar trends, but softer responses than the corresponding data recorded in post mortem human surrogate (PMHS) tests and linearly scaled to average male anthropometry. Finally, the pedestrian model was verified in a Car-to-Pedestrian Collison (CPC) simulation. The marker trajectories recorded in simulation were close to the data recorded on small PMHS in testing and the model predicted typical knee ligament ruptures. Therefore, we believe the F05-PS model, the first FE model developed based a female reconstructed geometry, could be used to improve vehicle front-end design for pedestrian protection and/or to investigate various pedestrian accidents.

3.1 INTRODUCTION

According to the World Health Organization (WHO), the total number of fatalities recorded in traffic accidents is about 1.25 million each year worldwide [1]. Among the road traffic fatalities in 2016, pedestrians comprised 23% (World), 27% (Europe), and 22% (Americas). In the United States, about 6,227 pedestrians were killed in 2018 [2], the highest level since 1990. [2] The percentage of injured pedestrians killed (16.9%) [3] is much higher than corresponding numbers for occupants (1%), pedal cyclists (1.8%), and motor cyclist (5.7%), which makes the pedestrian the most vulnerable traffic participant in the US [4].

Historically, the major challenge of crash dummy research was to improve design of both vehicles and restraint systems to reduce injuries for occupants. Recently, protection of pedestrians in a Car-to-Pedestrian Collison (CPC) has generated increased attention with regulations that involve three subsystem tests for adult pedestrian protection (leg, thigh, and head impact tests) and a head impact

test for the child pedestrian [5]. While these subsystem tests can help in reducing the stiffness of vehicle front-end components and consequently reduce the risk of injuries, neither the complex vehicle-pedestrian interaction nor the injury mechanisms can be characterized by these simple impact tests. Therefore, several pedestrian FE models [6-8], mostly representing 50th percentile male (M50), have been developed and pedestrian accidents have started to be investigated numerically [9]. However, both experimental [10] and numerical [6, 11, 12] studies showed that the pedestrian anthropometry plays a major role in pedestrian kinematics and injury mechanisms during a CPC. For example, the contact location of the head to the car front end and the pre-impact head velocity are strongly influenced by pedestrian height [13]. Hence, new FE models with various anthropometries are required to cover better human variation.

Female pedestrian fatalities showed less of a decline trend compared to male fatalities from 1975 to 2015 [14], so protection of female pedestrians during a CPC has drawn the attention of vehicle safety engineers. In this study, a computationally efficient FE model corresponding to a 5th percentile female (F05) anthropometry in walking posture was developed and validated. Reliable predictions of both pedestrian kinematics and risks of injuries during a CPC were the main requirements for this model in order to be useful in the development of new pedestrian-friendly vehicles.

3.2 METHODS

3.2.1. FE model development

The model was developed based on anthropometry of a recruited female subject (24 year-old, 149.9 cm, and 48.1 kg). Fifteen anthropometric measurements describing the subject were within 5 % deviation when compared to the anthropometry measurements of a 5th percentile female [15, 16]. An imaging protocol that leveraged multiple modalities was used to acquire surface and image data in a standing (pedestrian) posture (Figure 3.1, a) [17]. External anthropometry was collected via a 3D scanner (Faro, Platinum Model arm, 8 ft. (2.4 m), Lake Mary, FL). The subject assumed a natural standing posture with the legs side by side. A non-reflective apparatus was used to put light contact with the back during surface scanning to reduce the effect of swaying. The subject was able to preserve the head in the Frankfurt plane through the use of an adjustable height photo target on the opposing wall of the lab. The external anthropometry data and surface scans were integrated together for the generation of a non-uniform rational basis spline (NURBS) patchwork of the small female outer surface in this neutral standing posture. Surface data was symmetrized using methods described in literature [18]. These methods were used in the development of geometrical data for pedestrian models of different sizes [8].

The mesh of F05-PS FE model was obtained by morphing a previously developed 50th percentile male pedestrian model [8] (Figure 3.1, b). The M50-PS model (also in the neutral standing posture) was morphed to target small female geometry by using the outer surface and landmark data acquired from the small female subject using a radial basis interpolation function – thin plate spline approach [19]. Due to the morphing procedure, all modeling aspects including the number of nodes, element, material types, and contact definitions are carried forward from the M50-PS model [8]. Some local mesh refinement was required to improve mesh quality following the morphing. The defined material properties of the F05-PS model in the LS-Dyna (LSTC, Livermore, CA, USA)

software are based on the 50th percentile detailed male occupant model (M50-O) [20] as well as the M50-PS model [21]. The M50-O model was developed previously using a regional model development approach. The main body regions were independently meshed and validated by researchers from different worldwide universities. This included models of the head [22-24], neck [25-28], thorax [29-31], abdomen [32], pelvis [33], and lower extremity [34-37]. The regional models were integrated into one full body model and validated [38-41]. Additionally the neck of the model has been validated in low G braking conditions [42].

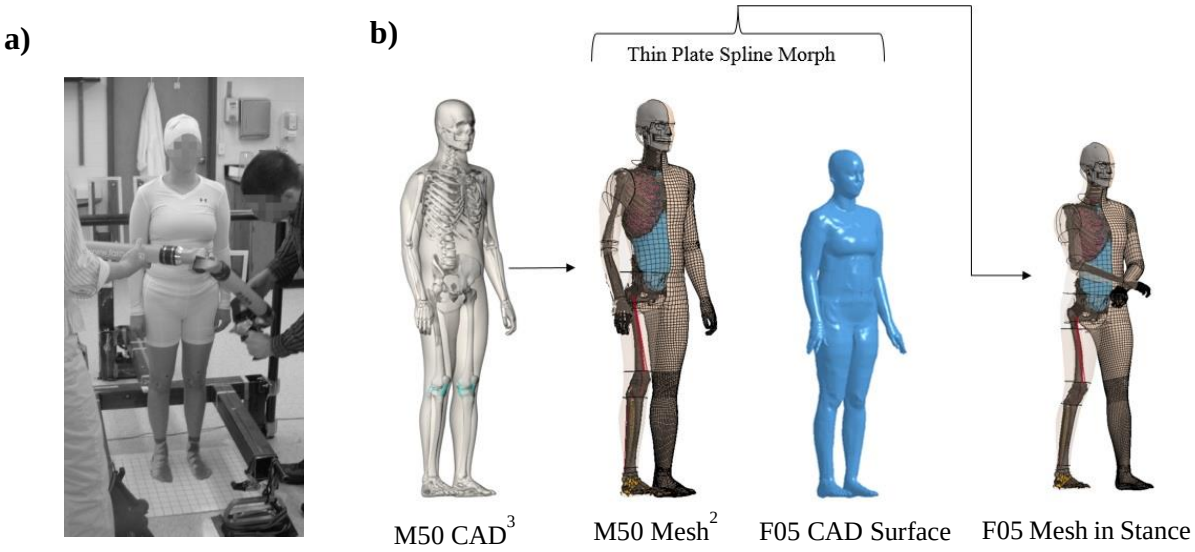

Figure 3.1 Model development: a) The subject was scanned in the standing posture using a 3D laser scanner. b) The schematic procedure of FE model mesh development

This model is a simplified version of the human body FE model, which was developed to evaluate the kinematics and kinetics of pedestrians with rapid run time. The model does not include internal viscera of the body, but rather was filled with an internal cavity component. Moreover, the brain was replaced by a single mass node at the location of the brain center of gravity and constrained to the skull. However, the F05-PS model includes detailed models of the pelvis and lower extremities, the first body parts impacted by the vehicle during a pedestrian accident, which showed to have a significant role on the kinematics of the whole body during CPC simulation. Therefore, the majority of pedestrian injuries (e.g. lower extremity, pelvis, ribs, neck etc.) could be predicted based on stress/strain data, while the injury of some upper body regions (e.g. head and abdomen) could be predicted based on structural data, such as acceleration and force, as in pedestrian rigid-body models [9].

The model was also designed to match the standard requirements of the European New Car Assessment Program (Euro NCAP) protocol [43], which calls for a heel to heel distance of 245 ± 10 mm, and H-point height of 820 mm ± 5% for the 5th percentile female. The upper extremities were adjusted using the same approach (Figure 3.1, b), to match previous testing work [44]. Overall, the F05-PS model has approximately 542,000 nodes and 830,000 elements (about 85% of deformable elements). To validate the pedestrian FE model at component level, four-point bending, lateral, and anterior-lateral blunt impact loadings were applied on the lower extremity

and the upper body, respectively. Then, the whole body model was validated in a CPC scenario. The whole validation process is presented in the following sections.

3.2.2 Validation of the knee joint under valgus bending

Combined valgus bending and shear loading of the knee joint have been recognized as the primary injury mechanisms for the knee ligaments during a CPC [45]. To validate the biomechanical response and injury tolerance of the knee joint under lateral loading, a four-point bending PMHS test reported in the literature was simulated [45]. The tested knee joints were acquired from 24 adult PMHS (68.3 ± 9.8 ages, 172 ± 7.8 cm height, and 75.2 ± 14.4 kg weight). The knee joint FE model was extracted from the F05-PS model and re-positioned manually to fit into the simulation setup (Figure 3.2). The ends of the three bones (femur, fibula, and tibia) were rigidly constrained to the bone cups. Every apparatus part was defined as rigid, except the load cell part, which was deformable to calculate the bending moment using a cross-section card [46]. The bone cups were attached to extension beams that were linked to the rotational joint supports. The support on the femur side was allowed to slide horizontally, while the other support was fixed. To load the knee joint under valgus bending, the extension beams were rotated at a knee angular rate of approximately 1 deg/ms in correspondence with a 40 km/h CPC impact [47]. In the simulation, the time histories of angular velocities were imposed to the rigid bars based on the data recorded in the PMHS tests.

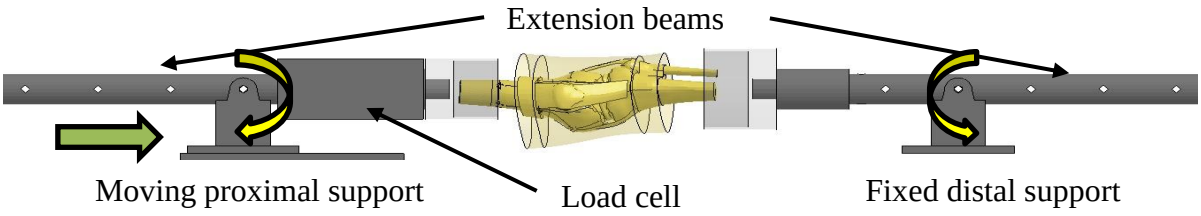

Figure 3.2 The FE simulation setup of four-point knee joint bending

3.2.3 Validation of the thoracic-abdominal region and pelvis under lateral impact loadings

The upper body section of the whole body FE model was validated against test data recorded on 14 PMHS specimens (53.8 ± 13.9 age, 67.2 ± 16.2 kg weight) subjected to blunt lateral impact loading [48]. The specimen was suspended upright with arms overhead then released at impact during PMHS test. A 23.4 kg and 150 mm diameter rigid impactor was freely suspended by a guided cable and accelerated approximately to 4.5, 6.7, or 9.4 m/s pre-impact speeds. Based on the PMHS test scenario, eight FE simulations were performed using the F05-PS model with combinations of impact regions (pelvis, abdomen, and thorax) and the impactor initial velocities. To avoid interference between arm and impactor during validation, the arm parts were removed and concentrated masses corresponding to each arm's mass were applied near each scapular region to preserve the pedestrian total mass (Figure 3.3). The pelvis was loaded laterally with an impactor aligned adjacent to the greater trochanter (Figure 3.3, a). The center of the impactor was aligned to the xiphoid process for the thorax impact and 7.5 cm down from the xiphoid process for the abdomen impact. Then, the impactor was rotated 60° from the anterior-posterior direction of the model before the model was impacted (Figure 3.3, b, c). During the simulation, the impact force time histories were recorded, and then compared to corresponding PMHS test data.

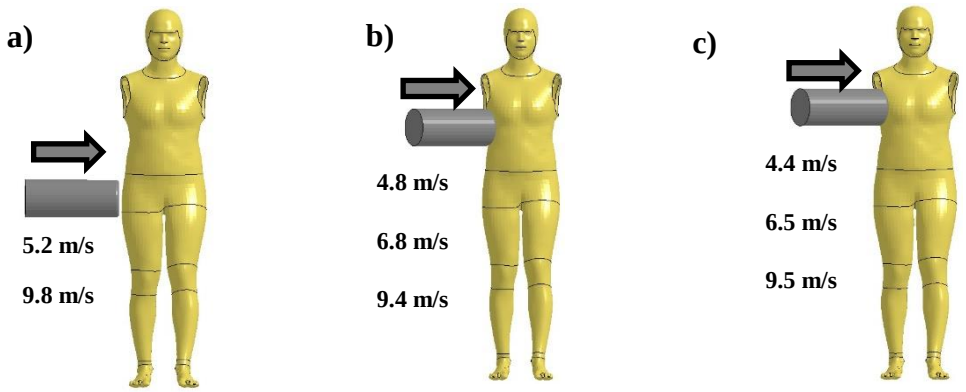

Figure 3.3 The upper body FE simulation setup for the F05-PS model: **a)** Pelvis, **b)** Abdomen, **c)** Thorax

3.2.4 Validation of the shoulder under lateral impact

Shoulder and arm injuries were reported as the most frequently upper extremity injuries during pedestrian accidents [49]. To validate the upper extremity in blunt impact scenario, a lateral impact simulation at the shoulder region was performed based on PMHS test data [50]. A rigid impactor with a mass of 23 kg and 150 mm diameter was aligned to the acromion of the right shoulder joint (Figure 3.4, a). Two impact FE simulations were performed on the F05-PS model at initial velocities of 4.5 m/s and 6.8 m/s.

3.2.5 Validation of the whole body

The whole F05-PS model was validated based on PMHS test data recorded in a CPC scenario [44]. The pedestrian model in a mid-stance posture was positioned laterally at the centerline of a mid-sized sedan vehicle FE model, which was truncated in half and mounted to a sled (Figure 3.4, b). This sedan was validated by its manufacturer against pedestrian subsystem test data [51]. The configuration used in testing [44] was also adopted by the pedestrian protocol of Euro NCAP [5]. A telemetry data acquisition system (TDAS) bag was attached to the PMHS to record pedestrian kinematic data. While the dimensions and the attachment of the TDAS bag were not documented in the literature, a TDAS mass (about 4.3 kg) was rigidly attached to the lumbar spines (L1~L4) as four concentrated mass nodes. Static/dynamic friction coefficients were defined as the average values reported in literature [52]: 0.26/0.25 (fabric-to-steel) for vehicle-to-pedestrian contact and 0.61/0.45 (fabric-to-fabric) for pedestrian-to-pedestrian contact. Prior testing, the PMHS was supported by a harness and released approximately 20-30 ms before the vehicle contact. In the simulation, prior to the impact at approximately 5 ms, acceleration due to gravity was applied to the pedestrian model and a force corresponding to its body weight was applied upward by the ground model in order to initiate the foot-ground contact. Then, the vehicle with 40 km/h initial velocity impacted the pedestrian FE model. This vehicle FE model was validated by its manufacturer against pedestrian subsystem test data [53].

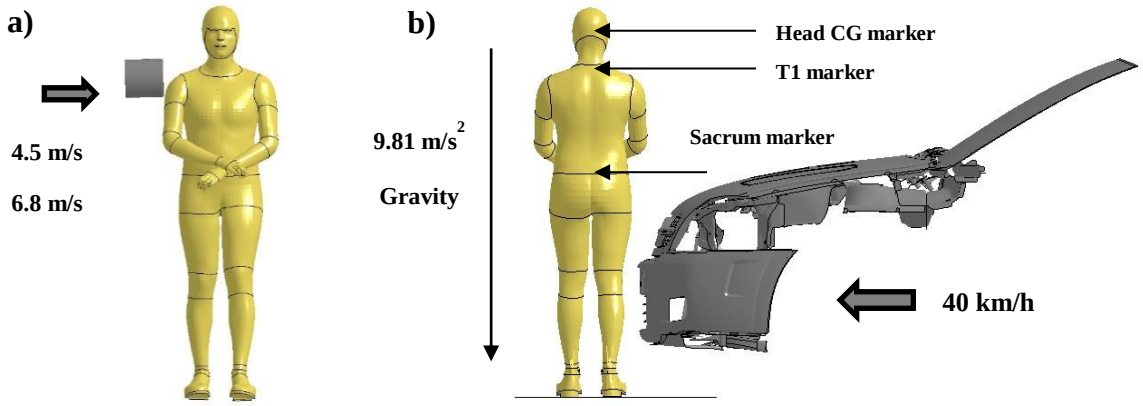

Figure 3.4 Schematic set up of validations: **a)** The shoulder lateral impact FE simulation, **b)** The whole body CPC simulation

In testing, the kinematic trajectories of the head's center of gravity (CG), first thoracic vertebra (T1), and sacrum relative to the car were recorded using the high-speed video [44]. The kinematic trajectories of FE model was recorded during CPC simulation and compared against the PMHS test data. The beginning and end timings were defined at the time of initial leg-bumper contact and the head-hood contact, respectively.

3.3 RESULTS

3.3.1 Validation of the pedestrian model at the component level

Overall, the valgus bending stiffness of the F05-PS knee model has a relatively similar trend as the curves obtained in testing, which were inertially compensated and geometrically scaled (based on the theory of dimensional analysis) to represent a 50th percentile adult male anthropometry (Figure 3.5) [45]. Initially, the load cell bending moments predicted by the FE models were lower than in testing, caused probably by the approximated setup inertia [8]. Then, the F05-PS model predicted lower stiffness than scaled test curves and M50-PS model. In terms of injury prediction, the F05-PS model predicted the ruptures of Medial Collateral Ligament (MCL) and Anterior Cruciate Ligament (ACL) in a knee angle range from 11° to 14.5°.

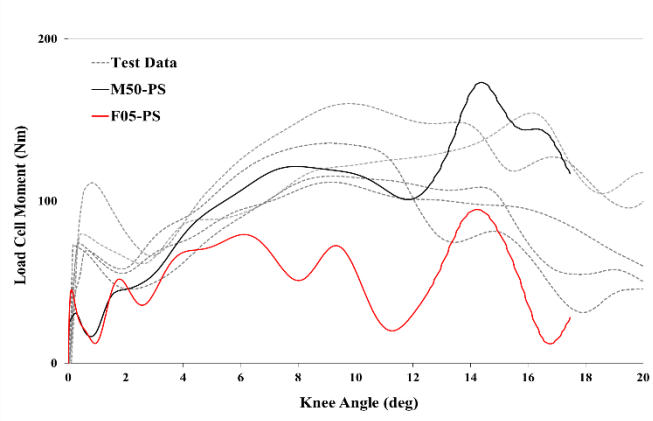

Figure 3.5 The response of knee joint under bending loading: PMHS tests vs FE simulations

The impact force time histories predicted by the F05-PS model under pelvis lateral loading were close to the lower boundary corridor (Fig. 6). It should be mentioned that the simulation responses were filtered (SAE 180) to reduce the noise and the published test corridors [48] were normalized to represent a 50th percentile adult male anthropometry.

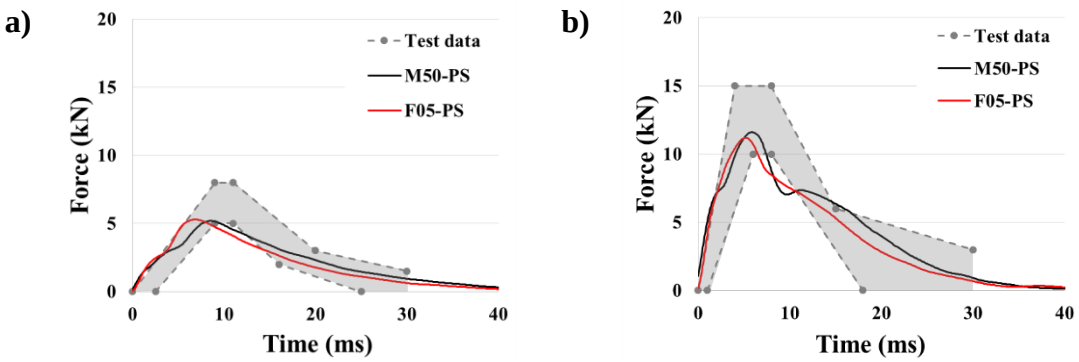

Figure 3.6 The time history of impact force at the pelvis: FE models vs. PMHS test data.
a) 5.2 m/s, **b)** 9.8 m/s initial impactor velocity

The time histories of impact force predicted by the F05-PS model during the thorax (Figure 3.7) and abdomen (Figure 3.8) impacts were compared against the corresponding PMHS test data [48]. The F05-PS model predicted lower peak forces than that of M50-PS model. At the beginning of the FE simulations (approximately 0 to 5 ms), the impact force gradients were close to the upper corridor of the PMHS test data. However, after the first peak force, a large decrease of the impact force predicted by the F05-PS model compared to the normalized PMHS corridor was observed in both thorax and abdomen simulations.

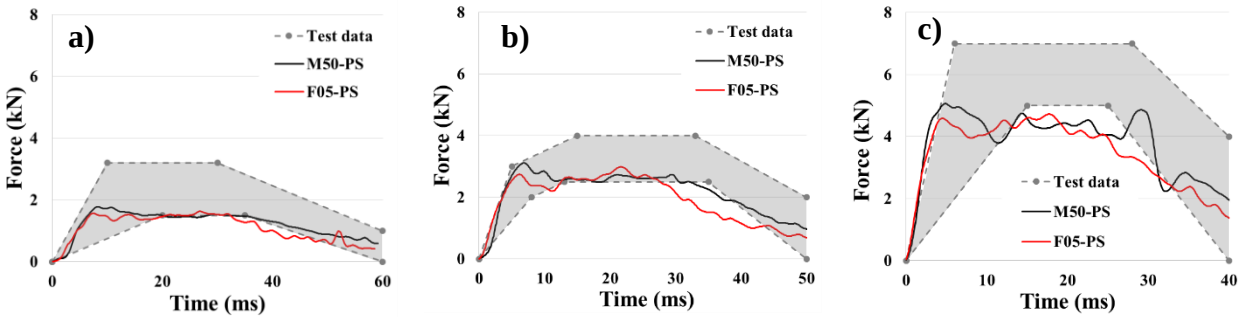

Figure 3.7 The time history of impact force at the thorax: FE models vs. PMHS test data.
a) 4.4 m/s, **b)** 6.5 m/s and, **c)** 9.5 m/s initial impactor velocity

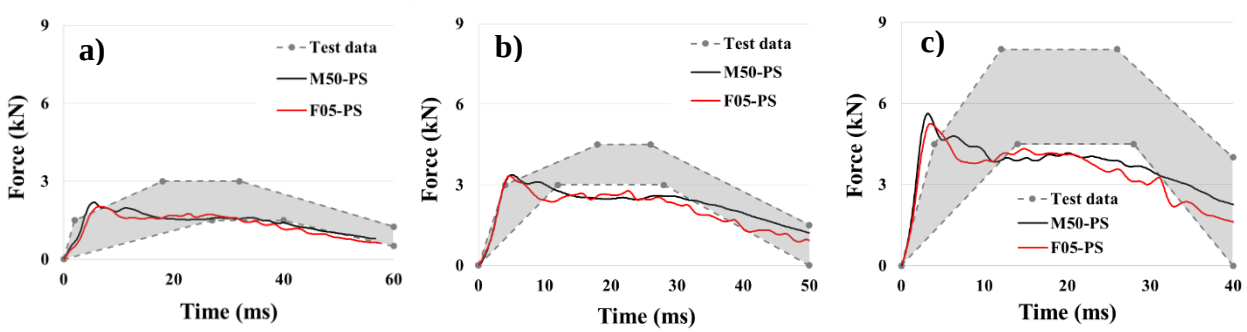

Figure 3.8 The time history of impact force at the abdomen: FE models vs. PMHS test data. **a)** 4.8 m/s, **b)** 6.8 m/s, and **c)** 9.4 m/s initial impactor velocity

The force time histories predicted by F05-PS model during shoulder impact simulations were close to the lower boundaries of the test corridors [50] (Figure 3.9) reported in literature [54-57] (average 73.3 ± 14.0 age, 62.2 ± 16.4 kg weight, and 370.6 ± 36.9 mm shoulder breath). It should be mentioned that these multi-linear corridors were obtained by scaling the force time histories relative to the M50 mass using a methodology proposed by Maltese et al [58]. Compared to the M50-PS model result [59], lower force peaks were predicted by the F05-PS model.

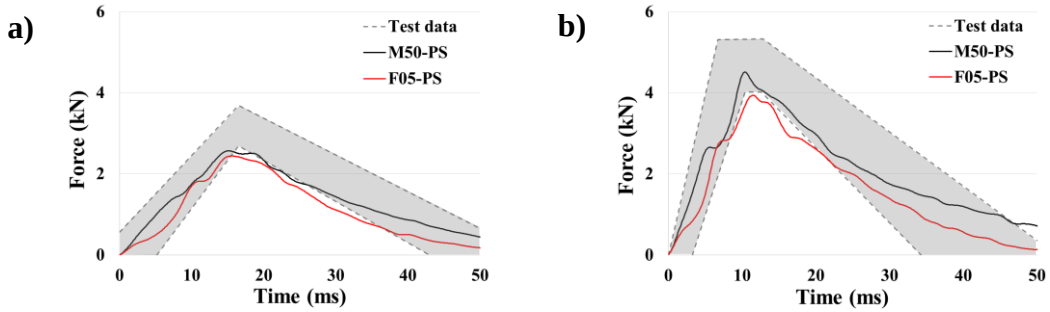

Figure 3.9 The time histories of impact force in lateral shoulder impact: FE model vs. PMHS test data. **a)** 4.5 m/s, **b)** 6.8 m/s impactor initial velocity

3.3.2 Validation of the pedestrian model in CPC simulation

The model kinematics in terms of upper body marker trajectories relative to the vehicle was extracted during the FE simulation and compared to corresponding PMHS test (Figure 3.10). The marker trajectories predicted by F05-PS model at the Head CG and T1 were close to the trajectories recorded on shorter PMHS specimens. The kinematic trajectory of the F05-PS model at sacrum was close to the one shorter specimen.

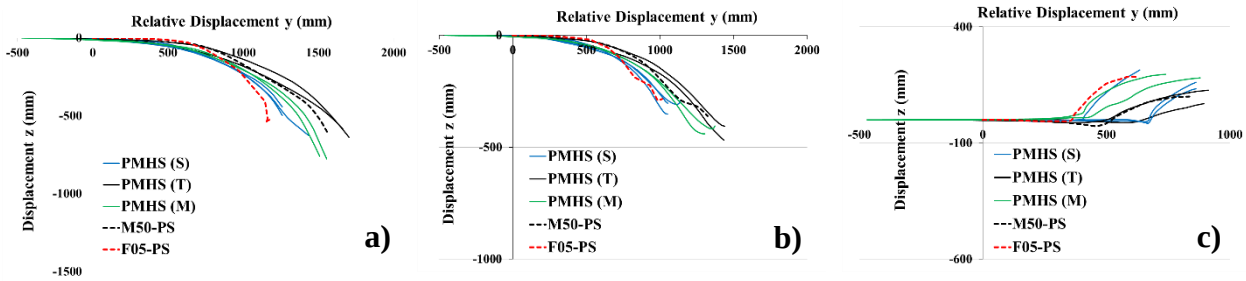

Figure 3.10 The F05-PS model kinematics-marker trajectories relative to the vehicle: FE model vs. PMHS tests:
a) Head CG, **b)** T1, **c)** Sacrum, S: shorter, M: mid-sized, T: taller specimen

While the time of head-vehicle contact (114 ms) was in the range of shorter PMHS data (112-116 ms), some discrepancies were observed in the head contact location [44]. For example, a shorter Wrap Around Distance (WAD) was observed in the F05-PS model (1658 mm) compared to the short PMHS test data (1860 and 1920 mm) caused probably by anthropometric differences between the model (1521 mm height) and short PMHS subjects (1631 and 1645 mm). In terms of injuries, the FE model predicted knee ligament injuries in both right (ACL/MCL) and left (ACL/LCL) lower extremities. Knee ligament ruptures (ACL/LCL) were recorded in the left knee of the shortest subject (1631 mm height), while tibia/fibula fractures were reported in other subjects' legs.

3.4 DISCUSSION

This study presents the development and validation of a small female FE model in walking posture. This is the first human FE model that is based on geometric data acquired from a living subject with anthropometric characteristics close to those of a 5th percentile female. Previous anthropometry of the F05 pedestrian FE model [6], or pedestrian anthropometric testing device (ATD) [10, 11] were obtained mainly by simple scaling from a 50th percentile male FE model which was followed by some improvements in pelvic and thoracic regions [6]. The mesh of our F05-PS model was obtained by a morphing approach that considerably reduced the development effort. The model characteristics including material properties and contact definitions were duplicated from the M50-PS model, which were developed from averaged test data obtained on a large number of samples (which usually included female data as well) [59]. While material characteristics may depend on gender and age, an update of material models is recommended when the corresponding data to young small females becomes available in the literature.

The F05-PS model was validated at the component level against impact loadings similar to those observed in a CPC scenario [8]. It should be mentioned that the majority of PMHS data presented in literature was scaled or obtained on subjects with anthropometry close to the 50th percentile male subject. While various scaling procedures were proposed in literature [60], their validations are difficult to perform, mostly due to the variations in human properties and various test setups used in component tests. Therefore, it was decided to compare the model responses to existing 50th percentile male PMHS test corridors, which could be considered an inherent limitation of this study. The responses of F05-PS model components were usually close to lower boundaries of test

corridors and showed softer stiffness than the corresponding responses of M50-PS model components. These results and the model stability during simulations generate confidence in the model. In addition, a simple (linear) scaling relationship between the responses of F05-PS and M50-PS was not determined, which suggests that the test setup and the material properties may play an important role in addition to anthropometry. In future studies, the model could be reevaluated when test data corresponding to 5th percentile female subjects becomes available.

The F05-PS knee model showed, as expected, a lower lateral bending stiffness than the M50-PS model and PMHS data corresponding average male anthropometry. However, the test output (the time history of load cell bending moment) depends on the dynamics of both the knee and test setup (identical in all simulations and tests). Therefore, to better validate the F05-PS knee model, additional tests of small female specimens are required in the same test configurations or in an improved test configuration that will allow an accurate calculation of the knee stiffness at its center location. In the CPC scenario, the knee could be subjected to complex conditions, which may include a shearing load in addition to bending depending on the position of vehicle bumper relative to the knee. Therefore, validations in complex conditions (bending and shearing) are recommended in future. The knee model biofidelity could be increased by including the structures neglected in the current model (e.g. surrounding muscles and tendons), by improving the geometry of knee capsule, and/or by modeling the synovial fluid. Updating material properties of the knee ligaments with an anisotropic material model [61] and validation of each ligament against test data may also improve the knee model.

The upper body validation responses under blunt lateral/anterior-lateral loadings at the regions of shoulder, pelvis, thorax, and abdomen were mostly within the PMHS test corridor (corresponding to M50 anthropometry), but usually close to the lower boundaries. The impact force responses of F05-PS thorax and abdomen showed an almost linear decrease toward the lower boundaries, after their inertial peaks. The simplified abdominal cavity probably causes this typical shape, observed in the responses of M50-PS model as well. Therefore, modeling internal organs [62] and including them into the rib cage cavity may improve the damping properties of the upper body in blunt impact conditions, and consequently the overall correlation of the model with the PMHS test data. In addition, we believe that a more biofidelic material model of flesh, especially in pelvic region, may improve the model responses as well.

Overall, the kinematic trajectories predicted by the F05-PS model in frontal plane were close to the corresponding trajectories recorded on short PMHS specimens. To further validate the model motion in sagittal plane as well as possible body rotation during impact, this data should be recorded in future PMHS tests. The F05-PS model predicted shorter head contact time to the vehicle hood and WAD, which is likely caused by the F05-PS stature, smaller compared to the shorter PMHS (152.1 cm of FE model vs. 163.1, 164, and 164.5 cm of short PMHSs).

In terms of injury, similar knee ligament ruptures (ACL/LCL) compared to the shortest female PMHS were observed, but no leg bone fractures were predicted. This could be caused by the anthropometric differences between the F05-PS model and tested PMHS. The front end vehicle geometry including the front bumper shape, and the relative position of knee to the bumper plays a significant role on the leg loadings during CPC and leg injuries [10, 13]. Hence, additional validations using female subjects with closer anthropometries relative to F05-PS model and various types of vehicles (e.g. sport utility vehicle, truck, and compact sized sedan) are suggested in the future. In addition, the current elastic-plastic material model with plastic strain failure criteria

assigned to cortical bone should be improved as previously suggested [36, 63]. Furthermore, to better understand the overall contributions of pedestrian anthropometry, vehicle geometry, and lower extremity material/failure properties, a sensitivity study [36, 63-66] should be performed in the future.

In conclusion, the F05-PS model showed close kinematic responses to the short PMHS test data and promising capability to predict the injury risk of pedestrians during lateral car impact. Therefore, the model could be used by automotive safety engineers to improve the design of vehicle front-end parts for better protection of the small pedestrian population. Compared to a previous 5th percentile female model (not publicly available), our model is expected to be released freely for academia, and to enhance the academic pedestrian safety research.

ACKNOWLEDGEMENTS

Funding for this study was provided by the Global Human Body Models Consortium. All findings and views reported in this manuscript are based on the opinions of the authors and do not necessarily represent the consensus or views of the funding organization.

REFERENCE

[1] WHO, "Road traffic injuries," 2016.
[2] R. Retting, "Pedestrian Traffic Fatalities by State: 2018 Preliminary data," GHSA2019.
[3] NHTSA, "Early Estimate of Motor Vehicle Traffic Fatalities in 2018," 2019.
[4] NHTSA, "Motor Vehicle Crashes: Overview," 2015.
[5] EuroNCAP, "Pedestrian Testing Protocol," 2019.
[6] R. Watanabe, T. Katsuhara, H. Miyazaki, Y. Kitagawa, and T. Yasuki, "Research of the relationship of pedestrian injury to collision speed, car-type, impact location and pedestrian sizes using human FE model (THUMS Version 4)," *Stapp car crash journal*, vol. 56, pp. 269-321, 2012.
[7] Y. Takahashi, Y. Kikuchi, A. Konosu, and H. Ishikawa, "Development and validation of the finite element model for the human lower limb of pedestrians," *Stapp car crash journal*, vol. 44, pp. 335-55, 2000.
[8] C. D. Untaroiu, W. Pak, Y. Meng, J. Schap, B. Koya, and F. S. Gayzik, "A Finite Element Model of a Mid-Size Male for Simulating Pedestrian Accidents," *ASME Journal of Biomedical Engineering*, 2017.
[9] C. D. Untaroiu, M. U. Meissner, J. R. Crandall, Y. Takahashi, M. Okamoto, and O. Ito, "Crash reconstruction of pedestrian accidents using optimization techniques," *International Journal of Impact Engineering*, vol. 36, pp. 210-219, Feb 2009.
[10] C. Untaroiu, J. Shin, J. Ivarsson, J. Crandall, Y. Takahashi, A. Akiyama, *et al.*, "Pedestrian kinematics investigation with finite element dummy model based on anthropometry scaling method," in *Proc. 20th Int. Technical Conf. Enhanced Safety of Vehicle*, 2007.
[11] R. Fredriksson, J. Shin, and C. D. Untaroiu, "Potential of pedestrian protection systems--a parameter study using finite element models of pedestrian dummy and generic passenger vehicles," *Traffic injury prevention*, vol. 12, pp. 398-411, 2011.

[12] C. D. Untaroiu, J. Shin, J. R. Crandall, R. Fredriksson, O. Bostrom, Y. Takahashi, *et al.*, "Development and validation of pedestrian sedan bucks using finite-element simulations: a numerical investigation of the influence of vehicle automatic braking on the kinematics of the pedestrian involved in vehicle collisions," *International Journal of Crashworthiness,* vol. 15, pp. 491-503, 2010.
[13] Y. Okamoto, T. Sugimoto, K. Enomoto, and J. Kikuchi, "Pedestrian head impact conditions depending on the vehicle front shape and its construction--full model simulation," *Traffic injury prevention,* vol. 4, pp. 74-82, 2003.
[14] IIHS, "General statistics of fatality facts," 2016.
[15] M. L. Davis, B. Koya, J. M. Schap, and F. S. Gayzik, "Development and full body validation of a 5th percentile female finite element model," *Stapp car crash journal,* vol. 60, p. 509, 2016.
[16] C. C. Gordon, T. Churchill, C. E. Clauser, B. Bradtmiller, and J. T. McConville, "Anthropometric survey of US army personnel: methods and summary statistics 1988," DTIC Document1989.
[17] F. Gayzik, D. Moreno, C. Geer, S. Wuertzer, R. Martin, and J. Stitzel, "Development of a full body CAD dataset for computational modeling: a multi-modality approach," *Annals of biomedical engineering,* vol. 39, p. 2568, 2011.
[18] F. Gayzik, D. Moreno, K. Danelson, C. McNally, K. Klinich, and J. D. Stitzel, "External landmark, body surface, and volume data of a mid-sized male in seated and standing postures," *Annals of biomedical engineering,* vol. 40, pp. 2019-2032, 2012.
[19] N. A. Vavalle, S. L. Schoell, A. A. Weaver, J. D. Stitzel, and F. S. Gayzik, "Application of radial basis function methods in the development of a 95th percentile male seated fea model," *Stapp car crash journal,* vol. 58, p. 361, 2014.
[20] N. A. Vavalle, M. L. Davis, J. D. Stitzel, and F. S. Gayzik, "Quantitative validation of a human body finite element model using rigid body impacts," *Annals of biomedical engineering,* vol. 43, pp. 2163-2174, 2015.
[21] D. Schwartz, B. Guleyupoglu, B. Koya, J. D. Stitzel, and F. S. Gayzik, "Development of a computationally efficient full human body finite element model," *Traffic injury prevention,* vol. 16, pp. S49-S56, 2015.
[22] H. Mao, L. Zhang, B. Jiang, V. V. Genthikatti, X. Jin, F. Zhu, *et al.*, "Development of a Finite Element Human Head Model Partially Validated With Thirty Five Experimental Cases," *Journal of biomechanical engineering,* vol. 135, p. 111002, 2013.
[23] E. G. Takhounts, M. J. Craig, K. Moorhouse, J. McFadden, and V. Hasija, "Development of Brain Injury Criteria (BrIC)," *Stapp car crash journal,* vol. 57, pp. 243-266, 2013.
[24] T. Yanaoka and Y. Dokko, "A Parametric Study of Age-Related Factors Affecting Intracranial Responses under Impact Loading Using a Human Head/Brain FE Model," presented at the International Research Council on Biomechanics Injury (IRCOBI), Gothenburg, Sweeden, 2013.
[25] J. A. DeWit and D. S. Cronin, "Cervical spine segment finite element model for traumatic injury prediction," *Journal of the mechanical behavior of biomedical materials,* vol. 10, pp. 138-150, 2012.
[26] J. B. Fice, D. S. Cronin, and M. B. Panzer, "Cervical spine model to predict capsular ligament response in rear impact," *Annals of biomedical engineering,* vol. 39, pp. 2152-2162, 2011.

[27] S. F. Mattucci, J. A. Moulton, N. Chandrashekar, and D. S. Cronin, "Strain rate dependent properties of younger human cervical spine ligaments," *Journal of the mechanical behavior of biomedical materials,* vol. 10, pp. 216-226, 2012.
[28] S. F. Mattucci, J. A. Moulton, N. Chandrashekar, and D. S. Cronin, "Strain rate dependent properties of human craniovertebral ligaments," *Journal of the mechanical behavior of biomedical materials,* vol. 23, pp. 71-79, 2013.
[29] Z. Li, M. W. Kindig, J. R. Kerrigan, C. D. Untaroiu, D. Subit, J. R. Crandall, *et al.*, "Rib Fractures Under Anterior-Posterior Dynamic Loads: Experimental and Finite-Element Study," *Journal of Biomechanics,* vol. 43, p. 228.234, 2010.
[30] Z. Li, M. W. Kindig, D. Subit, and R. W. Kent, "Influence of mesh density, cortical thickness and material properties on human rib fracture prediction," *Medical engineering & physics,* vol. 32, pp. 998-1008, 2010.
[31] D. Poulard, R. Kent, M. Kindig, Z. Li, and D. Subit, "Thoracic response targets for a computational model: A hierarchical approach to asses the biofidelity of a 50th-percentile occupant male finite element model," *J Mech Behav Biomed Mater,* 2015.
[32] A. Soni and P. Beillas, "Modelling hollow organs for impact conditions: a simplified case study," *Comput Methods Biomech Biomed Engin,* vol. [Epub ahead of print], Oct 24 2013.
[33] Y. H. Kim, J. E. Kim, and A. W. Eberhardt, "A new cortical thickness mapping method with application to an in vivo finite element model," *Comput Methods Biomech Biomed Engin,* vol. 17, pp. 997-1001, Oct 31 2012.
[34] J. Shin and C. Untaroiu, "Biomechanical and Injury Response of Human Foot and Ankle under Complex Loading," *J Biomech Eng,* vol. 135, Jul 1 2013.
[35] C. D. Untaroiu, N. Yue, and J. Shin, "A finite element model of the lower limb for simulating automotive impacts," *Ann Biomed Eng,* vol. 41, pp. 513-26, Mar 2013.
[36] N. Yue and C. D. Untaroiu, "A numerical investigation on the variation in hip injury tolerance with occupant posture during frontal collisions," *Traffic injury prevention,* vol. 15, pp. 513-522, 2014.
[37] N. Yue, J. Shin, and C. Untaroiu, "Development and validation of an occupant lower limb finite element model.," in *SAE Technical Paper* vol. 2011-01-1128, ed, 2011.
[38] A. R. Hayes, N. A. Vavalle, D. P. Moreno, J. D. Stitzel, and F. S. Gayzik, "Validation of simulated chestband data in frontal and lateral loading using a human body finite element model," *Traffic Inj Prev,* vol. 15, pp. 181-6, 2014.
[39] N. A. Vavalle, A. B. Thompson, A. R. Hayes, D. P. Moreno, J. D. Stitzel, and F. S. Gayzik, "Investigation of the Mass Distribution of a Detailed Seated Male Finite Element Model," *J Appl Biomech,* vol. [Epub ahead of print], Dec 17 2013.
[40] G. Park, T. Kim, J. R. Crandall, C. Arregui-Dalmases, and J. Luzon-Narro, "Comparison of Kinematics of GHBMC to PMHS on the Side Impact Condition," presented at the International Research Council on Biomechanics of Injury, Gothenburg, Sweden, 2013.
[41] N. A. Vavalle, D. P. Moreno, A. C. Rhyne, J. D. Stitzel, and F. S. Gayzik, "Lateral impact validation of a geometrically accurate full body finite element model for blunt injury prediction," *Ann Biomed Eng,* vol. 41, pp. 497-512, Mar 2013.
[42] GHBMC, "User Manual: M50 Occupant Version 4.3 for LS-DYNA," 2014.
[43] EuroNCAP, "Pedestrian testing protocol," 2010.
[44] J. R. Kerrigan, J. R. Crandall, and B. Deng, "Pedestrian kinematic response to mid-sized vehicle impact," *International journal of vehicle safety,* vol. 2, pp. 221-240, 2007.

[45] D. Bose, K. S. Bhalla, C. D. Untaroiu, B. J. Ivarsson, J. R. Crandall, and S. Hurwitz, "Injury tolerance and moment response of the knee joint to combined valgus bending and shear loading," *J Biomech Eng,* vol. 130, p. 031008, Jun 2008.
[46] LSTC, "LS-DYNA KEYWORD USER'S MANUAL," 2013.
[47] C. Untaroiu, K. Darvish, J. Crandall, B. Deng, and W. Jenne-Tai, "A finite element model of the lower limb for simulating pedestrian impacts," *Stapp car crash journal,* vol. 49, p. 157, 2005.
[48] D. C. Viano, "Biomechanical responses and injuries in blunt lateral impact," SAE Technical Paper 0148-7191, 1989.
[49] J.-L. Martin, A. Lardy, and B. Laumon, "Pedestrian injury patterns according to car and casualty characteristics in France," in *55th AAAM Annual Conference Annals of Advances in Automotive Medicine*, 2011.
[50] S.-W. Koh, J. M. Cavanaugh, M. J. Mason, and S. A. Petersen, "Shoulder injury and response due to lateral glenohumeral joint impact: an analysis of combined data," *Stapp car crash journal,* vol. 49, p. 291, 2005.
[51] J. R. Kerrigan, D. P. Parent, C. Untaroiu, J. R. Crandall, and B. Deng, "A new approach to multibody model development: pedestrian lower extremity," *Traffic Inj Prev,* vol. 10, pp. 386-97, Aug 2009.
[52] V. Kothari and M. Gangal, "Assessment of frictional properties of some woven fabrics," 1994.
[53] J. R. Kerrigan, D. P. Parent, C. Untaroiu, J. R. Crandall, and B. Deng, "A new approach to multibody model development: pedestrian lower extremity," *Traffic injury prevention,* vol. 10, pp. 386-397, 2009.
[54] J. H. Bolte IV, M. H. Hines, R. G. Herriott, J. D. McFadden, and B. R. Donnelly, "Shoulder impact response and injury due to lateral and oblique loading," *Stapp car crash journal,* vol. 47, p. 35, 2003.
[55] J. H. Bolte, M. H. Hines, J. D. McFadden, and R. A. Saul, "Shoulder response characteristics and injury due to lateral glenohumeral joint impacts," *Stapp car crash journal,* vol. 44, pp. 261-280, 2000.
[56] S. Compigne, Y. Caire, T. Quesnel, and J.-P. Verries, "Non-injurious and injurious impact response of the human shoulder three-dimensional analysis of kinematics and determination of injury threshold," *Stapp car crash journal,* vol. 48, pp. 89-123, 2004.
[57] D. R. Marth, "Biomechanics of the shoulder in lateral impact," MS Thesis, Wayne State University, 2002.
[58] M. R. Maltese, R. H. Eppinger, H. H. Rhule, B. R. Donnelly, F. A. Pintar, and N. Yoganandan, "Response corridors of human surrogates in lateral impacts," *Stapp Car Crash J,* vol. 46, pp. 321-51, Nov 2002.
[59] C. D. Untaroiu, J. B. Putnam, J. Schap, M. L. Davis, and F. S. Gayzik, "Development and preliminary validation of a 50th percentile pedestrian finite element model," in *ASME 2015 IDETC/CIE Conference*, Boston, MA, USA, 2015, p. 7.
[60] A. Petitjean, X. Trosseille, N. Yoganandan, and F. A. Pintar, "Normalization and scaling for human response corridors and development of injury risk curves," in *Accidental Injury*, ed: Springer, 2015, pp. 769-792.
[61] J. A. Weiss and J. C. Gardiner, "Computational modeling of ligament mechanics," *Critical Reviews™ in Biomedical Engineering,* vol. 29, 2001.

[62] Y. C. Lu and C. D. Untaroiu, "A statistical geometrical description of the human liver for probabilistic occupant models," *Journal of Biomechanics,* vol. 47, pp. 3681-3688, Nov 28 2014.
[63] C. D. Untaroiu, N. Yue, and J. Shin, "A finite element model of the lower limb for simulating automotive impacts," *Annals of biomedical engineering,* vol. 41, pp. 513-526, 2013.
[64] Y. Han, J. K. Yang, K. Mizuno, and Y. Matsui, "Effects of Vehicle Impact Velocity, Vehicle Front-End Shapes on Pedestrian Injury Risk," *Traffic Injury Prevention,* vol. 13, pp. 507-518, 2012.
[65] J. B. Putnam, J. T. Somers, and C. D. Untaroiu, "Development, calibration, and validation of a head-neck complex of THOR mod kit finite element model," *Traffic injury prevention,* vol. 15, pp. 844-54, 2014.
[66] L. M. Saez, L. J. G. Casanova, E. A. Fazio, and A. G. Alvarez, "Behaviour of high bumper vehicles in pedestrian scenarios with full finite element human models," *International Journal of Crashworthiness,* vol. 17, pp. 1-10, Feb 2012.

Chapter 4

Development and Validation of a Finite Element Model of an Average Male for Investigating Pedestrian Accidents

Wansoo Pak, Berkan Guleyupoglu, Bharath Koya, Scott F. Gayzik, Eric Song,

Costin D. Untaroiu

Manuscript in preparation

ABSTRACT

The pedestrian is one of the most vulnerable road users and comprises approximately 23% of the road crash-related fatalities in the world. To protect a pedestrian during Car-to-Pedestrian Collisions (CPC), subsystem impact tests have been performed. However, these tests cannot characterize either complex vehicle-pedestrian interaction or the injury mechanisms. The main purpose of this study was to develop and validate a detailed pedestrian Finite Element (FE) model corresponding to a 50^{th} percentile male to predict crash-induced injuries observed in pedestrian accidents. The model geometry was reconstructed using a multi-modality protocol from medical images and exterior scanned data corresponding to a mid-sized male subject volunteer and included the internal organs, muscles and vessels. The lower extremity, shoulder and upper body of the FE model were validated against Post Mortem Human Surrogate (PMHS) test data recorded in valgus bending, CPC impact and lateral/anterior-lateral blunt impact tests, respectively. Then, the whole-body pedestrian model was verified in CPC simulations in the same conditions as PMHS impact testing with a mid-sized sedan and simplified generic vehicles. In the component validations, the responses of the FE model were mostly within PMHS test corridors. The kinematic trajectories predicted by the FE model during CPC validations showed similar trends corresponding to PMHS test data. The biofidelic kinetic/kinematic responses and crash-induced injury prediction of this model recommend using it in automotive safety research for the development of new pedestrian-friendly vehicles.

4.1 INTRODUCTION

According to the World Health Organization (WHO), the total number of fatalities recorded in traffic accidents worldwide is about 1.35 million each year [1]. Among the road traffic deaths, in 2016, pedestrian fatalities represented 23% (World), 27% (Europe) and 22% (Americas) of total traffic fatalities. Historically, the major challenge of automotive safety research was to improve the design of both vehicles and restraint systems to reduce injuries for vehicle occupants. Consequently, the occupant fatalities have declined 46% in the United States since 1975 [2]. While the total fatalities in traffic crashes have decreased from 2006 to 2015, the pedestrian fatalities

have increased [3]. In 2015, approximately 5,376 pedestrians were killed and 70,000 were injured in traffic crashes in the United States [3]. Therefore, pedestrian protection during Car-to-Pedestrian Collisions (CPC) accidents continue to generate increased attention.

To mitigate the number of pedestrian morbidity and mortality in traffic accidents, several test protocols were proposed to evaluate new vehicles for pedestrian protection [4-7]. Mainly, these protocols involve subsystem tests using isolated impactors corresponding to various body regions (e.g. leg, thigh and child/adult head). These subsystem tests can help in reducing the stiffness of vehicle front-end components and consequently reduce the risk of injuries. However, neither the complex vehicle-pedestrian interaction nor the injury mechanisms can be characterized by these simple impact tests. Additionally, several computational models of pedestrian humans or dummies [8-13] have been developed and validated. However, these pedestrian models have several limitations related to simplified geometries and material models available at the time the models were developed and validated. For example, some simplified body parts (modelled usually with lump masses) may lead to unrealistic mass distribution and possibly affects the kinematics and injury response.

The primary goal of this study was to develop and validate a refined Finite Element (FE) model corresponding to a 50^{th} percentile male anthropometry in a walking posture. A high level of detail in terms of mesh refinement and modeled structures were used in this model to better predict kinetic/kinematic responses as well as the crash-induced injuries in CPC accident. Hence, the model included not only the muscular-skeletal structures but also the brain, vessels and internal organs. The specific regions of the whole-body FE model were validated against the Post Mortem Human Surrogate (PMHS) test data. Then, the whole-body was validated in a CPC scenario with a mid-sized sedan and simplified generic vehicles.

4.2 METHODS

4.2.1 Development of the Pedestrian Finite Element Model

The geometry of a 50^{th} percentile male pedestrian (M50-P) model corresponds to the anthropometry of a recruited male subject (174.9 cm and 78 kg) was developed [14] (Figure 4.1). Fifteen anthropometric measurements describing the subject demonstrated a close match to the anthropometry of a 50^{th} percentile North American male [15]. A multi-modality protocol was used to acquire data in a standing posture [16]. External anthropometry was collected via a 3D scanner (Faro, Platinum Model arm, 8ft. (2.4 m), Lake Mary, FL). The subjects were instructed to walk towards a line on the floor and to stop with both feet parallel to assume a natural posture. The feet of the subject were traced on poster board and an apparatus was used to put light contact on the back during surface scanning to reduce the effect of swaying. A photo target was used to keep the head in the Frankfurt plane. The external anthropometry data and surface scans were integrated together for the generation of a Non-Uniform Rational Basis Spline (NURBS) patchwork of the average male outer surface in this neutral standing posture.

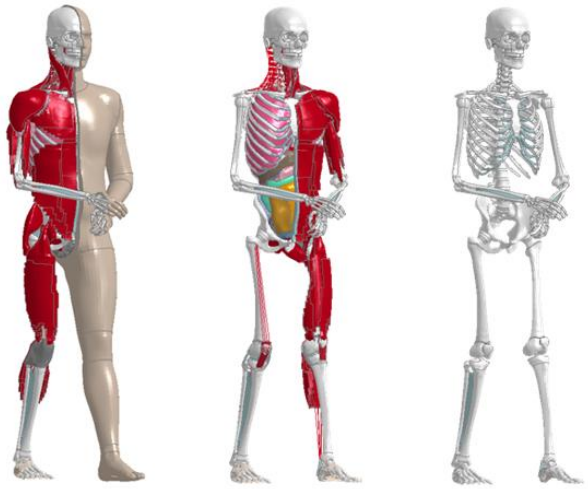

Figure 4.1 50-P FE model showing different structures

This pedestrian FE model was developed in LS-Dyna software (LSTC, Livermore, CA) based on the 50th percentile male occupant model (M50-O). The Global Human Body Models Consortium (GHBMC) occupant model was developed using a regional model development approach. The main body regions were independently meshed and validated by researchers from different worldwide universities. This included models of the head [17-19], neck [20-23], thorax [24-26], abdomen [27], pelvis [28] and lower extremity [29-31]. The regional models were integrated into one full body model and validated [32-37]. Additionally the neck of the model has been validated in low G braking conditions [38].

All material models and the mesh of all bony structures are identical to the occupant model. On a regional basis, some regions are essentially the same model as the occupant (e.g. Head and minor adjustments to the Neck), others were remeshed in order to acehive the standing posture. These include the viscera of the thorax and abdomen, skeletal muscle of the pelvis and lower extremities. The ligamentous and cartilagenous structures of the knee use the same material models as the occupant but were remeshed to reflect the extended knee CAD data. Skeletal muscles were modelled as beam elements [39] and the external soft tissue envelope was meshed with hexahedral elements.

4.2.2 Validation of the Knee Joint

In traffic accidents, a valgus bending of the knee has been recognized as the primary soft tissue injury in pedestrians [40]. To validate biomechanical and injury responses of the knee joint under lateral loading, a four-point bending FE simulation was performed [41]. The tested knee joints were acquired from 24 adult PMHS (68.3 ± 9.8 ages, 172 ± 7.8 cm and 75.2 ± 14.4 kg). The knee joint of the M50-P model was extracted and then re-positioned manually to fit into the simulation setup (Figure 4.2). The ends of the three bones (femur, fibula and tibia) were positioned approximatively in the center of the cups and then rigidly constrained to the bone cups in a depth of 76 mm (the interior length of the cup). Each part of the apparatus was defined as rigid, except the load cell part attached to the bone cup, which was deformable in order to calculate the bending moment. The bone cups were attached to extension beams that were linked to the rotational joint supports. The initial anterior-posterior knee axis was approximately parallel with the axis defined

by the support centers. The support on the femur side was allowed to slide horizontally, while the other support was fixed. In the original test setup, an impact fork was used to load the extension bars. The stiffness properties of the three revolute joints used in this setup were unknown and modeling of the contact between the steel ram and aluminum extension bars may add some errors as well. Therefore, the boundary conditions of the specimen were assigned based on the time histories of the angular velocity for the extension beams, recorded in testing. As a result, the knee joint was loaded under valgus bending with a knee angular rate of approximately 1 deg/ms in correspondence with a 40 km/h CPC impact [42].

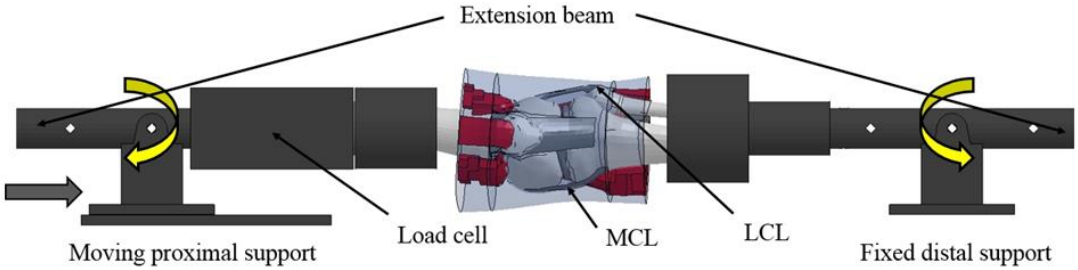

Figure 4.2 FE simulation setup for knee joint bending loading

4.2.3 Validation of the Lower Extremity

After the knee joint validation, a response of the entire lower extremity was validated in CPC impact. The M50-P model was laterally impacted by the simplified generic vehicles represented as a sedan, SUV and Van. Then, the angle of the right leg during impact was calculated and compared against the PMHS test data. In PMHS tests, the initial coordinates of the sacrum up (SU), sacrum low (SL) and greater trochanter (GT) points as well as the kinematic trajectories of the SU and SL during impact were recorded [43]. To calculate the angle of the right lower extremity, three reference points associated to the GT, right knee and right ankle were defined on the M50-P model based on the Euro NCAP technical bulletins 024 [44]. Since the kinematic trajectory of the GT was not recorded in tests, the kinematics of the GT point were calculated from the initial distance between the SU and GT and the SL and GT.

$$d_1{}^2 = (x_1 - x)^2 + (z_1 - z)^2 \qquad (1)$$

$$d_2{}^2 = (x_2 - x)^2 + (z_2 - z)^2 \qquad (2)$$

From equations (1) and (2), the distance between the SU and GT (d_1) and the SU and GT (d_2) can be calculated from the initial coordinates (Figure 4.3). The kinematics of the GT were calculated from the given distances d_1, d_2 and the time histories of the coordinates relative to the vehicle at SU (x_1, z_1) and SL (x_2, z_2). The time histories of the lower extremity angle during impact was then computed in the coronal plane using the kinematics at the SU, SL and GT points.

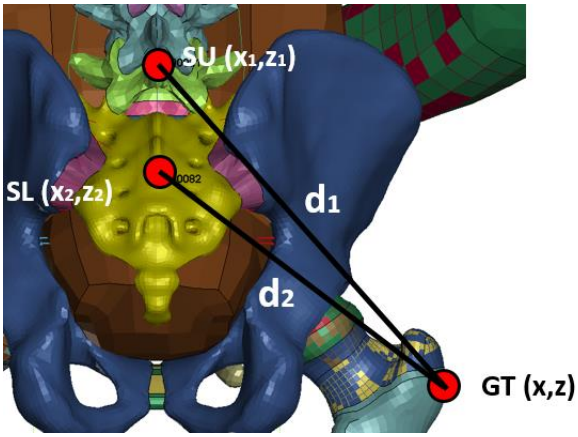

Figure 4.3 Reference points of the sacrum up, sacrum low and greater trochanter

4.2.4 Validation of the Upper Body

The shoulder and arm were reported as the most frequent injured upper extremities during pedestrian accidents [45]. To validate the model of upper extremity region, a simulation of lateral blunt impact to the shoulder was performed using the same setup used in PMHS testing [46]. In validation, a rigid impactor with a mass of 23 kg and 150 mm diameter was aligned to the acromion of the right shoulder joint (Figure 4.4, a). Then, the impactor with initial velocities of 4.5 m /s and 6.8 m /s laterally impacted to the M50-P model. During validation, the impact forces time histories obtained in simulations were compared to a test corridor [46] obtained from similar data reported in literature [47-50] (average 73.3 ± 14.0 age, 62.2 ± 16.4 kg weight and 370.6 ± 36.9 mm shoulder breath).

The upper body section of the whole-body FE model was validated against test data collected from 14 PMHS specimens (53.8 ± 13.9 age, 67.2 ± 16.2 kg weight) subjected to blunt lateral/anterior-lateral impact loadings [51]. In testing, the specimen was suspended upright with arms overhead then released at impact. Then, a 23.4 kg rigid impactor suspended by a guided cable was accelerated at various pre-impact speeds (Figure 4.4, b-d). Based on the PMHS test scenario, eight FE simulations were performed using the M50-P model under various combinations of impacted regions (pelvis, abdomen and thorax) and impactor initial velocities. To avoid interference between arms and the impactor, the upper extremities were removed but a concentrated mass corresponding to each arm was applied near the scapular region to maintain the total mass. The pelvis was loaded laterally with the impactor aligned adjacent to the greater trochanter (Figure 4.4, d). The center of the impactor was aligned to the xiphoid process for the thorax impact and 7.5 cm down from the xiphoid process for the abdomen impact. Then, the impactor was rotated 60° around the vertical (z) axis (Figure 4.4, b, c). The impact forces recorded on the simulations were compared to corresponding PMHS test data. To reduce the noise, all model responses were filtered with SAE 180 Hz.

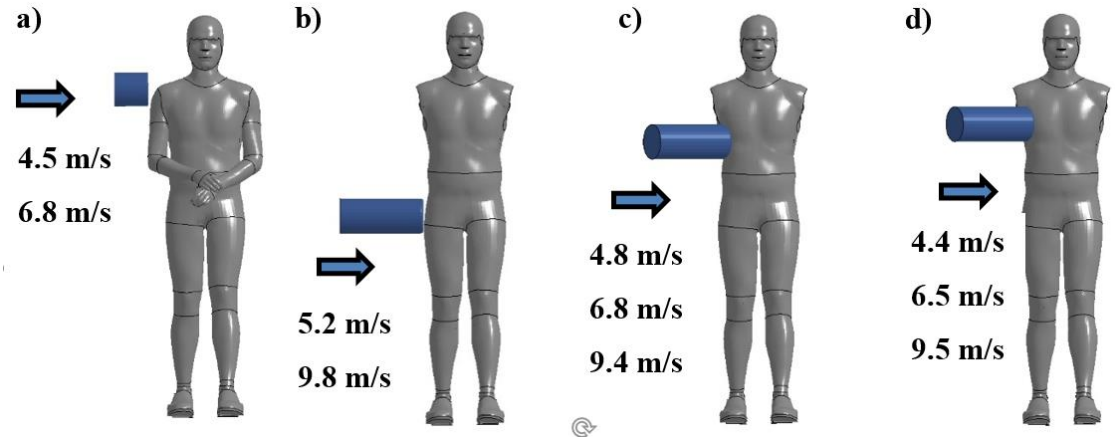

Figure 4.4 Simulation setup for the a) shoulder, b) pelvis, c) abdomen and d) thorax

4.2.5 Validation of the Whole-Body

The whole-body M50-P model was validated in a CPC scenario with a mid-sized sedan and simplified generic vehicles based on PMHS test data [43, 52]. In both tests, the PMHS positioned laterally at the centerline of a vehicle to represent the most frequent pedestrian accident scenario [53]. The body of PMHS was supported by a harness and released before the vehicle impact. Then, the vehicle with an initial velocity of 40 km/h impacted to the PMHS. The mid-sized sedan used in first validation was truncated half and mounted to a sled (Figure 4.5). This sedan was validated by its manufacturer against pedestrian subsystem test data [54]. For the generic vehicles, three types of vehicle profile represent a sedan, SUV and Van (Figure 4.6) was developed by the LAB (Laboratory of Accidentology and Biomechanics, PSA, Renault, France) and mounted on a sled [43]. In the test, the position of each specimen relative to the vehicle buck was modified with respect to its anthropometry and the shape of generic vehicle profiles to maximize the geometrical correspondence between different cases. For example, the knee reference point, which is 10 mm below the center of anterior and posterior edge of a tibia plateau, of each specimens are aligned with 82 mm above the SUV bumper tube center. In addition, the upper body kinematics of PMHS was scaled based on the SAE J2868 while no scaling was applied on the lower extremities since only translational displacement was experienced [43]. During testing, markers were attached to the PMHS and the kinematic trajectories were recorded relative to the vehicle using the high-speed video.

The posture of the M50-P model was set to mid-stance with the legs apart walking towards the vehicle centerline then the rearward leg was impacted first by the vehicle, based on the PMHS test setup [52]. For the first validation with mid-sized sedan, nodes corresponding to markers attached to the PMHS were defined in the pedestrian model at the head's center of gravity (CG) and about 60 mm behind of the T1 and sacrum due to the consideration of the screw length (Figure 4.5). In addition, an about 4.3 kg mass was added as four concentrated mass nodes rigidly to the M50-P lumbar spine (L1-L4) to maintain the total specimen body weight, which was the Telemetry Data Acquisition System (TDAS) bag attached to the PMHS [52]. Static/dynamic friction coefficients are defined as the average values reported in literature [55]: 0.26/0.25 (fabric-to-steel) for vehicle-to-pedestrian contact and 0.61/0.45 (fabric-to-fabric) for pedestrian-to-pedestrian contact. Before the M50-P model impacted by mid-sized sedan, the gravity acceleration was assigned to the whole-body and a force corresponding to its body weight was applied upward by the ground model to

initiate the foot-ground contact prior to the impact at about 5 ms in simulation. For the second validation with the simplified generic vehicles, nodes corresponding to markers attached to the PMHS were defined at the head, shoulder, T1, T4, T12, sacrum up, sacrum low, right knee and right ankle (Figure 4.6). Similar static/dynamic friction coefficients as in previous CPC validation were defined for vehicle-to-pedestrian contacts and for pedestrian-to-pedestrian contacts. The beginning and the end of the outputs were defined at the time of initial right leg-bumper contact and the initial time of the head-hood contact, respectively.

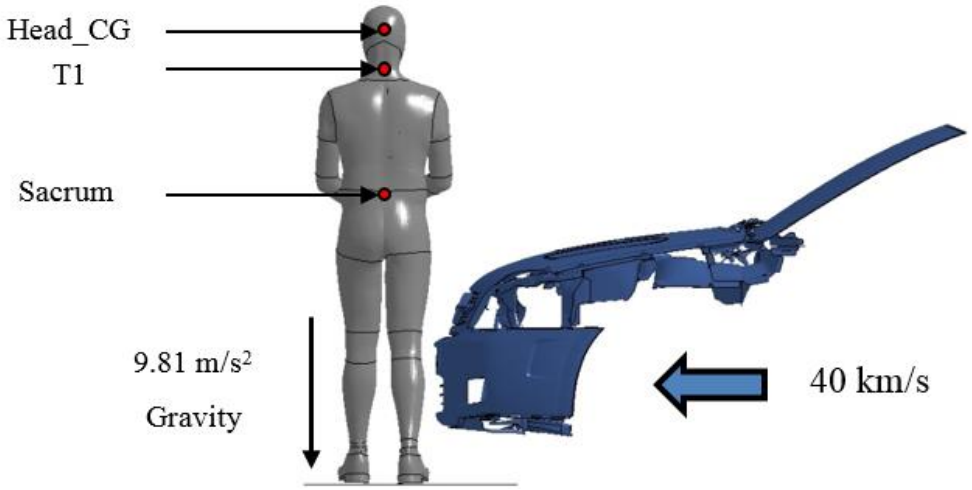

Figure 4.5 Whole-body validation setup with mid-sized sedan vehicle

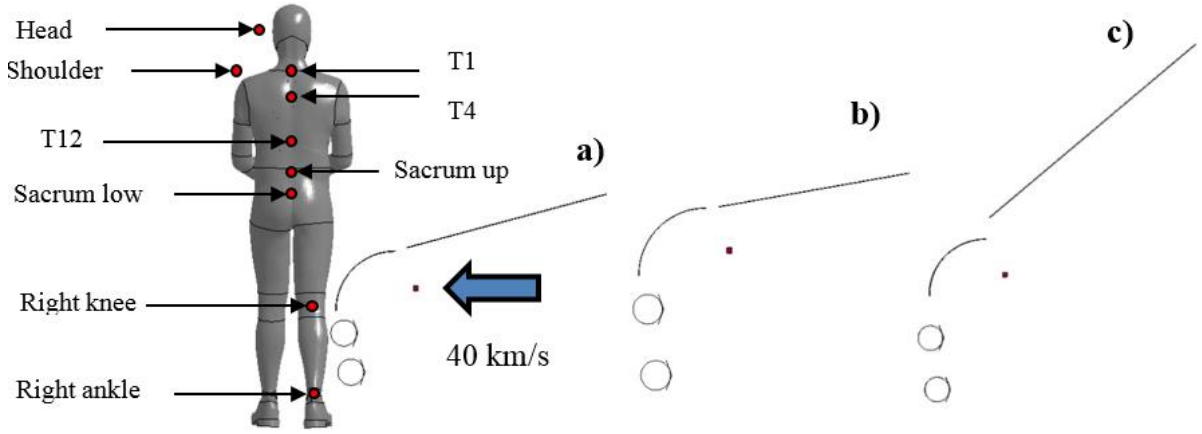

Figure 4.6. Whole-body validation setup with simplified generic vehicles; a) sedan, b) SUV and c) Van

4.3 RESULTS

Overall, the M50-P model comprised of a total number of 1,251,274 nodes and 2,324,738 elements (approximately 97 % deformable elements) significantly more precise than the simplified 50th percentile male pedestrian model (M50-PS), which has about 538,000 nodes and 827,000 elements (85% of deformable elements) [13].

4.3.1 Validation at Component Level

The knee bending stiffness of the M50-P model showed a relatively similar trend as the curves corresponding to the PMHS test data (Figure 4.7). It should be mentioned that the PMHS test curves were scaled to represent a 50th percentile adult male anthropometry [41]. In terms of the soft tissue injury, the M50-P model predicted the ruptures of Anterior Cruciate Ligament (ACL) and Medical Collateral Ligament (MCL) in a knee angle range from 10.5° to 15.5°. It should be mentioned that MCL ruptures were also observed in all PMHS tests in a range of knee angles from 10.5° to 18°.

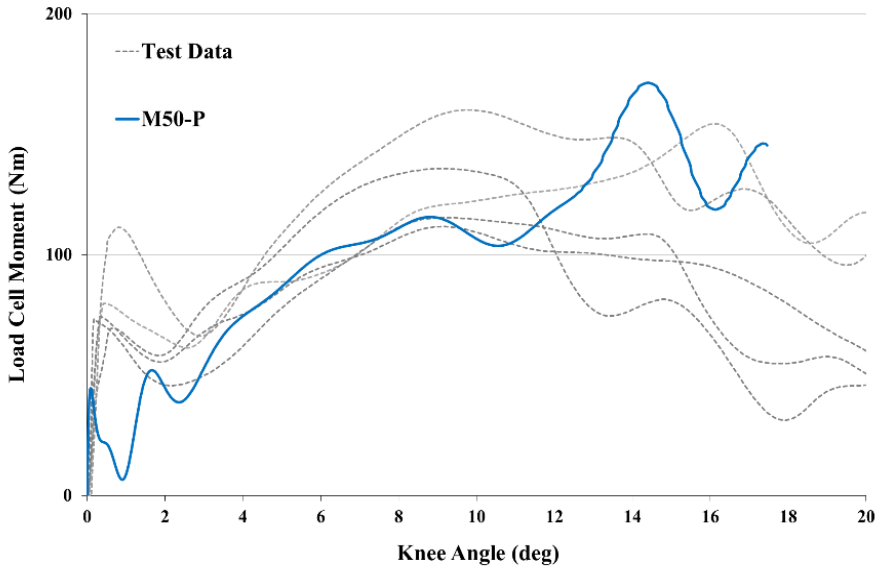

Figure 4.7 Load cell moment of knee joint under bending loading: PMHS tests vs. M50-P model

The angle of the right lower extremity, which was impacted first by the vehicle in CPC validations, was compared to the PMHS tests with the sedan, SUV and Van vehicles. Initially, the lower extremity angle showed a slight discrepancy between the M50-P and the PMHS responses. However, the overall magnitude and phase of the lower extremity angle were similar to the PMHS test data in all validations (Figure 4.8).

a)

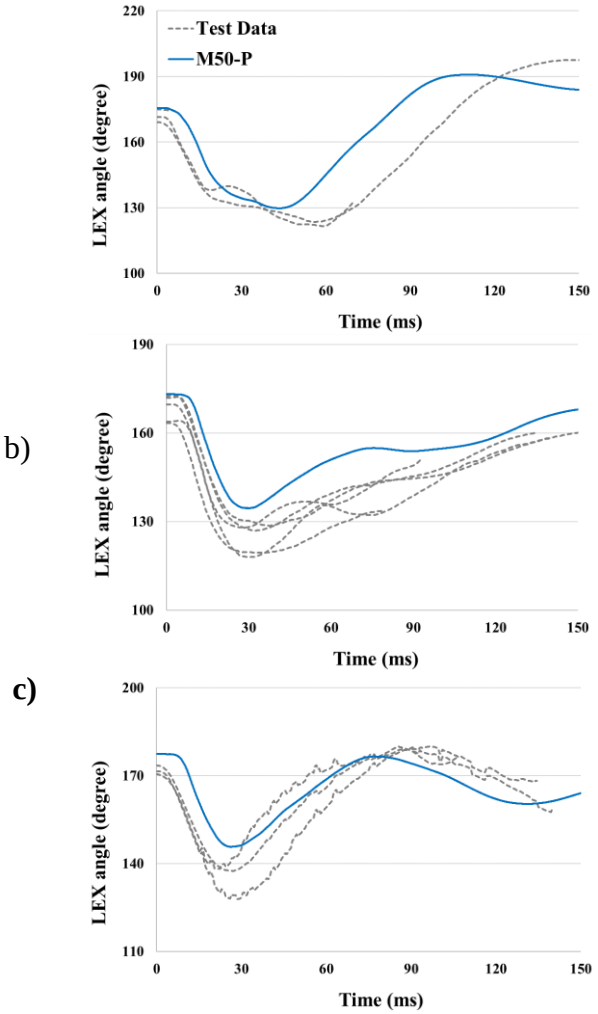

Figure 4.8. Angle of the right lower extremity (LEX) during impact: a) sedan, b) SUV, c) Van

The shoulder validation result of M50-P model under blunt lateral loading are mostly within the PMHS test corridor (Figure 4.9). However, the peak force predicted by M50-P model showed lower than that of the PMHS test corridor in both lower and higher impact velocities.

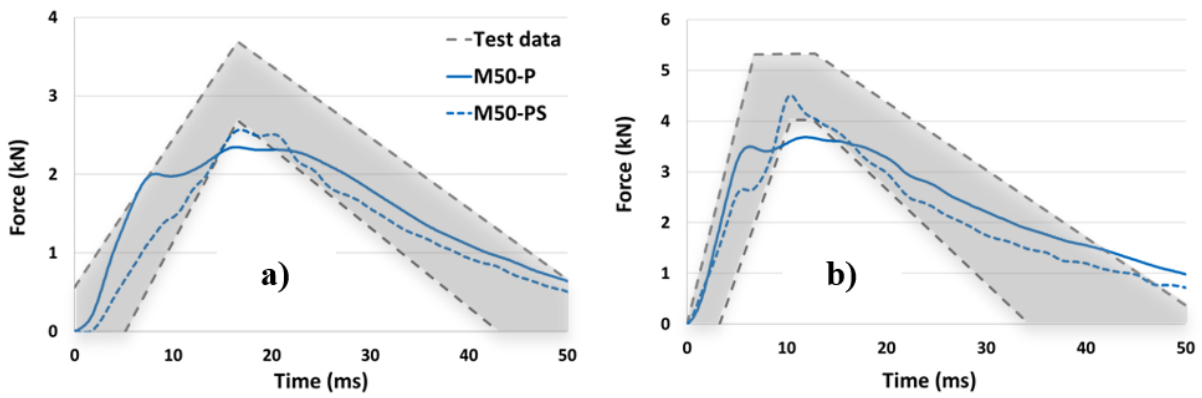

Figure 4.9 Time histories of impact force at shoulder: a) 4.5 m/s, b) 6.8 m/s initial impactor velocity

The impact force predicted by the M50-P model under pelvic lateral loading was close to the mean corridor at lower impact velocity (5.2 m/s). At higher impact velocity (9.8 m/s), the impact force was close to the mean corridor until it reached to the peak force then, a oscillation in FE response was observed between the lower and the upper boundary corridors (Figure 4.10).

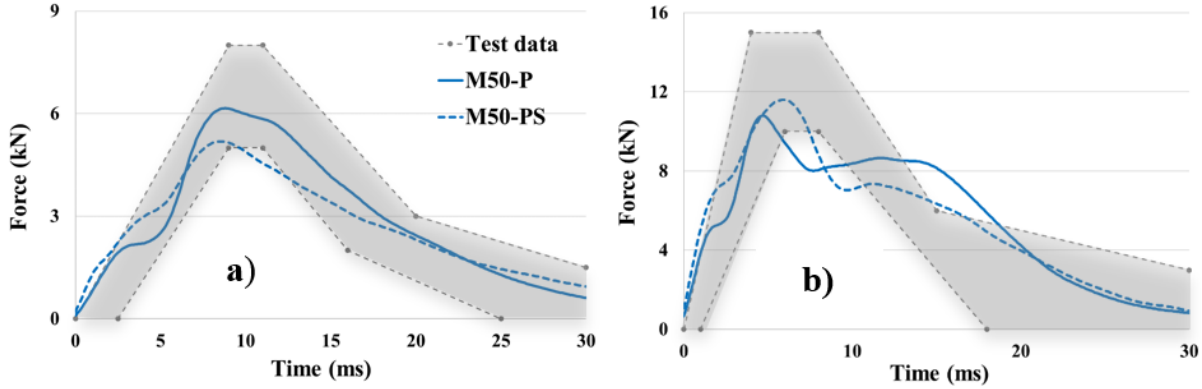

Figure 4.10 Time histories of impact force at pelvis: a) 5.2 m/s, b) 9.8 m/s initial impactor velocity

Overall, the upper-body validation responses predicted by the M50-P model were mostly within the PMHS test corridor (Figure 4.11-12). From the abdomen validations, the M50-P model predicted the responses close to the upper corridor until it reached to the peak force, and decreased to the lower corridor. In thorax validations, the impact force of the M50-P model, at lower impact velocity (4.4 m/s), was close to the mean test corridor. In higher velocities, the impact forces of M50-P model were close to the upper corridor, and then it started to decrease, being slightly out of the lower test corridors for a small time period (5-8 ms).

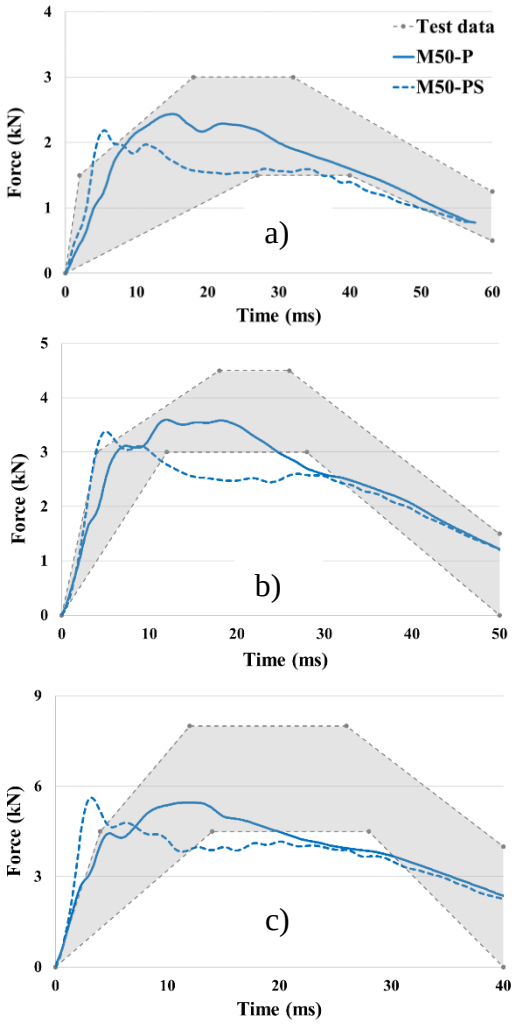

Figure 4.11 Time histories of impact force at abdomen: a) 4.8 m/s, b) 6.8 m/s, c) 9.4 m/s initial impactor velocity

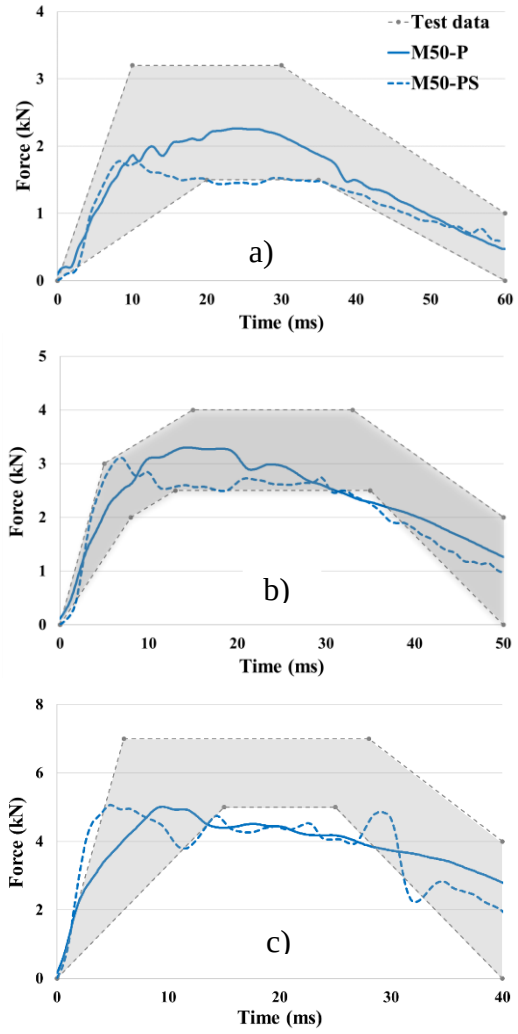

Figure 4.12 Time histories of impact force at thorax: a) 4.4 m/s, b) 6.5 m/s, c) 9.5 m/s initial impactor velocity

4.3.2 Validation in Car-to-Pedestrian Impact

The kinematic trajectories of the M50-P model relative to the mid-sized sedan were compared to PMHS test data [52]. The kinematics of M50-P model in coronal plane were close to the corresponding trajectories recorded on taller PMHS specimens (Figure 4.13). In comparison of the kinematic motion, the M50-P model predicted almost identical response as the T7 specimen, especially at the lower extremities and head kinematics (Figure 4.14). Additionally, the head contact to the vehicle time and the Wrap-Around-Distance (WAD) predicted by the M50-P model were close to the corresponding data recorded in the T7 specimen (Table A1, Appendix).

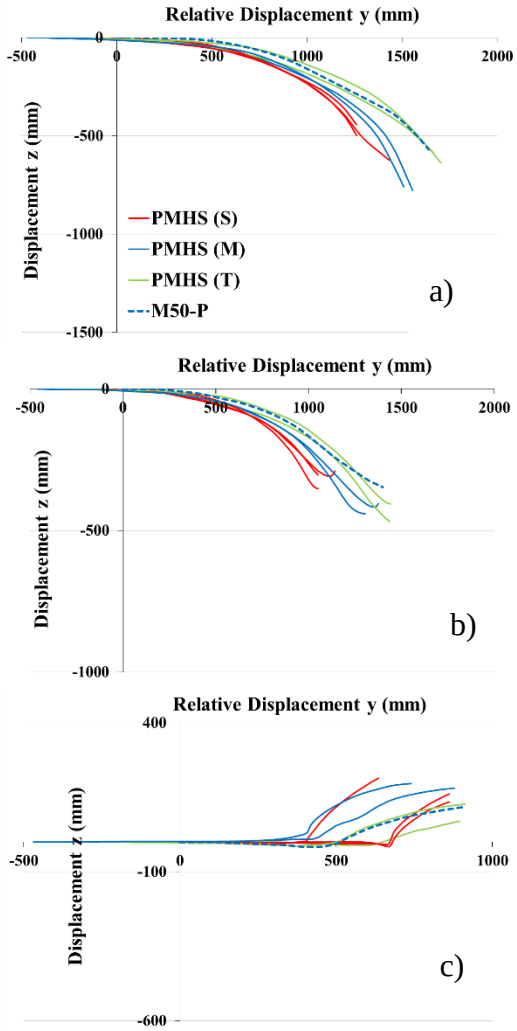

Figure 4.13 Kinematic trajectories relative to the mid-sized sedan: a) Head CG, b) T1, c) Sacrum, S: shorter, M: mid-size, T: Taller specimen

In terms of injury prediction, the M50-P model showed ruptures of the joint ligaments from the right knee (MCL/ACL) and the left knee (LCL/ACL). In addition, a right fibula fracture was observed in the M50-P model. While in one PMHS a MCL rupture was observed in the right knee as in the model, the tibia/fibula fractures were observed in other four PMHS. The typical injury pattern in PMHS tests in the left lower extremity was LCL/ACL ruptures (five tests) as in the pedestrian FE model. In addition, pelvic fractures were observed in all PMHS tests, except for the test of the tallest PMHS (T6).

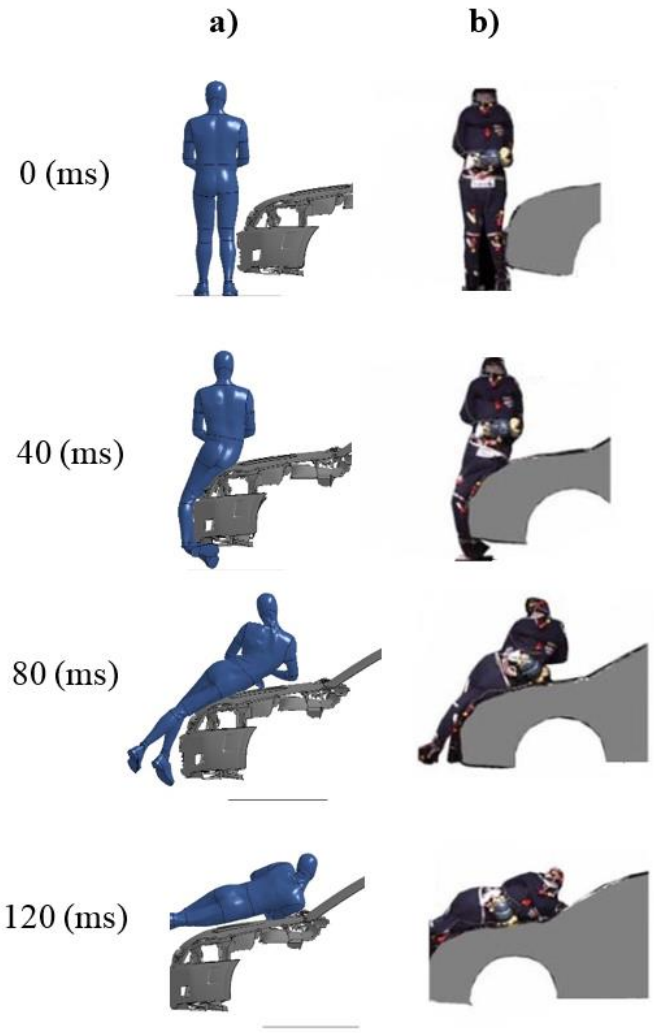

Figure 4.14 Comparison of the kinematic responses in video images for PMHS and animation for FE model: a) M50-P model and b) T7 specimen

The kinematic trajectories of the M50-P model relative to the simplified generic vehicles were compared to the scaled PMHS test data (Table A2, Appendix) [43]. Overall, a kinematics predicted by the M50-P model were similar to those of the scaled PMHS data (Figure 4.15 and Figure A1-3, Appendix). However, some discrepancies of kinematic responses between M50-P model and PMHS were observed especially at the knee with high bumper vehicles (SUV and Van).

In terms of injury, the M50-P model predicted similar results with respect to the ligament rupture and bone fracture compared to the PMHS data [43]. In the right lower extremity, 91% of MCL and 45% of ACL ruptures were reported in tests. With respect to the hard tissue injury, 63% of fibula and 18% of femur fractures were reported. The M50-P model predicted the rupture of MCL and ACL in all simulations. In addition, the femur and fibula fractures were predicted only from the sedan buck simulation.

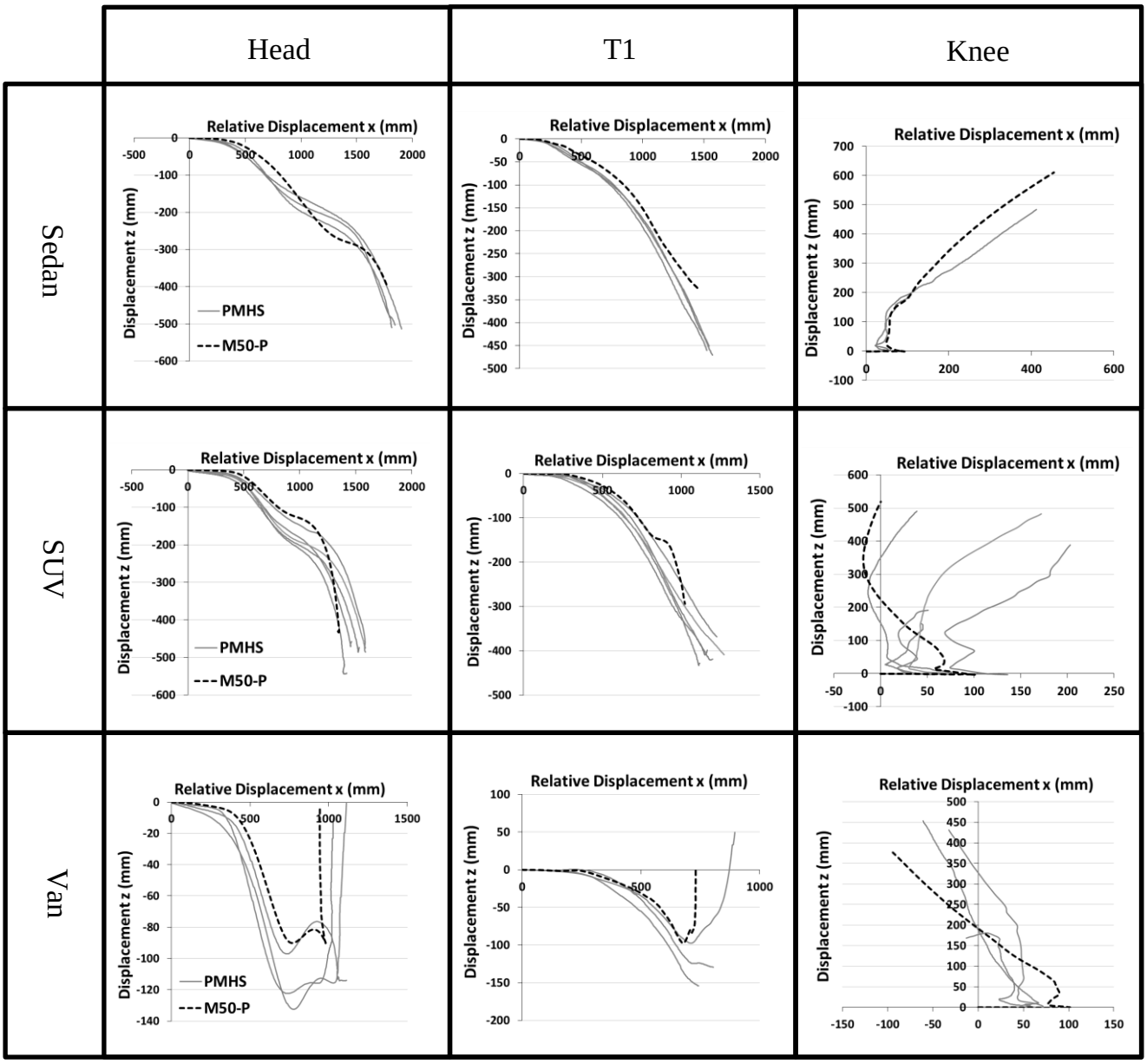

Figure 4.15 Kinematic trajectories of pedestrian during the CPC impact by the simplified generic vehicles: FE data vs. PMHS data

From the left lower extremity, 82% of LCL and 54% of ACL injuries were reported in tests. In addition, 18% of fibula fracture was observed. The M50-P model predicted the rupture of LCL and ACL in all simulations but no bone fracture. Lastly, the PMHS have 36% of sacral ala and 36% of acetabulum fractures. The M50-P model predicted pelvic bone fractures at sacral ala with SUV and Van simulations and right acetabulum fractures with all vehicles.

4.4 DISCUSSION

This study presents the development and validation of a detailed pedestrian FE model corresponding to a 50th percentile male anthropometry. This pedestrian FE model is distinct from previous models in two aspects. First, the model geometric data was reconstructed using a multimodality protocol from medical images and exterior scanned data corresponding to an average anthropometric male volunteer. The previous pedestrian FE models were developed using individuals with anthropometry that differed from a 50th percentile male [42, 56] or using commercial databases [8, 56], which possessed limitations (e.g. only exterior surfaces of bones). Second, this model was developed as a detailed version to predict kinetic/kinematic responses and can additionally predict crash-induced injuries in CPC accidents due to the modeling of the detailed structures of human body. While the detailed pedestrian FE model is not as computationally efficient as the simplified pedestrian FE model [13], it is capable of predicting biofidelic responses and injury biomechanics.

At the knee joint validation, the load cell bending moment, as predicted by the M50-P model, was lower than the PMHS test data until about 2°. This possibly caused by differences in the inertial properties of the test setup (model setup vs. physical setup). The knee joint stiffness of the M50-P model showed mainly similar responses but a higher peak value observed at about 15°. While this model was developed as a detailed version, the complexity of the human knee joint was not modelled explicitly. Improvement of the knee model may include improving the geometry of the knee capsule (which was approximated, not reconstructed from medical images), updating the material model of ligaments, and/or modeling the synovial fluid. In terms of injury, the M50-P model predicted MCL and ACL ruptures which are the most frequent injuries observed in all 40 PMHS knee bending tests (52.5% MCL ruptures and 10 % ACL & MCL ruptures) [41].

In the lower extremity validation during CPC impacts, the M50-P model predicted mostly similar magnitude and phase of the right knee angle (in coronal plane) against the PMHS results in all simulations. The discrepancy in the initial angle of the right lower extremity is likely caused by the anthropometric variation of tested specimens. To increase the model biofidelity regarding the lower extremity, the angle of the leg in sagittal plane is suggest to validate when the test data available. It should be mentioned that the M50-P model is currently the only one pedestrian model validated the knee angle during the CPC impact with different vehicles based on the most recent PMHS tests.

In shoulder validation, no fracture was observed by the M50-P model during the eight impacts with various impact velocities. From the PMHS tests, 13 out of 38 bone fractures (34%) were reported [46]. In pelvic lateral impact validation, a different pattern and lower peak value of impact force predicted by the M50-P model were observed in a higher impact velocity. It is believed that a more biofidelic material model of flesh based on the compressive test may improve the response

of the model in this loading condition. For the anterior-lateral impact responses on the thorax and abdomen, the M50-P model predicted more biofidelic responses compared to the simplified pedestrian FE model reported previously [13]. This better performance could be the effect of adding the internal organs into the rib cage of M50-P model that improved the damping properties of the upper body.

The kinematic responses of the whole-body pedestrian FE model in the mid-sized sedan CPC simulation predicted close not to the corresponding mid-size specimens, but taller specimens, as were classified by Kerrigan et al. [52]. In addition, the head contact to the vehicle and the WAD predicted by the M50-P model were close to the result of a T7 specimen (Table A1, Appendix). While the height of the M50-P model is close to the mid-size specimens (176.1 cm FE model vs. 172.9/174.3 cm specimens), there are some arguments to explain the current results. First, the gender difference and discrepancy of body weight (77.3 kg FE model vs. 90.6/92.9 kg female specimens) are possible factors for disagreement. Second, a larger height of the right Greater Trochanter (GT) for the M50-P model (907 mm) than that of mid-size specimens (802 and 826 mm) is also one of the important factors for disagreement. This is because the taller PMHS showed that the body began to slide up the hood after the pelvis contacted the hood, whereas the shorter PMHS observed the initiation of rotation of the body when the pelvis was pinned at the hood leading edge in testing [52]. Last, the boundary condition of contact between the whole-body and the vehicle possessed a potential discrepancy because the friction coefficient between the vehicle used in testing and the TYVEX body suit was not identified.

Since the shape of vehicle front-end may plays a major role regarding kinematics and injury outcomes in pedestrian accidents [57], a further validation with different vehicles in CPC scenario was also performed. The M50-P model kinematics showed mostly similar to those of the PMHS responses. However, some discrepancies of kinematics between M50-P and PMHS were observed. While the position of the generic vehicles was adjusted to each specimens in testing, a different pattern of kinematics may induced by differences of the long bone length (femur and tibia) and stiffness of knee joint. In addition, an average weight and height of PMHS specimens (69 kg and 1660 mm) has a gap compared to the M50-P model (77 kg and 1761 mm). While the PMHS data was scaled to take into account the anthropometric variation, previous studies showed that linear scaling approaches have significant limitations [58]. These limitations could be removed in future by development of subject specific pedestrian models based on the M50-P model.

In terms of injury prediction in mid-sized sedan CPC validation, the M50-P model showed some discrepancies compared to the PMHS test data. The higher risk of knee ligament injuries predicted by the model could be caused by the position of the pedestrian knee relative to the vehicle bumper/leading edge and/or the FE failure modeling approach. A higher knee height in the model than the PMHS mid-size specimens generated different loadings on the leg and might influence significantly leg injuries as it was reported previously in literature [59, 60]. In CPC validations with the simplified generic vehicles, the lower extremity injuries with respect to the soft tissue predicted by the M50-P model are similar to those of the PMHS tests reported by Song et al. [43]. However, a bone injury, such as crack and fracture, was not predicted accurately. As in previous pedestrian FE models, the element elimination was used to predict the injuries. However, it is known that this approach is mesh sensitive and cannot represent adequately the failure propagation and post-failure response of the FE model. Therefore, it is recommended in the future using improved numerical approaches of tissue failure as extended FE method or cohesive FE modeling

[61]. In addition, the bone parts were modeled with solid elements to represent to the trabecular bone and shell elements to represent to the cortical bone. Representing bone with these elements could disguise imperfections in the bone that could serve to initiate crack propagation, and accordingly, fracture of the bone is not accurate to predict. Hence, a more robust method to predict fracture initiation is recommended in the future. In addition, for a better comparison between FE and PMHS results, it is suggested morphing the detailed pedestrian model to the PMHS specific geometries before performing CPC simulations.

4.5 CONCLUSION

Overall, the M50-P model showed biofidelic responses based on the corresponding PMHS test data in both the component and whole-body validations. Additionally, promising capability to predict the injury risks of pedestrians during lateral vehicle impact was observed in the full-scale impact scenario. Compared to previous pedestrian models developed by various auto manufactures, which are proprietary, this detailed M50-P model will be publically available for academic researchers and could be used to better understand the pedestrian injury biomechanics.

ACKNOWLEDGEMENTS

All findings and views reported in this manuscript are based on the opinions of the authors and do not necessarily represent the consensus or view of the funding organization. Work was supported by the Global Human Body Models Consortium, LLC and NHSTA under GHBMC Project No.: WFU-006.

REFERENCE

[1] WHO, "Global status report on road safety," 2018.
[2] IIHS, "General statistics," 2016.
[3] NHTSA, "Traffic Safety Facts 2015," 2017.
[4] ANCAP, "ANCAP Assessment Protocol-Pedestrian Protection v9.0.2," 2018.
[5] CNCAP, "CNCAP Management Regulation," 2018.
[6] EuroNCAP, "Pedestrian Testing Protocol v8.5," 2019.
[7] JNCAP, "Pedestrian Head Protection Performance Test procedure," 2018.
[8] Y. Takahashi, Y. Kikuchi, A. Konosu, and H. Ishikawa, "Development and validation of the finite element model for the human lower limb of pedestrians," *Stapp car crash journal*, vol. 44, pp. 335-55, 2000.
[9] C. D. Untaroiu, J. B. Putnam, J. Schap, M. L. Davis, and F. S. Gayzik, "Development and preliminary validation of a 50th percentile pedestrian finite element model," in *ASME 2015 IDETC/CIE Conference*, Boston, MA, USA, 2015, p. 7.

[10] P. J. Arnoux, D. Cesari, M. Behr, L. Thollon, and C. Brunet, "Pedestrian lower limb injury criteria evaluation: a finite element approach," *Traffic Inj Prev,* vol. 6, pp. 288-97, Sep 2005.
[11] M. Iwamoto, K. Omori, H. Kimpara, Y. Nakahira, A. Tamura, I. Watanabe, *et al.*, "Recent Advances in THUMS: Development of Individual Internal Organs, Brain, Small Female, and Pedestrian Model," in *4th European LS-DYNA Conference*, Ulm (Germany), 2003.
[12] F. H. Mo, P. J. Arnoux, D. Cesari, and C. Masson, "Investigation of the injury threshold of knee ligaments by the parametric study of car-pedestrian impact conditions," *Safety Science,* vol. 62, pp. 58-67, Feb 2014.
[13] C. D. Untaroiu, W. Pak, Y. Meng, J. Schap, B. Koya, and S. Gayzik, "A Finite Element Model of a Midsize Male for Simulating Pedestrian Accidents," *J Biomech Eng,* vol. 140, Jan 1 2018.
[14] F. Gayzik, D. Moreno, K. Danelson, C. McNally, K. Klinich, and J. D. Stitzel, "External landmark, body surface, and volume data of a mid-sized male in seated and standing postures," *Annals of biomedical engineering,* vol. 40, pp. 2019-2032, 2012.
[15] C. C. Gordon, T. Churchill, C. E. Clauser, B. Bradtmiller, and J. T. McConville, "Anthropometric survey of US army personnel: methods and summary statistics 1988," DTIC Document1989.
[16] F. Gayzik, D. Moreno, C. Geer, S. Wuertzer, R. Martin, and J. Stitzel, "Development of a full body CAD dataset for computational modeling: a multi-modality approach," *Annals of biomedical engineering,* vol. 39, p. 2568, 2011.
[17] H. Mao, L. Zhang, B. Jiang, V. V. Genthikatti, X. Jin, F. Zhu, *et al.*, "Development of a Finite Element Human Head Model Partially Validated With Thirty Five Experimental Cases," *Journal of biomechanical engineering,* vol. 135, p. 111002, 2013.
[18] E. G. Takhounts, M. J. Craig, K. Moorhouse, J. McFadden, and V. Hasija, "Development of Brain Injury Criteria (BrIC)," *Stapp car crash journal,* vol. 57, pp. 243-266, 2013.
[19] T. Yanaoka and Y. Dokko, "A Parametric Study of Age-Related Factors Affecting Intracranial Responses under Impact Loading Using a Human Head/Brain FE Model," presented at the International Research Council on Biomechanics Injury (IRCOBI), Gothenburg, Sweeden, 2013.
[20] J. A. DeWit and D. S. Cronin, "Cervical spine segment finite element model for traumatic injury prediction," *Journal of the mechanical behavior of biomedical materials,* vol. 10, pp. 138-150, 2012.
[21] J. B. Fice, D. S. Cronin, and M. B. Panzer, "Cervical spine model to predict capsular ligament response in rear impact," *Annals of biomedical engineering,* vol. 39, pp. 2152-2162, 2011.
[22] S. F. Mattucci, J. A. Moulton, N. Chandrashekar, and D. S. Cronin, "Strain rate dependent properties of younger human cervical spine ligaments," *Journal of the mechanical behavior of biomedical materials,* vol. 10, pp. 216-226, 2012.
[23] S. F. Mattucci, J. A. Moulton, N. Chandrashekar, and D. S. Cronin, "Strain rate dependent properties of human craniovertebral ligaments," *Journal of the mechanical behavior of biomedical materials,* vol. 23, pp. 71-79, 2013.
[24] Z. Li, M. W. Kindig, J. R. Kerrigan, C. D. Untaroiu, D. Subit, J. R. Crandall, *et al.*, "Rib Fractures Under Anterior-Posterior Dynamic Loads: Experimental and Finite-Element Study," *Journal of Biomechanics,* vol. 43, p. 228.234, 2010.

[25] Z. Li, M. W. Kindig, D. Subit, and R. W. Kent, "Influence of mesh density, cortical thickness and material properties on human rib fracture prediction," *Medical engineering & physics,* vol. 32, pp. 998-1008, 2010.
[26] D. Poulard, R. Kent, M. Kindig, Z. Li, and D. Subit, "Thoracic response targets for a computational model: A hierarchical approach to asses the biofidelity of a 50th-percentile occupant male finite element model," *J Mech Behav Biomed Mater,* 2015.
[27] A. Soni and P. Beillas, "Modelling hollow organs for impact conditions: a simplified case study," *Comput Methods Biomech Biomed Engin,* vol. [Epub ahead of print], Oct 24 2013.
[28] Y. H. Kim, J. E. Kim, and A. W. Eberhardt, "A new cortical thickness mapping method with application to an in vivo finite element model," *Comput Methods Biomech Biomed Engin,* vol. 17, pp. 997-1001, Oct 31 2012.
[29] C. D. Untaroiu, N. Yue, and J. Shin, "A finite element model of the lower limb for simulating automotive impacts," *Ann Biomed Eng,* vol. 41, pp. 513-26, Mar 2013.
[30] N. Yue and C. D. Untaroiu, "A numerical investigation on the variation in hip injury tolerance with occupant posture during frontal collisions," *Traffic Injury Prevention,* vol. 15, pp. 513-522, 2014.
[31] N. Yue, J. Shin, and C. Untaroiu, "Development and validation of an occupant lower limb finite element model.," in *SAE Technical Paper* vol. 2011-01-1128, ed, 2011.
[32] A. R. Hayes, N. A. Vavalle, D. P. Moreno, J. D. Stitzel, and F. S. Gayzik, "Validation of simulated chestband data in frontal and lateral loading using a human body finite element model," *Traffic Inj Prev,* vol. 15, pp. 181-6, 2014.
[33] N. A. Vavalle, A. B. Thompson, A. R. Hayes, D. P. Moreno, J. D. Stitzel, and F. S. Gayzik, "Investigation of the Mass Distribution of a Detailed Seated Male Finite Element Model," *J Appl Biomech,* vol. [Epub ahead of print], Dec 17 2013.
[34] G. Park, T. Kim, J. R. Crandall, C. Arregui-Dalmases, and J. Luzon-Narro, "Comparison of Kinematics of GHBMC to PMHS on the Side Impact Condition," presented at the International Research Council on Biomechanics of Injury, Gothenburg, Sweden, 2013.
[35] N. A. Vavalle, M. L. Davis, J. D. Stitzel, and F. S. Gayzik, "Quantitative Validation of a Human Body Finite Element Model Using Rigid Body Impacts," *Annals of Biomedical Engineering,* pp. 1-12, 2014.
[36] N. A. Vavalle, B. C. Jelen, D. P. Moreno, J. D. Stitzel, and F. S. Gayzik, "An evaluation of objective rating methods for full-body finite element model comparison to PMHS tests," *Traffic Inj Prev,* vol. 14 Suppl, pp. S87-94, 2013.
[37] N. A. Vavalle, D. P. Moreno, A. C. Rhyne, J. D. Stitzel, and F. S. Gayzik, "Lateral impact validation of a geometrically accurate full body finite element model for blunt injury prediction," *Ann Biomed Eng,* vol. 41, pp. 497-512, Mar 2013.
[38] GHBMC, "User Manual: M50 Occupant Version 4.3 for LS-DYNA," 2014.
[39] M. L. Davis, B. Koya, J. M. Schap, and F. S. Gayzik, "Development and Full Body Validation of a 5th Percentile Female Finite Element Model," *Stapp Car Crash J,* vol. 60, pp. 509-544, Nov 2016.
[40] G. Teresiński and R. Mądro, "Knee joint injuries as a reconstructive factors in car-to-pedestrian accidents," *Forensic science international,* vol. 124, pp. 74-82, 2001.
[41] D. Bose, K. S. Bhalla, C. D. Untaroiu, B. J. Ivarsson, J. R. Crandall, and S. Hurwitz, "Injury tolerance and moment response of the knee joint to combined valgus bending and shear loading," *J Biomech Eng,* vol. 130, p. 031008, Jun 2008.

[42] C. Untaroiu, K. Darvish, J. Crandall, B. Deng, and W. Jenne-Tai, "A finite element model of the lower limb for simulating pedestrian impacts," *Stapp car crash journal,* vol. 49, p. 157, 2005.
[43] E. Song, J. Uriot, P. Potier, D. Dubois, P. Petit, X. Trosseille, *et al.*, "Reference PMHS Tests to Assess Whole-Body Pedestrian Impact Using a Simplified Generic Vehicle Front-End," in *IRCOBI Conference Proceedings*, 2017.
[44] EuroNCAP, "Technical Bulletins 024 - Pedestrian Human Model Certification v1.1," 2019.
[45] J.-L. Martin, A. Lardy, and B. Laumon, "Pedestrian injury patterns according to car and casualty characteristics in France," in *55th AAAM Annual Conference Annals of Advances in Automotive Medicine*, 2011.
[46] S. W. Koh, J. M. Cavanaugh, M. J. Mason, S. A. Petersen, D. R. Marth, S. W. Rouhana, *et al.*, "Shoulder injury and response due to lateral glenohumeral joint impact: an analysis of combined data," *Stapp Car Crash J,* vol. 49, pp. 291-322, Nov 2005.
[47] J. H. Bolte IV, M. H. Hines, R. G. Herriott, J. D. McFadden, and B. R. Donnelly, "Shoulder impact response and injury due to lateral and oblique loading," *Stapp car crash journal,* vol. 47, p. 35, 2003.
[48] J. H. Bolte, M. H. Hines, J. D. McFadden, and R. A. Saul, "Shoulder response characteristics and injury due to lateral glenohumeral joint impacts," *Stapp car crash journal,* vol. 44, pp. 261-280, 2000.
[49] S. Compigne, Y. Caire, T. Quesnel, and J.-P. Verries, "Non-injurious and injurious impact response of the human shoulder three-dimensional analysis of kinematics and determination of injury threshold," *Stapp car crash journal,* vol. 48, pp. 89-123, 2004.
[50] D. R. Marth, "Biomechanics of the shoulder in lateral impact," MS Thesis, Wayne State University, 2002.
[51] D. C. Viano, "Biomechanical responses and injuries in blunt lateral impact," SAE Technical Paper 0148-7191, 1989.
[52] J. R. Kerrigan, J. R. Crandall, and B. Deng, "Pedestrian kinematic response to mid-sized vehicle impact," *International journal of vehicle safety*, vol. 2, pp. 221-240, 2007.
[53] R. Fredriksson, E. Rosén, and A. Kullgren, "Priorities of pedestrian protection—a real-life study of severe injuries and car sources," *Accident analysis & prevention,* vol. 42, pp. 1672-1681, 2010.
[54] J. R. Kerrigan, D. P. Parent, C. Untaroiu, J. R. Crandall, and B. Deng, "A new approach to multibody model development: pedestrian lower extremity," *Traffic Inj Prev,* vol. 10, pp. 386-97, Aug 2009.
[55] V. Kothari and M. Gangal, "Assessment of frictional properties of some woven fabrics," 1994.
[56] R. Watanabe, T. Katsuhara, H. Miyazaki, Y. Kitagawa, and T. Yasuki, "Research of the relationship of pedestrian injury to collision speed, car-type, impact location and pedestrian sizes using human FE model (THUMS Version 4)," *Stapp car crash journal,* vol. 56, pp. 269-321, 2012.
[57] Y. Han, J. Yang, K. Mizuno, and Y. Matsui, "Effects of vehicle impact velocity, vehicle front-end shapes on pedestrian injury risk," *Traffic injury prevention*, vol. 13, pp. 507-518, 2012.
[58] C. D. Untaroiu, J. Shin, J. R. Crandall, R. Fredriksson, O. Bostrom, Y. Takahashi, *et al.*, "Development and validation of pedestrian sedan bucks using finite-element simulations: a numerical investigation of the influence of vehicle automatic braking on the kinematics

of the pedestrian involved in vehicle collisions," *International Journal of Crashworthiness*, vol. 15, pp. 491-503, 2010.

[59] Y. Okamoto, T. Sugimoto, K. Enomoto, and J. Kikuchi, "Pedestrian head impact conditions depending on the vehicle front shape and its construction--full model simulation," *Traffic injury prevention,* vol. 4, pp. 74-82, 2003.

[60] C. Untaroiu, J. Shin, J. Ivarsson, J. Crandall, Y. Takahashi, A. Akiyama, *et al.*, "Pedestrian kinematics investigation with finite element dummy model based on anthropometry scaling method," in *Proc. 20th Int. Technical Conf. Enhanced Safety of Vehicle*, 2007.

[61] C. D. Untaroiu, Y. C. Lu, S. K. Siripurapu, and A. R. Kemper, "Modeling the biomechanical and injury response of human liver parenchyma under tensile loading," *Journal of the Mechanical Behavior of Biomedical Materials,* vol. 41, pp. 280-291, Jan 2015.

Chapter 5

Pedestrian Biomechanical and Injury Responses regarding Pre-Impact Posture and Vehicle Type

Manuscript in preparation

ABSTRACT

Pedestrians are the most vulnerable road users and 2018 reported the highest number of pedestrian fatalities number in nearly three decades. In this study, five computational human body models, representing 50th percentile male in gait cycle, were developed. Using these models, the Car-to-Pedestrian Collision (CPC) impact simulations were performed with four generic vehicle finite element (FE) models representing the family car, roadster, multi-purpose vehicle, and sport utility vehicle in order to investigate the pedestrian kinetic/kinematic responses in various accident scenarios. In the impacts with the high-profile vehicles (MPV and SUV), the pedestrian models usually slide above the bonnet leading edge and shorter wrap around distance (WAD) was observed than in the case of the low-profile vehicles (FCR and RDS). The pedestrian postures showed to influence the post-impact rotation of the pedestrian and consequently, the impacted head region. The pedestrian posture also influenced the risk of injuries in the lower extremities. Higher risk of knee ligament injuries were observed in the swing phase posture compared to the stance phase, in which higher bending moments were observed. The findings of this study should be taken into consideration when examining pedestrian protection protocols. In addition, the results of this study can be used to improve the design of active safety systems used to protect pedestrians in collisions.

5.1 INTRODUCTION

Currently, road traffic crashes are represent the eighth leading cause of death across all age groups in the world. According to the World Health Organization (WHO), the number of road traffic fatalities continues to rise steadily and reached more than 1.35 million each year, and has caused up to 50 million injuries [1]. Between 2008 and 2018, the United States experienced a 41 % increase in pedestrian fatalities, while the number of all other traffic deaths decreased by 6 % [2-4]. In 2018, the number of pedestrians killed in motor vehicle crashes was 6,227, the highest number in nearly three decades [2].

In vehicle-pedestrian interactions, the pedestrian biomechanical and injury responses are heavily affected by various pre-impact conditions including: height of the hip-point (H-point), upper extremity posture, and vehicle type. Variations in height of the H-point during gait may result in

different pelvic-vehicle hood interactions, potentially altering pedestrian injury responses. Upper extremity position has an effect on whole-body kinematics and leads to variations in head contact time [5-7]. In terms of the vehicle type, the kinetic/kinematic responses of the pedestrian in a Car-to-Pedestrian Collision (CPC) depends on the shape of the vehicle's front-end. In 2017, nearly 89 % of pedestrian fatalities were caused by front impact with passenger cars and light trucks [3]. The majority of passenger cars impact the pedestrian's below their center of gravity, but larger or taller vehicles such as: Light trucks and Vans (LTV), Sport Utility Vehicles (SUV), and Multi-Purpose Vehicles (MPV) can impact the pedestrian at or above their center of gravity resulting in different biomechanical responses [8]. For example, LTV-to-pedestrian crashes pose higher head and chest injury risks and report higher pedestrian fatalities than passenger car-to-pedestrian collisions [9, 10]. Thereby, it is critical to investigate the relationships between different pre-impact conditions and the associated pedestrian injury risks in order to protect pedestrians in traffic accidents.

CPC studies have examined the effect of pedestrian posture and vehicle type in vehicle-pedestrian interactions using Post Mortem Human Surrogate (PMHS), a multibody pedestrian model (MADYMO), and computational human body model. Each of these studies' research techniques have critical limitations in examining the influence of the pedestrian gait and vehicle type in biomechanical and injury responses. Physical testing with PMHS provides reliable and valuable information but the testing is expensive, un-repeatable, and subjects are not available in various anthropometries. Furthermore, PMHS have a very limited number of collision scenarios that can be analyzed due to tissue break down and model positioning complications. In PMHS based pedestrian studies, the subject's upper extremities were usually tied together to minimize the potential effect of varying upper-body kinematics on whole-body responses to ensure repeatable kinematics [11, 12]. In studies using the MADYMO model, which consists of ellipsoid rigid bodies, the model kinematics generally showed some overall agreement with the PMHS test data across various impact conditions [13, 14]. However, the contact modelling issues of multibody models and their difficulties to investigate injury prediction based on strain/stress criteria rise some questions regarding their accuracy levels. Lastly, Li et al. conducted a study using a computational human body model to investigate the influence of gait in pedestrian accidents [15]. However, only the positions of the lower extremities were considered and the upper extremity posture was not accounted for.

To properly investigate the influence of pedestrian gait and vehicle type in vehicle-pedestrian interactions, the test subject must be reproducible, cost-effective, and respond in a similar fashion to a living human. Therefore, the Global Human Body Models Consortium (GHBMC) pedestrian human body finite element (FE) model was used in this study. This model has been developed and validated against PMHS test data at the component and whole-body level. To evaluate the effect of pedestrian posture in gait and vehicle type on pedestrian biomechanical and injury responses, the GHBMC 50th percentile male pedestrian (M50-PS) FE model was subjected to change its posture, including upper and lower extremities. Then, four different vehicle FE models were used to investigate the effect of vehicle front-end shape in CPC scenarios.

5.2 METHODS

5.2.1 Development and Validation of the 50th Percentile Male Pedestrian Finite Element Model

The M50-PS model was developed based on the GHBMC 50th percentile male detailed occupant (M50-O) model. The geometry of the M50-O model, such as the Computer Aided Design (CAD) data, was independently meshed and validated by researchers from various institutions. The component validations included models of the head [16-18], neck [19-22], thorax [23-25], abdomen [26], pelvis [27] and lower extremity [28-31]. The regional models were integrated into one full body occupant model and further validated [32-35]. After all validations against 17 various frontal and lateral impact tests [36], the mesh of the M50-PS model was mostly adopted from the M50-O model. Additional validation of the M50-PS model were performed at the component level (knee joint, shoulder, pelvis, thorax, and abdomen) against loading condition corresponding to pedestrian accidents. Finally, the whole-body M50-PS model was validated in a CPC impact scenario against PMHS test data [37]. The kinematic response of the M50-PS model in CPC simulation was close to the corresponding response of the mid-sized PMHS specimens. Recently, this GHBMC M50-PS model was accepted by the Euro NCAP, as listed in the Technical Bulletin (TB) 013 and pedestrian testing protocol [38, 39].

5.2.2 Positioning of the pedestrian model

To investigate the influence of gait posture on the pedestrian kinematics and injury outcomes, five pedestrian models in different postures were developed from the original M50-PS model. The pedestrian walking posture were defined based on the gait functions of joint angles and the height of the H-point reported in previous study [40]. The GHBMC M50-PS model was positioned in five different posture corresponding to 0, 20, 40, 60, and 80 % of the gait cycle.

The shoulder, elbow, hip, knee, and ankle joints were subjected to modification in each gait cycle model. To calculate these angles, anatomic landmarks for the pedestrian FE model were defined based on the recommendations of the International Society of Biomechanics (ISB) [41, 42]. The shoulder angle was defined as the angle between the horizontal plane and the humerus axis. The elbow angle was defined as the angle between the humerus reference axis and the connection between the midpoint of the medial epicondyle (EM) and the lateral epicondyle (EL) and the most caudal-medial point on the ulnar styloid (US). The humerus reference axis was defined as the connection between two points: SC and HM. The point SC was defined as the midpoint of the most latero-dorsal point of the angulus acromialis (AA) and the most ventral point of the processus coracoideus (PC). Similarly, HM was defined as the midpoint of the most caudal-lateral point on the EL and the most caudal-medial point on the EM. The hip angle was defined as the angle between the horizontal plane and the femur reference axis. The femur reference axis was defined as the connection between the center of the nodes of the acetabulum and the midpoint (F) between the epicondylus femoralis medialis (FEM) and the epicondylus femoralis lateralis (FEL). The knee angle was defined between the femur reference axis and the midpoint (M) between the tip of the medial malleolus (MM) and tip of the lateral malleolus (LM). The ankle angle was defined between the axis of the F and M and the axis of the two points at frontal and rear of the shoe sole, which are close to the second metatarsal and calcaneus bone, respectively (Figure 5.1). The target angles for each gait are provided in Table 5.1.

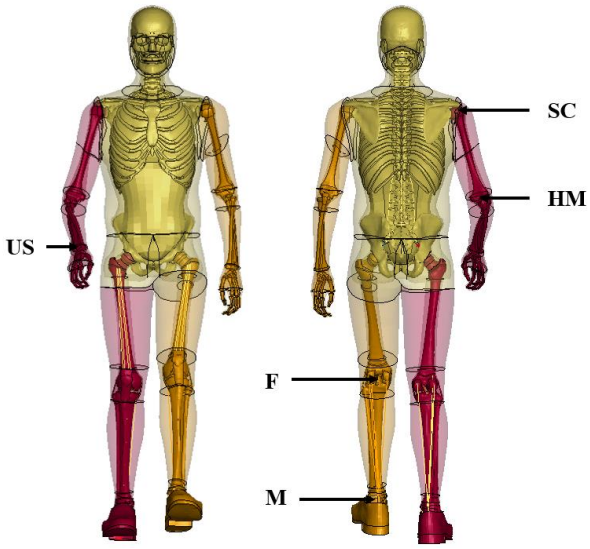

Figure 5.1 The anatomic landmarks on the M50-PS model (40 % gait cycle)

The whole process of changing pedestrian posture was mainly performed in PIPER open source software (v1.0.2, www.piper-project.org) [43], but some manual adjustments were required to improve the mesh quality of the models by using the Hypermesh software (Altair Engineering, Troy, MI).

Table 5.1 Angle at each of joint in the gait cycle [40]

Gait cycle (%)	Shoulder (L/R) (degrees)	Elbow (L/R) (degrees)	Hip (L/R) (degrees)	Knee (L/R) (degrees)	Ankle (L/R) (degrees)
0	97.3 / 68.7	140.8 / 138.8	75.6 / 112.5	173.4 / 174.1	78.7 / 86.9
20	86.8 / 80.6	145.6 / 145.9	103.9 / 100.4	121.9 / 164.0	94.9 / 85.0
40	71.5 / 95.8	39.3 / 143.2	114.1 / 78.9	165.1 / 170.6	83.8 / 74.8
60	72.1 / 93.0	142.9 / 140.9	111.6 / 85.8	163.9 / 128.1	90.6 / 101.4
80	87.8 / 78.8	142.9 / 144.0	88.4 / 112.7	173.2 / 133.4	81.4 / 81.7
100	97.3 / 68.7	140.8 / 138.8	75.5 / 112.5	173.4 / 174.1	78.7 / 86.9

5.2.3 Generic vehicle FE models

Pedestrian kinematics and injury responses are accurate and reliable when computational CPC simulations are performed using validated full-scale vehicle FE models. Unfortunately, automotive companies rarely release their vehicle FE models publically because of the proprietary nature of the model. Even if these models were readily available, researchers would have difficulty using them because of the enormous computational cost associated with these incredibly sophisticated FE models. Therefore, four publically available FE models of generic vehicles [44] were used in this research (Figure 5.2). The geometries of the generic vehicles that correspond to the Family Car/Sedan (FCR), Roadster (RDS), Multi-Purpose Vehicle (MPV), and Sport Utility Vehicle (SUV) were parameterized based on outer structures provided by European car manufacturers. After model development, generic vehicles were calibrated and validated based on the target curves of structural behavior obtained from impactor simulations run with the current European car FE models that were validated for pedestrian protection tests. These four generic vehicle FE models, comprised of a spoiler, bumper, grill, bonnet leading, bonnet, and windshield, could be used in CPC simulations in order to drastically reduce the computational cost and obtain reliable results.

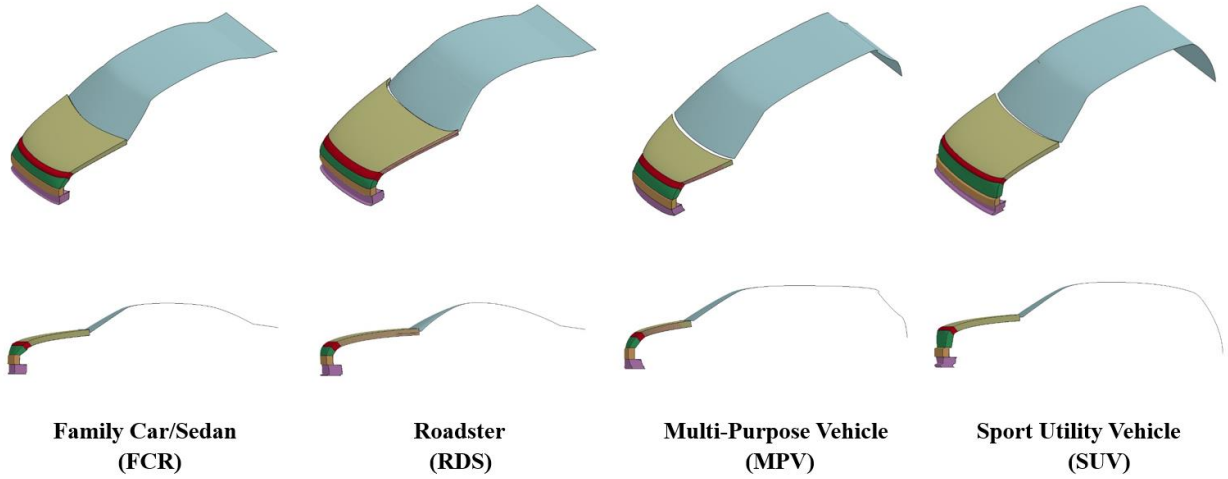

Figure 5.2 Overview of the generic vehicle FE models

5.2.4 Car-to-Pedestrian Collision simulation setup

To investigate pedestrian kinematics and injury outcomes with respect to posture and vehicle type, CPC scenarios were simulated using the four different generic vehicles and the whole-body M50-PS model in the five different gait postures (0, 20, 40, 60, and 80 % of gait cycle). The pedestrian models were positioned laterally at the vehicle centerline and the right leg was impacted first by a generic vehicle with a 40 km/h velocity (Figure 5.3). This configuration is the most frequent CPC impact scenario. According to the Pedestrian Crash Data Study (PCDS) data, about 70 % of pedestrian were impacted by vehicles laterally [11, 45]. Before impact, gravity was assigned to the whole-body pedestrian model and a force corresponding to its body weight was applied upward by the ground for the initial contact between the pedestrian and ground. The static/dynamic coefficient of friction between the pedestrian's shoes and ground was defined as 0.8/0.65, which are in the range of rubber-to-dry asphalt friction coefficient data reported in ligature (from 0.5 to 0.8) [46, 47]. For the pedestrian and vehicle-pedestrian contact, the static/dynamic coefficient of

friction was defined as average data reported in literature [48]: 0.26/0.25 (fabric-to-steel) for vehicle-to-pedestrian contact and 0.61/0.45 (fabric-to-fabric) for pedestrian-to-pedestrian contact. The start and the end of the outputs were defined at the time of initial vehicle-pedestrian contact and the time of initial vehicle-pedestrian head contact, respectively.

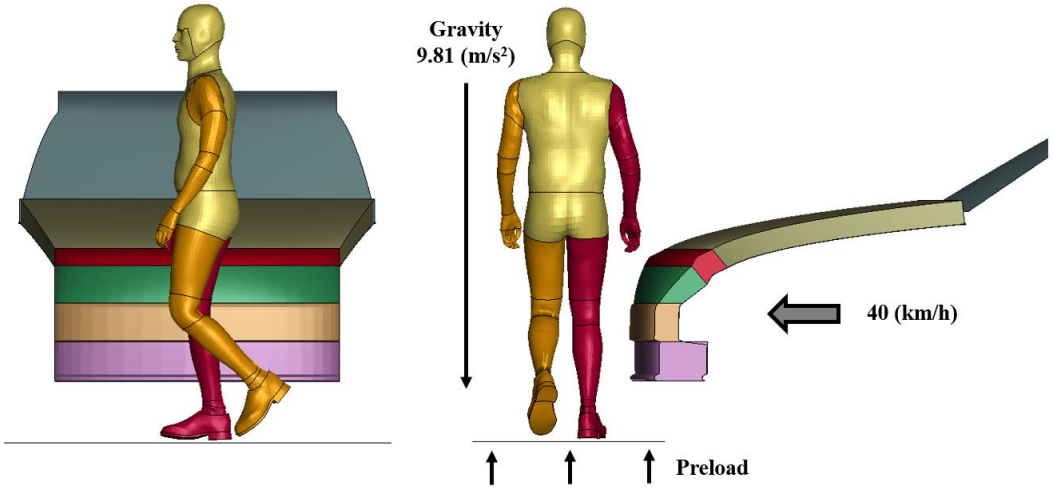

Figure 5.3 Overview of the CPC impact simulations setup (20 % gait with FCR)

To predict the pedestrian injury response, the bending moments at center of the length of femur and tibia were recorded. To reduce the noise and avoid unrealistic values, all bending moments were filtered with the SAE 180 Hz. In addition, to predict soft tissue injury at the knee joint, the knee angles of both legs were recorded during CPC impact. The knee angle was measured between the mid of femur, the F point, and the mid of tibia in the coronal plane (Figure 5.1). While the location and time of the initial head contact to the vehicle were identified in each CPC simulation, the values of head injury data was not calculated mainly due to modeling inaccuracies of the windshield (a frequent vehicle region impacted by the pedestrian's head). The M50-PS model in gait postures have assigned failure criteria in lower extremities (e.g. bone and knee ligaments) and they could predict injuries using an element elimination approach. However, this approach has some limitations in terms of failure propagation and post injury behavior, so it was turned off in CPC simulations. Instead of this approach, the risk of failure was estimated based on structural parameters such as the maximum bending moments in mid-thigh/leg and maximum valgus knee angle.

5.3 RESULTS

Joint angles of all five pedestrian models are within ±5° tolerance from the target joint angles (Figure 5.4). The models show good stability in the all CPC simulations.

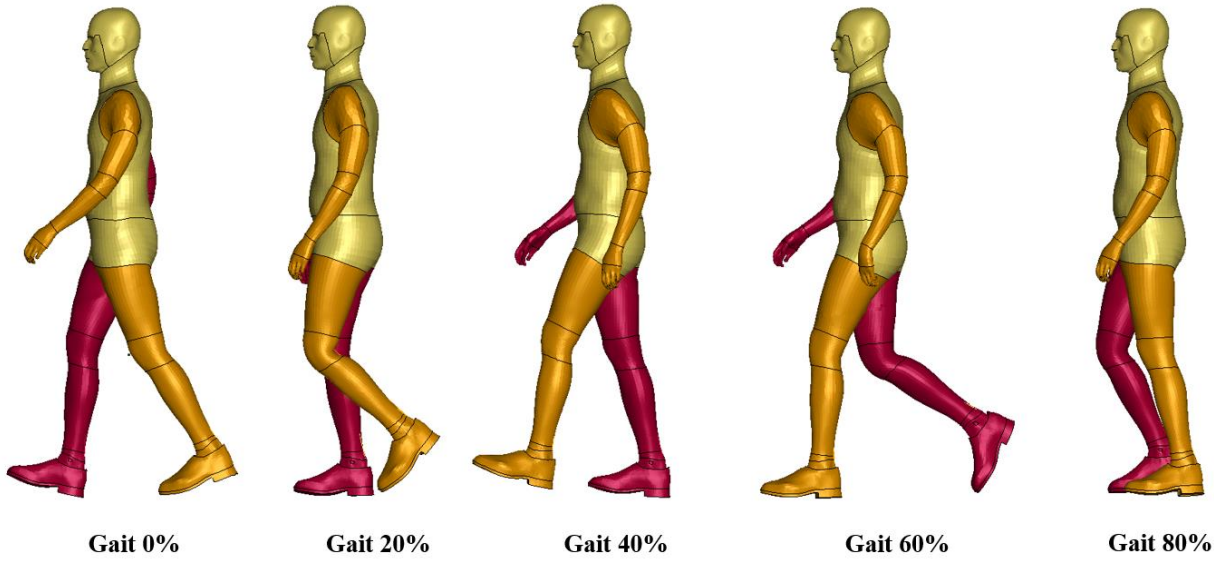

Figure 5.4 M50-PS finite element models in gait cycle

The M50-PS models in gait predicted different kinematic responses when posture and vehicle type were varied. When the pedestrian was impacted by the high-profile vehicles (MPV and SUV), shorter wrap around distance (WAD) was observed than in the case of the low-profile vehicles (FCR and RDS) (Figure 5.5, a). The WAD variation due to the pedestrian posture was also smaller in the high-profile vehicles (maximum 86.3/62.2 mm difference with MPV/SUV) than in the case of the low-profile vehicles (maximum 127.3/139.3 mm difference with FCR/RDS).

Similarly, head impact time (HIT) varied with respect to the pedestrian posture and vehicle type. The longer HIT values were observed when the pedestrian was impacted by the low-profile vehicles than in the cases when the pedestrian was impacted by the high-profile vehicles (Figure 5.5, b). The maximum HIT variation (45 ms) was recorded between the maximum HIT from 0 % gait with RDS and the minimum HIT from 0 % gait with SUV.

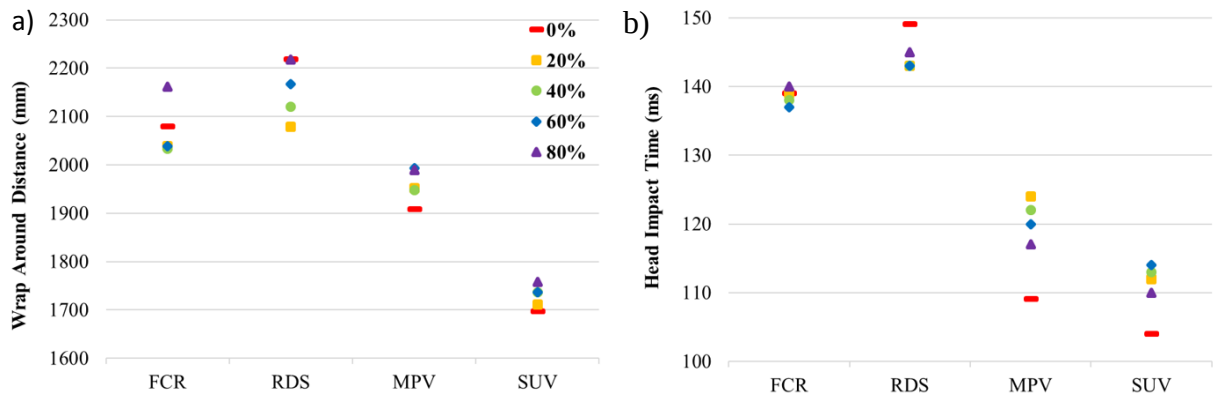

Figure 5.5 Head impact time (HIT) and Wrap around distance (WAD) of gait cycle models

The initial head impact points were examined on both the pedestrian and vehicle. The head impact points on the vehicles predicted by the M50-PS models showed insignificant difference with respect to posture. The vehicle impact points were recorded on the SUV's hood, while the corresponding points were on the windshield in the impacts with other vehicles. In terms of the head impact location on the pedestrian, different points were predicted by the M50-PS models across different gait cycle (Figure 5.6).

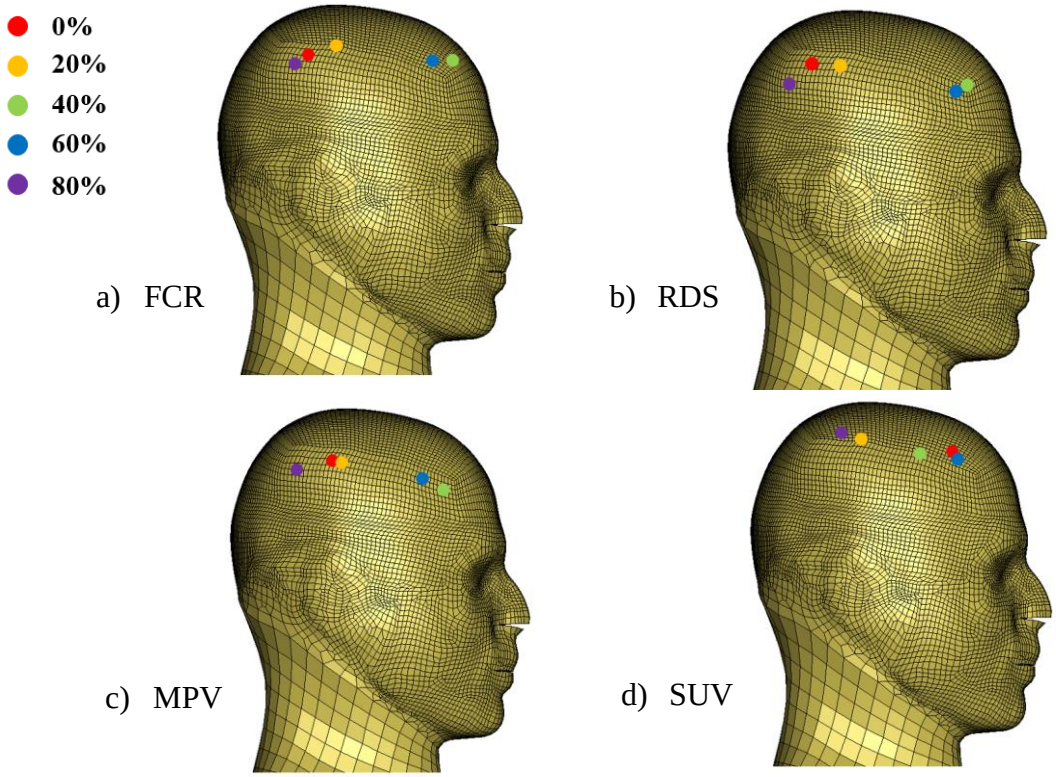

Figure 5.6 The initial head impact location

In terms of injury prediction at the lower extremities, the bending moments at the middle of the femur and tibia were recorded and compared between models. The maximum bending moments at the mid-thigh and mid-leg varied based on gait posture and vehicle type (Figure 5.7). The probability of injury for mid-thigh and mid-leg were calculated based on the formulas reported in literature [49]. The posture corresponding to 20 % gait cycle showed the highest probability of thigh/leg injury in most scenarios.

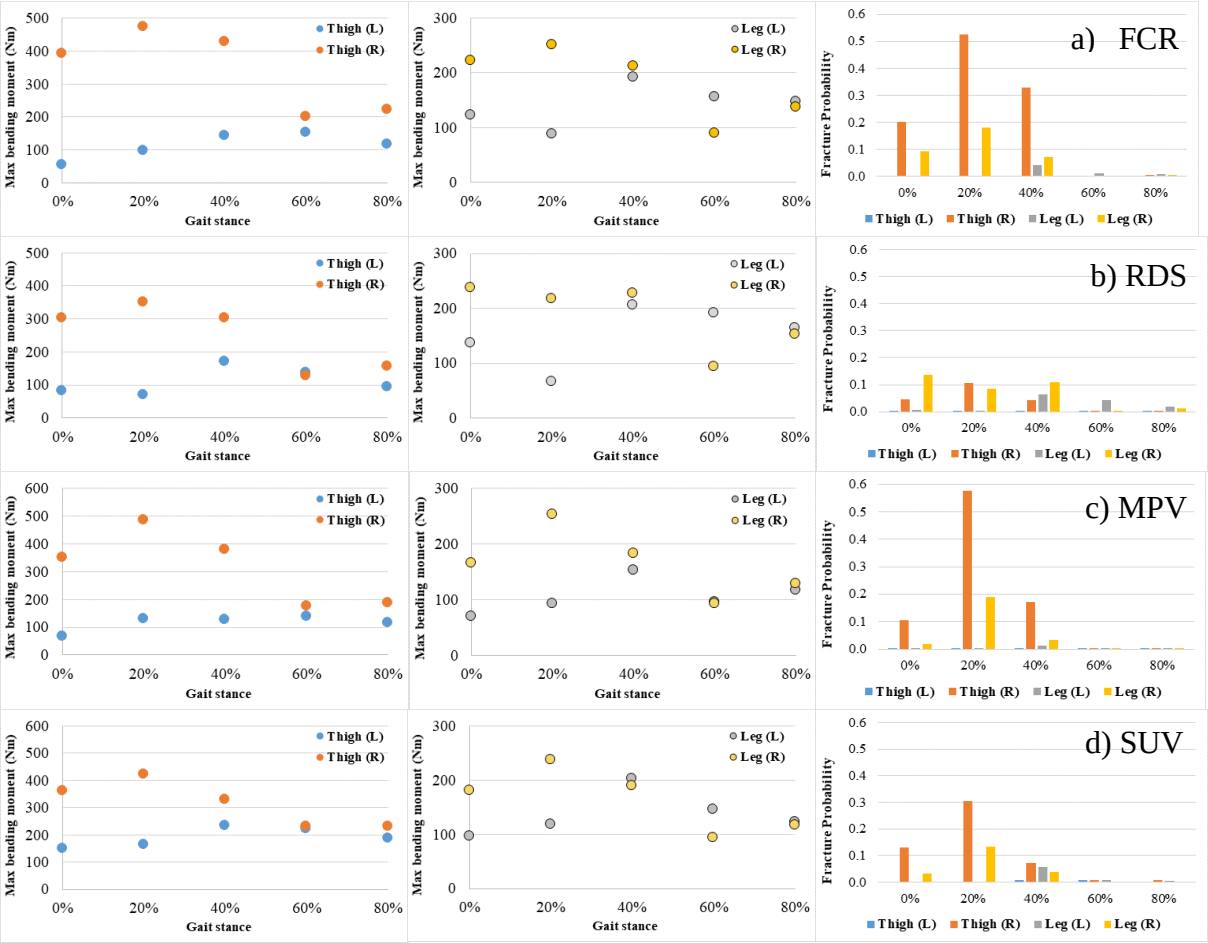

Figure 5.7 The maximum bending (L-M) in thighs and legs during gait cycle for various

During CPC impacts, the maximum valgus knee bending angle was calculated in order to predict knee ligament injuries. In all cases, the right leg predicted a larger maximum angle than the left leg, except when the 20 % gait model was impacted with the SUV (Figure 5.8). As a result, the medial collateral ligament (MCL) failure probability calculated based on the formulas reported in literature [50] on right leg showed high values (Table 5.2). The highest knee angles were observed from the right knee in the 60 and 80 % gait model in all CPC impact scenarios. Unlike others, the 20 % gait predicted the highest valgus bending angle at the left knee regardless of vehicle type.

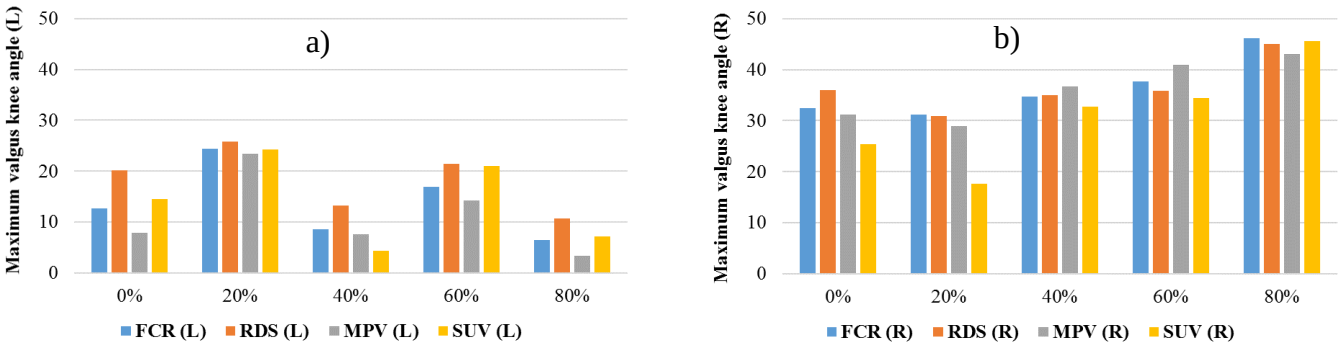

Figure 5.8 The maximum valgus knee bending angle: a) left and b) right lower extremity

Table 5.2 MCL injury probability on right leg [50]

	0 %	**20 %**	**40 %**	**60 %**	**80 %**
FCR	0.98	0.96	0.99	1.0	1.0
RDS	1.0	0.96	0.99	1.0	1.0
MPV	0.96	0.92	1.0	1.0	1.0
SUV	0.80	0.36	0.98	0.99	1.0

5.4 DISCUSSION

In this study, the effects corresponding to two pre-impact variables of pedestrian accidents (e.g. pedestrian posture and vehicle type) were examined using a validated pedestrian FE model of a 50^{th} percentile male. This is the first study, which investigates various CPC impact scenarios using a validated pedestrian FE model in various gait postures as well as different vehicle types.

The development of M50-PS models in gait posture was the most time-consuming part of this study. The majority of the M50-PS model's joints (e.g. hip, knee) include ligaments, so changing the posture is much more difficult than the simplified human models, which was modelled simple mechanical joints [13]. While a specialized software for this changing of model posture task was used (PIPER), some element distortions and contact penetrations were observed in the output models. Therefore, the models were further improved and debugged in CPC simulations until high quality metrics of all elements were obtained as in the original M50-PS model. Additionally, the final models showed stable in CPC impacts with various vehicles, providing its good robustness.

Head injuries are the leading cause of death in pedestrian accidents [8, 51]. Determining the point of initial head impact on the pedestrian is crucial to predicting head injuries. Several studies found a lower injury tolerance for lateral impacts than for anteroposterior and axial impact in humans [52-54]. Furthermore, a highest probability of concussion was observed when the head was impacted on the side/temporal region based on the analysis of concussions in college-level sports players [55].

The CPC impact simulations that used the pedestrian FE models positioned in 0, 20, and 80 % gait posture predicted the initial head impact point within the parietal head region for all vehicle types except the SUV. It was observed that this head impact location was influenced by the pre-impact position of the pedestrian's initially impacted leg (right in this study). For the gait postures of 0, 20, and 80 %, the right leg was anterior to the body, so when it was impacted by the vehicle, it implied a rotation of the pedestrian's lower body to rotate left in the longitudinal axis. Consequently, the upper body rotated towards the vehicle, causing the initial head impact at the parietal bone region. Conversely, when the model was in 40 and 60 % of gait, the right leg was posterior to the body, which caused the lower body to rotate to the right. This lower body rotation caused an initial head impact point at the frontal bone region. For the CPC impact with SUV, the upper body began to rotate along the anteroposterior axis as soon as the bonnet leading edge (BLE) contacted the greater trochanter (GT). In this case, the gait posture of lower extremities had a smaller influence on the rotation of upper body, which is observed some different pattern in the SUV impact.

In all scenarios except on the SUV, the initial head impact point on the vehicle was observed within the windshield region. In the case of SUV impacts, the initial head impact point was recorded on the vehicle hood region, which include the high-stiffness parts of vehicle, such as the engine compartment. When the pedestrian is impacted by high-profile vehicles, their pivot point is higher than when they are impacted by low-profile vehicles. In addition, the SUV has a longer bonnet length compared to the MPV, which caused the initial head contact to the vehicle hood region. The head impact times show to vary with respect to vehicle types and pedestrian postures (Figure 5.5, b). This observation is useful to set up the deployment time of active bonnet system, which was developed and installed on a production vehicle recently [56]. This active bonnet system creates a buffer space between the high-stiffness engine parts and the pedestrian when a pedestrian contact is detected. However, these active safety system should be carefully validated across various CPC scenarios because various HIT regarding pedestrian's posture was predicted. Therefore, the results presented in this study could be used in future to improve the design of new active safety systems for pedestrian protection, which may select the optimum activation time.

Higher valgus knee bending angles were observed in the right knee corresponding to the first lower extremity impacted by the vehicle (Figure 5.8). While the MCL injury probability were high in almost all cases (except 20 % gait with SUV impact), the highest values (close to 1) were predicted from the impacts with low-profile vehicles (FCR and RDS) and for the postures corresponding to the gait in swing phase (60 and 80 %). Interestingly, the lowest long bone fracture probability of thigh/leg were observed in these postures, which are in swing phase for all impact scenarios. This suggest an inverse correlation between the probability of MCL injuries and lower extremity bone injuries.

There are several limitations to this study. One limitation was the pedestrian was positioned relative to the vehicle centerline in this study. In contrast, real world CPC impact can happen at a variety of vehicle-pedestrian alignments and these should be investigated as well. This study is limited in the validity of the pedestrian model's knee ligament geometries. The geometries of the lower extremities soft tissues were deformed caused by the model positioning. The deformed knee ligament geometries were not verified due to a lack of medical images and PMHS test data of the knee at the simulated joint angles. This validation should be considered to increase the model biofidelity in injury prediction of soft tissue at the knee joint, once data is available.

The European Experimental Vehicles Committee (EEVC) Work Groups proposed a lateral bending angle of 15 degrees as the thresholds for knee injuries[57, 58]. Three bending tests, using isolated lower limbs conducted by Kerrigan et al. and Bhalla et al., reported the medial collateral ligament (MCL) rupture at about 12.7 degrees [59, 60]. However, the injury of the knee joint is associated with bending as well as shear displacement. In addition, the injury thresholds were established from experiments that used a straight knee, which is unsuitable to apply same threshold to the bent knee. Hence, the MCL injury probability calculated in this study should be improved when the bent knee test are available.

Despite these limitations, the results of this study should be taken into consideration when examining the pedestrian testing protocols. This study shows that varying pre-impact conditions, including pedestrian posture and vehicle type causes variation in pedestrian kinetic/kinematic responses, which may result in different injury outcomes. In order to protect the pedestrian, testing needs to examine various pedestrian accident scenarios.

ACKNOWLEDGEMENTS

All findings and views reported in this manuscript are based on the opinions of the authors and do not necessarily represent the consensus or view of the funding organization. Work was supported by the Global Human Body Models Consortium, LLC and NHSTA under GHBMC Project No.: WFU-006.

REFERENCE

[1] WHO, "Global Status Report on Road Safety," 2018.
[2] GHSA, "Pedestrian Traffic Fatalities by State," 2019.
[3] NHTSA, "Traffic Safety Facts (2017 Data)," 2019.
[4] NHTSA, "Early Estimate of Motor Vehicle Traffic Fatalities in 2018," 2019.
[5] C. Klug, F. Feist, M. Raffler, W. Sinz, P. Petit, J. Ellway, *et al.*, "Development of a Procedure to Compare Kinematics of Human Body Models for Pedestrian Simulations," in *IRCOBI Conference: International Research Council on the Biomechanics of Injury*, 2017.
[6] R. Paas, C. Masson, and J. Davidsson, "Head boundary conditions in pedestrian crashes with passenger cars: six-degrees-of-freedom post-mortem human subject responses," *International journal of crashworthiness*, vol. 20, pp. 547-559, 2015.

[7] G. Schroeder, "Injury mechanism of pedestrians during a front-end collision with a late model car," in *JSAE Spring Convention, 2000*, 2000.
[8] J. R. Crandall, K. S. Bhalla, and N. Madeley, "Designing road vehicles for pedestrian protection," *Bmj*, vol. 324, pp. 1145-1148, 2002.
[9] B. Y. Henary, J. Crandall, K. Bhalla, C. N. Mock, and B. S. Roudsari, "Child and adult pedestrian impact: the influence of vehicle type on injury severity," in *Annual Proceedings/Association for the Advancement of Automotive Medicine*, 2003, p. 105.
[10] D. E. Lefler and H. C. Gabler, "The emerging threat of light truck impacts with pedestrians," Rowan University, 2001.
[11] C. Kam, J. Kerrigan, M. Meissner, C. Drinkwater, D. Murphy, J. Bolton, *et al.*, "Design of a full-scale impact system for analysis of vehicle pedestrian collisions," *SAE transactions*, pp. 2268-2282, 2005.
[12] J. R. Kerrigan, J. R. Crandall, and B. Deng, "Pedestrian kinematic response to mid-sized vehicle impact," *International journal of vehicle safety*, vol. 2, pp. 221-240, 2007.
[13] N. Leglatin, M. Blundell, and G. Blount, "The simulation of pedestrian impact with a combined multibody finite elements system model," *Journal of Engineering Design*, vol. 17, pp. 463-477, 2006.
[14] J. van Hoof, R. de Lange, and J. S. Wismans, "Improving pedestrian safety using numerical human models," SAE Technical Paper2003.
[15] G. Li, J. Yang, and C. Simms, "The influence of gait stance on pedestrian lower limb injury risk," *Accident Analysis & Prevention*, vol. 85, pp. 83-92, 2015.
[16] H. Mao, L. Zhang, B. Jiang, V. V. Genthikatti, X. Jin, F. Zhu, *et al.*, "Development of a Finite Element Human Head Model Partially Validated With Thirty Five Experimental Cases," *Journal of biomechanical engineering*, vol. 135, p. 111002, 2013.
[17] E. G. Takhounts, M. J. Craig, K. Moorhouse, J. McFadden, and V. Hasija, "Development of Brain Injury Criteria (BrIC)," *Stapp car crash journal*, vol. 57, pp. 243-266, 2013.
[18] T. Yanaoka and Y. Dokko, "A Parametric Study of Age-Related Factors Affecting Intracranial Responses under Impact Loading Using a Human Head/Brain FE Model," presented at the International Research Council on Biomechanics Injury (IRCOBI), Gothenburg, Sweeden, 2013.
[19] J. A. DeWit and D. S. Cronin, "Cervical spine segment finite element model for traumatic injury prediction," *Journal of the mechanical behavior of biomedical materials*, vol. 10, pp. 138-150, 2012.
[20] J. B. Fice, D. S. Cronin, and M. B. Panzer, "Cervical spine model to predict capsular ligament response in rear impact," *Annals of biomedical engineering*, vol. 39, pp. 2152-2162, 2011.
[21] S. F. Mattucci, J. A. Moulton, N. Chandrashekar, and D. S. Cronin, "Strain rate dependent properties of younger human cervical spine ligaments," *Journal of the mechanical behavior of biomedical materials*, vol. 10, pp. 216-226, 2012.
[22] S. F. Mattucci, J. A. Moulton, N. Chandrashekar, and D. S. Cronin, "Strain rate dependent properties of human craniovertebral ligaments," *Journal of the mechanical behavior of biomedical materials*, vol. 23, pp. 71-79, 2013.
[23] Z. Li, M. W. Kindig, J. R. Kerrigan, C. D. Untaroiu, D. Subit, J. R. Crandall, *et al.*, "Rib Fractures Under Anterior-Posterior Dynamic Loads: Experimental and Finite-Element Study," *Journal of Biomechanics*, vol. 43, p. 228.234, 2010.

[24] Z. Li, M. W. Kindig, D. Subit, and R. W. Kent, "Influence of mesh density, cortical thickness and material properties on human rib fracture prediction," *Medical engineering & physics,* vol. 32, pp. 998-1008, 2010.
[25] D. Poulard, R. Kent, M. Kindig, Z. Li, and D. Subit, "Thoracic response targets for a computational model: A hierarchical approach to asses the biofidelity of a 50th-percentile occupant male finite element model," *J Mech Behav Biomed Mater,* 2015.
[26] A. Soni and P. Beillas, "Modelling hollow organs for impact conditions: a simplified case study," *Comput Methods Biomech Biomed Engin,* vol. [Epub ahead of print], Oct 24 2013.
[27] Y. H. Kim, J. E. Kim, and A. W. Eberhardt, "A new cortical thickness mapping method with application to an in vivo finite element model," *Comput Methods Biomech Biomed Engin,* vol. 17, pp. 997-1001, Oct 31 2012.
[28] J. Shin and C. Untaroiu, "Biomechanical and Injury Response of Human Foot and Ankle under Complex Loading," *J Biomech Eng,* vol. 135, Jul 1 2013.
[29] C. D. Untaroiu, N. Yue, and J. Shin, "A finite element model of the lower limb for simulating automotive impacts," *Ann Biomed Eng,* vol. 41, pp. 513-26, Mar 2013.
[30] N. Yue and C. D. Untaroiu, "A numerical investigation on the variation in hip injury tolerance with occupant posture during frontal collisions," *Traffic injury prevention,* vol. 15, pp. 513-522, 2014.
[31] N. Yue, J. Shin, and C. Untaroiu, "Development and validation of an occupant lower limb finite element model.," in *SAE Technical Paper* vol. 2011-01-1128, ed, 2011.
[32] A. R. Hayes, N. A. Vavalle, D. P. Moreno, J. D. Stitzel, and F. S. Gayzik, "Validation of simulated chestband data in frontal and lateral loading using a human body finite element model," *Traffic Inj Prev,* vol. 15, pp. 181-6, 2014.
[33] N. A. Vavalle, A. B. Thompson, A. R. Hayes, D. P. Moreno, J. D. Stitzel, and F. S. Gayzik, "Investigation of the Mass Distribution of a Detailed Seated Male Finite Element Model," *J Appl Biomech,* vol. [Epub ahead of print], Dec 17 2013.
[34] G. Park, T. Kim, J. R. Crandall, C. Arregui-Dalmases, and J. Luzon-Narro, "Comparison of Kinematics of GHBMC to PMHS on the Side Impact Condition," presented at the International Research Council on Biomechanics of Injury, Gothenburg, Sweden, 2013.
[35] N. A. Vavalle, D. P. Moreno, A. C. Rhyne, J. D. Stitzel, and F. S. Gayzik, "Lateral impact validation of a geometrically accurate full body finite element model for blunt injury prediction," *Ann Biomed Eng,* vol. 41, pp. 497-512, Mar 2013.
[36] C. D. Untaroiu, J. Shin, N. Yue, Y.-H. Kim, J.-E. Kim, and A. W. Eberhardt, "A finite element model of the pelvis and lower limb for automotive impact applications," *12th International LSDYNA users conferenceDearborn, MI, USA,* 2012.
[37] C. D. Untaroiu, W. Pak, Y. Meng, J. Schap, B. Koya, and S. Gayzik, "A Finite Element Model of a Midsize Male for Simulating Pedestrian Accidents," *Journal of biomechanical engineering,* vol. 140, p. 011003, 2018.
[38] EuroNCAP, "Pedestrian CAE Models v1.5," 2017.
[39] EuroNCAP, "Pedestrian Testing Protocol v8.5," 2018.
[40] C. D. Untaroiu, M. U. Meissner, J. R. Crandall, Y. Takahashi, M. Okamoto, and O. Ito, "Crash reconstruction of pedestrian accidents using optimization techniques," *International Journal of Impact Engineering,* vol. 36, pp. 210-219, 2009.
[41] G. Wu, S. Siegler, P. Allard, C. Kirtley, A. Leardini, D. Rosenbaum, *et al.*, "ISB recommendation on definitions of joint coordinate system of various joints for the reporting

of human joint motion—part I: ankle, hip, and spine," *Journal of biomechanics,* vol. 35, pp. 543-548, 2002.
[42] G. Wu, F. C. Van der Helm, H. D. Veeger, M. Makhsous, P. Van Roy, C. Anglin, *et al.*, "ISB recommendation on definitions of joint coordinate systems of various joints for the reporting of human joint motion—Part II: shoulder, elbow, wrist and hand," *Journal of biomechanics,* vol. 38, pp. 981-992, 2005.
[43] T. Janak, Y. Lafon, P. Petit, and P. Beillas, "Transformation Smoothing to use after Positioning of Finite Element Human Body Models," 2018.
[44] C. Klug, F. Feist, M. Raffler, W. Sinz, P. Petit, J. Ellway, *et al.*, "Development of a Procedure to Compare Kinematics of Human Body Models for Pedestrian Simulations," in *IRCOBI Conference Proceedings*, 2017.
[45] A. Chidester and R. Isenberg, "Final report–the pedestrian crash data study," *National Highway Traffic Safety Administration Paper,* 2001.
[46] S.-W. Koh, J. M. Cavanaugh, M. J. Mason, and S. A. Petersen, "Shoulder injury and response due to lateral glenohumeral joint impact: an analysis of combined data," *Stapp car crash journal,* vol. 49, p. 291, 2005.
[47] R. Fredriksson, E. Rosén, and A. Kullgren, "Priorities of pedestrian protection—a real-life study of severe injuries and car sources," *Accident analysis & prevention,* vol. 42, pp. 1672-1681, 2010.
[48] V. Kothari and M. Gangal, "Assessment of frictional properties of some woven fabrics," 1994.
[49] J. R. Kerrigan, D. Drinkwater, C. Kam, D. Murphy, B. Ivarsson, J. Crandall, *et al.*, "Tolerance of the human leg and thigh in dynamic latero-medial bending," *International Journal of Crashworthiness,* vol. 9, pp. 607-623, 2004.
[50] Y. Takahashi, F. Matsuoka, H. Okuyama, and I. Imaizumi, "Development of injury probability functions for the flexible pedestrian legform impactor," *SAE International journal of passenger cars-mechanical systems,* vol. 5, pp. 242-252, 2012.
[51] Y.-W. Yun, J.-W. Lee, G.-H. Kim, and P. Gyung-Jin, "Pedestrian Protection Test and Results: Utilization for Regulations in Korea," in *23rd International Technical Conference on the Enhanced Safety of Vehicles (ESV) National Highway Traffic Safety Administration*, 2013.
[52] S. Kleiven, "Influence of impact direction on the human head in prediction of subdural hematoma," *Journal of neurotrauma,* vol. 20, pp. 365-379, 2003.
[53] L. Zhang, K. H. Yang, and A. I. King, "Comparison of brain responses between frontal and lateral impacts by finite element modeling," *Journal of neurotrauma,* vol. 18, pp. 21-30, 2001.
[54] L. Zhang, K. H. Yang, and A. I. King, "A proposed injury threshold for mild traumatic brain injury," *Journal of biomechanical engineering,* vol. 126, pp. 226-236, 2004.
[55] J. S. Delaney, V. Puni, and F. Rouah, "Mechanisms of injury for concussions in university football, ice hockey, and soccer: a pilot study," *Clinical Journal of Sport Medicine,* vol. 16, pp. 162-165, 2006.
[56] Y. Inomata, N. Iwai, Y. Maeda, S. Kobayashi, H. Okuyama, and N. Takahashi, "Development of the pop-up engine hood for pedestrian head protection," in *21st International Technical Conference on the Enhanced Safety of Vehicles (ESV 2009)*, 2009.
[57] E. E. V. C. W. G. o. P. Protection, "Proposals for Methods to Evaluate Pedestrian Protection for Passenger Cards: Final Report," 1994.

[58] E. E. V. C. W. G. o. P. Protection, "Improved test methods to evaluate pedestrian protection afforded by passenger cars," 1998.
[59] K. S. Bhalla, D. Bose, N. Madeley, J. Kerrigan, J. R. Crandall, D. C. Longhitano*, et al.*, "Evaluation of the response of mechanical pedestrian knee joint impactors in bending and shear loading," in *Proceedings: International Technical Conference on the Enhanced Safety of Vehicles*, 2003, pp. 12 p.-12 p.
[60] J. R. Kerrigan, K. S. Bhalla, N. J. Madeley, J. R. Funk, D. Bose, and J. R. Crandall, "Experiments for establishing pedestrian-impact lower limb injury criteria," SAE Technical Paper 0148-7191, 2003.

Chapter 6

Conclusion

6.1 LIMITATIONS AND FUTURE WORK

In this study, pedestrian finite element (FE) models were developed and validated in order to investigate the sensitivity of injury risk probabilities of a pedestrian involved in Car-to-Pedestrian Collision (CPC) accident on the vehicle and pedestrian pre-impact variables. The pedestrian FE models were validated in component tests and whole-body CPC impact simulations based on the Post Mortem Human Surrogate (PMHS) test data. After model development and validation, five pedestrian models corresponding to the 50^{th} percentile male were developed to represent the whole walking gait cycle. Using these models and four different type of vehicles, the effect of pre-impact variables such as pedestrian posture and vehicle type were investigated.

As many studies related to human models used in impact biomechanics, current study has some limitations, which should be acknowledged. First, the pedestrian FE models were validated only in lateral impact because this is the most frequent accident scenario [1] and PMHS test data is available in only this configuration [2, 3]. However, additional whole-body validation is recommended to be performed to increase model biofidelity, when the PMHS test data in ventral and dorsal impacts will be available.

Another limitation of the pedestrian FE models is that the geometry and the material properties of body parts were not exactly matched to the PMHS specimens used in the validation tests. While various scaling methods were suggested in literature [4], these methods are unable to be validated due to the nature of human variation and various test setup configuration used in testing. In addition, pedestrian FE models scaled by the whole height and weight corresponding to PMHS specimens possess limitations such as different body part anthropometries and disregarded material properties of body parts. Lastly, the test data used in model validations were usually obtained from aged PMHS specimens (68.3 ± 9.8 [5], 53.8 ± 13.9 [6], 73.3 ± 14.0 [7], 60.0 ± 15.2 [2], and 74.9 ± 8.0 [3] years-old). Instead of applying the scaling methods, advanced morphing methodologies should be applied in the future for matching the geometries of PMHS specimens used in testing [8].

The geometries of the soft tissue in the knee joint (e.g. knee ligaments) were deformed during the development of the pedestrian gait models. In terms of injury prediction, the geometry may plays important role. However, the deformed soft tissues were not verified in this study due to a lack of the medical images and PMHS test data of the knee at the simulated joint angles. Therefore, the geometries of knee ligaments are suggested to be verified in the future when the medical images of the knee at the simulated joint angles will be available.

Lastly, the results of study investigating the effect of pre-impact variables were not verified since no physical tests exist to compare the correlations. The results predicted by the gait models can be compared to the Pedestrian Crash Data Study (PCDS) in order to find correlations in the future. Despite of inadequate information such as the exact pedestrian posture during impact, this comparison may improve the reliability of the models in gait cycle and thus could be used to improve the current test procedure for pedestrian protection in various accident scenarios.

6.2 CONCLUSION

In this study, pedestrian FE models corresponding to 5^{th} female, 50^{th} male, and 95^{th} male anthropometries were developed and validated. Overall, the responses predicted by the FE models showed good correlations to the corresponding PMHS test data. Using these models, the kinetic/kinematic responses of pedestrian during vehicle-pedestrian interaction were investigated in various impact scenarios, which are unable or possess limitations in physical tests. Some limitations were observed in this study, however, the results of this study should be taken into consideration when examining the pedestrian testing protocols. Generally, the pedestrian models developed in this study could be used by safety researchers in the design of front-end of new vehicles and/or in the development of new regulations in order to protect pedestrians.

REFERENCE

[1] R. Fredriksson, E. Rosén, and A. Kullgren, "Priorities of pedestrian protection—a real-life study of severe injuries and car sources," *Accident analysis & prevention*, vol. 42, pp. 1672-1681, 2010.

[2] J. R. Kerrigan, J. R. Crandall, and B. Deng, "Pedestrian kinematic response to mid-sized vehicle impact," *International journal of vehicle safety*, vol. 2, pp. 221-240, 2007.

[3] E. Song, J. Uriot, P. Potier, D. Dubois, P. Petit, X. Trosseille, *et al.*, "Reference PMHS Tests to Assess Whole-Body Pedestrian Impact Using a Simplified Generic Vehicle Front-End," in *IRCOBI Conference Proceedings*, 2017.

[4] A. Petitjean, X. Trosseille, N. Yoganandan, and F. A. Pintar, "Normalization and scaling for human response corridors and development of injury risk curves," in *Accidental Injury*, ed: Springer, 2015, pp. 769-792.

[5] D. Bose, K. S. Bhalla, C. D. Untaroiu, B. J. Ivarsson, J. R. Crandall, and S. Hurwitz, "Injury tolerance and moment response of the knee joint to combined valgus bending and shear loading," *J Biomech Eng*, vol. 130, p. 031008, Jun 2008.

[6] D. C. Viano, "Biomechanical responses and injuries in blunt lateral impact," SAE Technical Paper 0148-7191, 1989.

[7] S. W. Koh, J. M. Cavanaugh, M. J. Mason, S. A. Petersen, D. R. Marth, S. W. Rouhana, *et al.*, "Shoulder injury and response due to lateral glenohumeral joint impact: an analysis of combined data," *Stapp Car Crash J*, vol. 49, pp. 291-322, Nov 2005.

[8] K. M. Yates and C. D. Untaroiu, "Finite element modeling of the human kidney for probabilistic occupant models: Statistical shape analysis and mesh morphing," *Journal of biomechanics,* vol. 74, pp. 50-56, 2018.

Appendix A

Table A1 Summary data of the PMHS specimens in sedan CPC (Kerrigan et al. 2007)

Specimen/gender	Height (mm)	Weight (kg)	Initial height of right GT (mm)	Head contact time (ms)	WAD to head contact (mm)
S1/F	1631	63.5	784	112	1860
S2/F	1640	88.8	806	116	1860
S3/F	1645	82.5	837	116	1920
M4/F	1729	90.6	802	120	1935
M5/F	1743	92.9	826	124	2045
T6/M	1790	87.0	895	128	2230
T7/M	1843	91.6	952	136	2200
M50-P	1761	77.3	907	140	2205

Table A2 Summary data of the PMHS specimens in generic vehicle CPC (Song et al. 2017)

Test#	Age/gender	Configuration	Height (mm)	Weight (kg)
01	62/M	SUV	1630	82
02	82/M	SUV	1630	62
03	87/M	SUV	1660	75
04	81/M	SUV	1600	59
05	80/M	SUV	1560	74
06	73/M	Van	1730	87
07	75/M	Van	1730	62
08	64/M	Van	1710	65
09	78/M	Sedan	1680	64
10	76/M	Sedan	1690	58
11	66/M	Sedan	1630	74

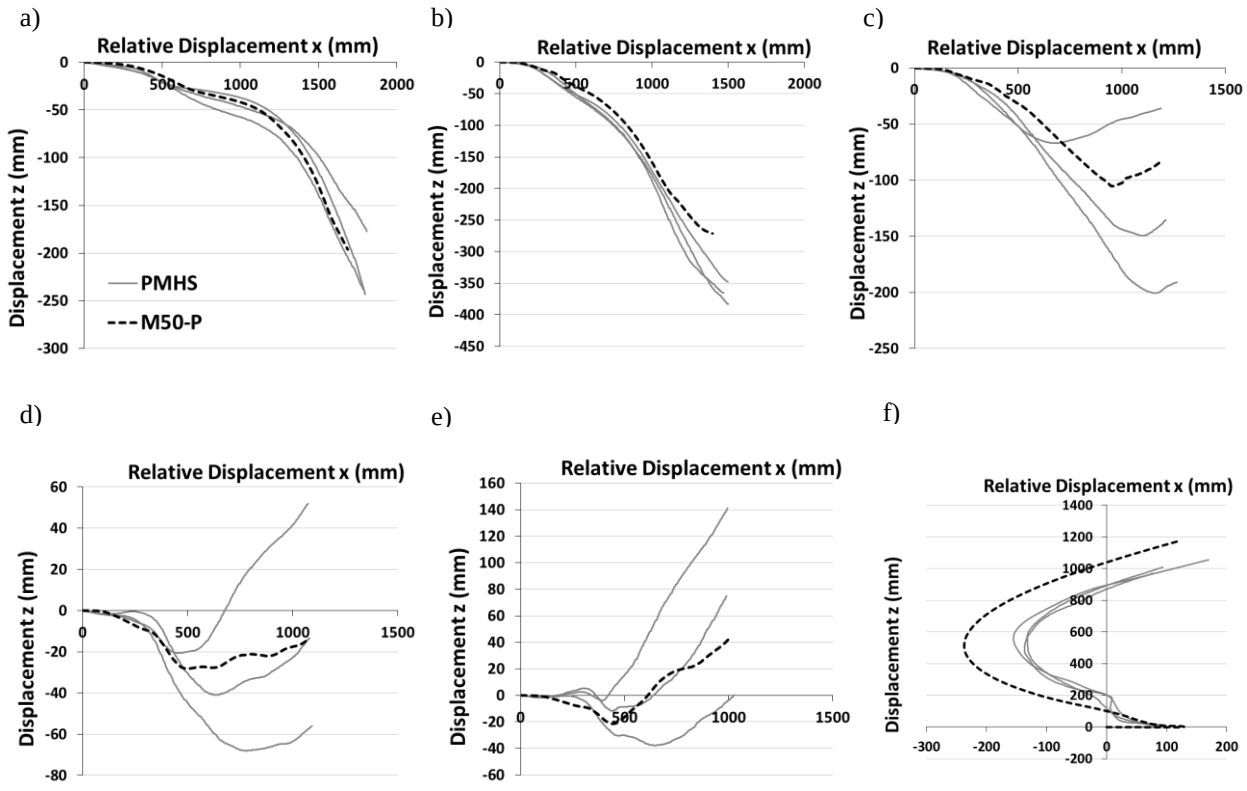

Figure A1 Kinematic trajectories relative to the simplified sedan buck:

a) shoulder, b) T4, c) T12, d) sacrum up, e) sacrum low, f) ankle

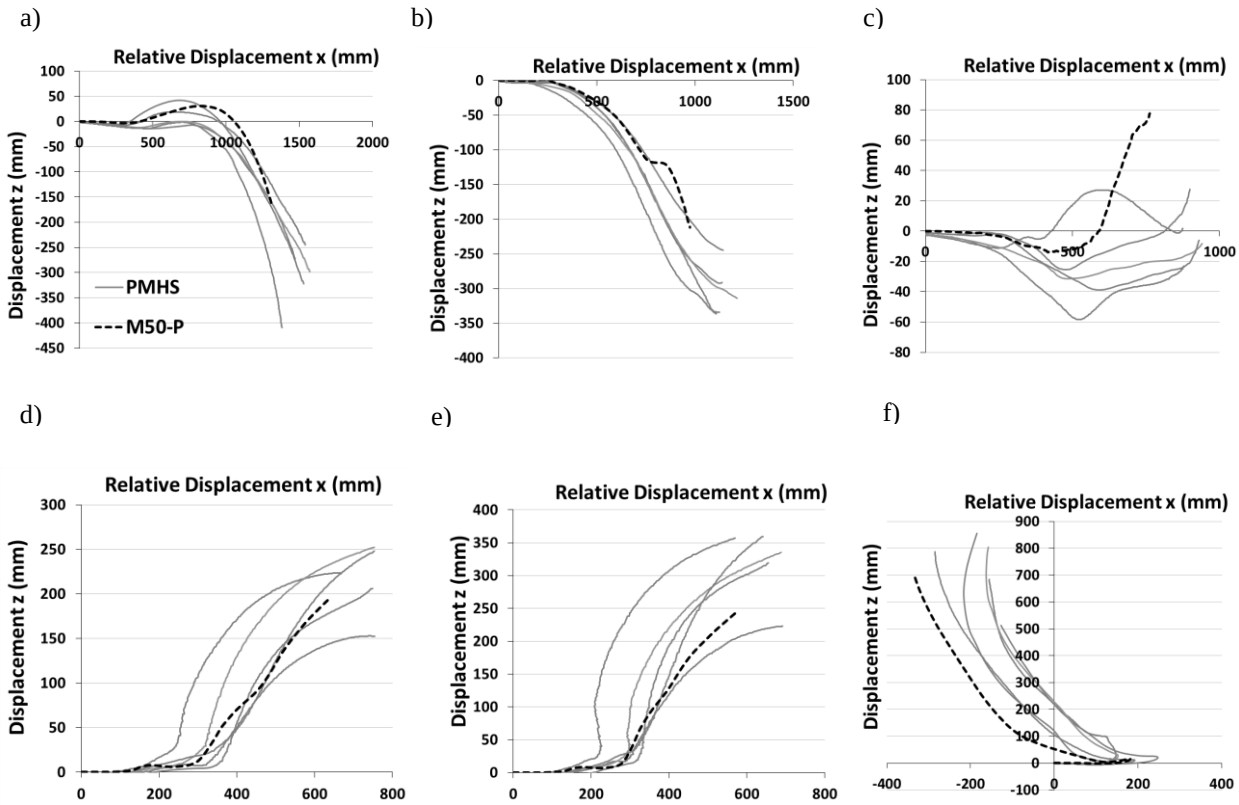

Figure A2 Kinematic trajectories relative to the simplified SUV buck:

a) shoulder, b) T4, c) T12, d) sacrum up, e) sacrum low, f) ankle

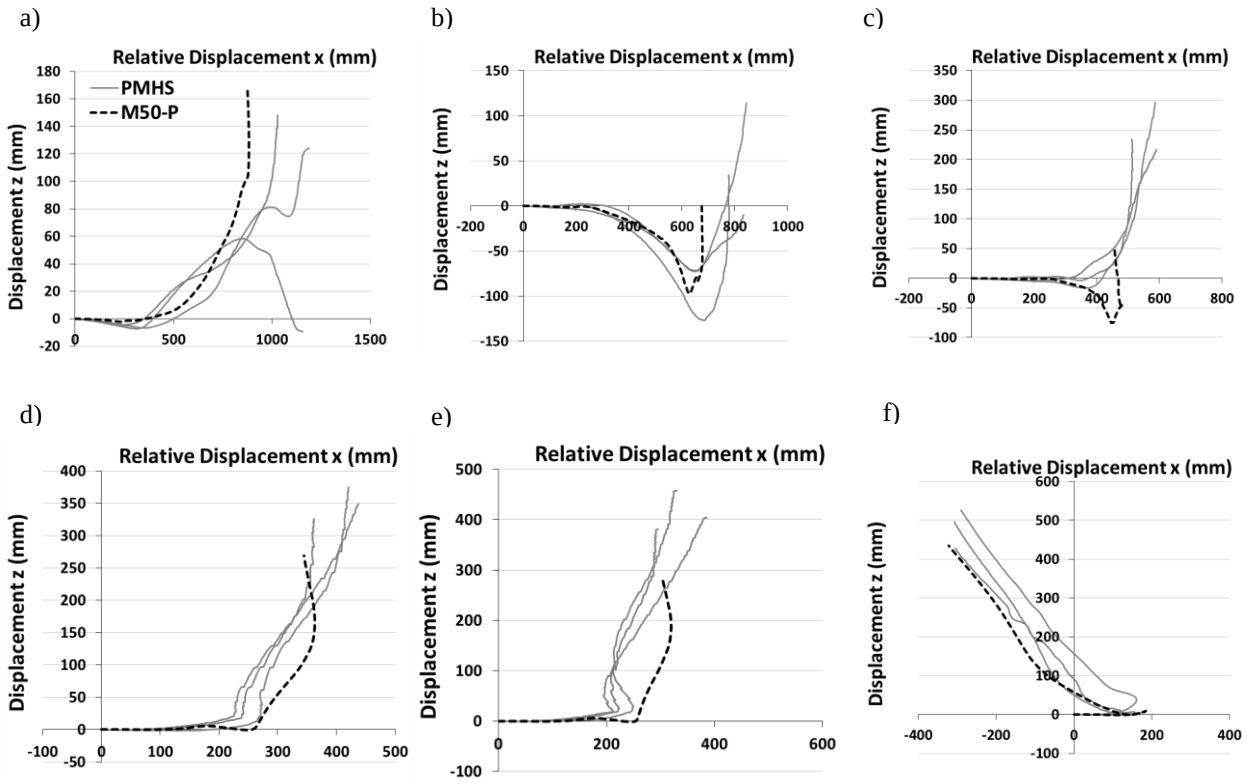

Figure A3 Kinematic trajectories relative to the simplified Van buck:

a) shoulder, b) T4, c) T12, d) sacrum up, e) sacrum low, f) ankle